THE

MUON COMPONENT OF

EXTENSIVE AIR SHOWERS

Thesis submitted by

PETER ROBERT BLAKE

for the degree of

DOCTOR OF PHILOSOPHY

in the University of London.

November 1965

ABSTRACT

Investigation of the muon component of Cosmic Ray extensive air showers serves as a means of studying the nature of the extremely high energy particles ($> 10^{14}$ eV) that reach the earth from space and the interactions they produce with atmospheric nuclei. Direct observation of these primaries is impossible because of their low intensity.

The present knowledge concerning the development of showers is reviewed in Chapter 1 together with a discussion about the origin of the high energy primaries producing them. Emphasis is put on the importance of the muon component.

Chapter 2 deals with the design of the muon density detectors used in the experiment described later in the thesis. Calibration and response uniformity tests are described. The liquid scintillators used are shielded by lead to absorb out the "soft" electron-photon component of the showers. The results of an experiment to determine the minimum thickness of lead absorber needed are presented and interpreted in Chapter 3.

The pulse height response spectra produced by secondary cosmic rays in various detectors are discussed in Chapter 4. The problem of the origin of "local showers" is presented

but the solution is left open.

In Chapter 5 the main experiment to measure the mean lateral distribution of muons in EAS is described. Results are presented on the variation of muon density with shower size and possible interpretations discussed. A lateral density distribution in the distance range 300 metres — 1,000 metres from the axis of showers of size 2×10^7 particles is presented. Comparison is made with other experiments and with theoretical calculations. An attempt is also made to determine any variation of lateral distribution with zenith angle and with shower size.

The variation of the ratio of muon density to electron density in showers with distance from the axis and with zenith angle is discussed in Chapter 6 using results obtained from comparing the response of the shielded detector with that of unshielded scintillators and Cherenkov tanks. Finally an outline of future work on muon density measurements at Haverah Park is given.

THE MUON COMPONENT OF EXTENSIVE AIR SHOWERS

CONTENTS

CHAPTER 1. THE STRUCTURE AND ORIGIN OF EXTENSIVE AIR SHOWERS — Page

1.1	Introduction.	1
1.2	Early Work.	4
1.3	The Structure of EAS.	5
1.4	Investigations of the Lateral Distribution of Charged Secondaries.	8
1.5	Energy of the Primary Particles.	10
1.6	The Size Spectrum.	11
1.7	The Longitudinal Development.	12
1.8	Fluctuations in the Development of Showers.	17
1.9	The Study of the Cores of EAS.	18
1.10	The Muon Component of EAS.	21
1.11	The Composition of High Energy Primaries.	30
1.12	Time Variations and Isotropy of EAS Primaries.	32
1.13	The Origin of Cosmic Rays.	35
1.14	Scope of the Present Work.	39

CHAPTER 2. THE DESIGN OF MUON DETECTORS AT HAVERAH PARK

2.1	The Haverah Park EAS Array.	41

CHAPTER 2. Continued. Page

2.2	Muon Density Detectors.	45
2.3	The Siting of the Detectors.	45
2.4	Area Considerations.	46
2.5	Detector Details.	48
2.6	Design Considerations.	49
2.7	Calibration and Single Particle Pulse Height Distribution.	56
2.8	Uniformity of Response.	60
2.9	Stability.	62
2.10	Shielding.	63

CHAPTER 3. THE ABSORPTION IN LEAD OF THE ELECTRON-PHOTON COMPONENT OF EAS

3.1	Introduction.	64
3.2	Experimental Details.	66
3.3	Experimental Procedure.	69
3.4	Identification of Core Positions.	71
3.5	Results.	72
3.6	Absorption of the Electron-Photon Component.	75
3.7	Interaction and Absorption of the Muon Component.	88
3.8	The Effect of the Nuclear Active Component.	91
3.9	The Proportion of Penetrating Particles.	93

CHAPTER 3. Continued. Page

3.10 Conclusions. 94

CHAPTER 4. THE PULSE HEIGHT SPECTRUM PRODUCED BY SECONDARY COSMIC RAYS

4.1 Introduction. 96

4.2 Apparatus. 96

4.3 The Integral Spectrum Obtained from the Liquid Scintillators. 97

4.4 Single Particles. 99

4.5 The Contribution of Extensive Air Showers. 101

4.6 Local Showers. 102

4.7 The Spectrum from a Plastic Scintillator. 103

4.8 The Pulse Height Spectrum from a Cherenkov Tank 104

4.9 Conclusion. 110

CHAPTER 5. THE MEAN LATERAL DENSITY DISTRIBUTION OF MUONS IN SHOWERS OF SIZE $5 \times 10^6 - 10^8$

5.1 Introduction. 112

5.2 Experimental Details. 114

5.3 Calibration and Checks on Response. 119

5.4 Shower Analysis. 122

5.5 Treatment of Muon Density Measurements. 124

CHAPTER 5. Continued. Page

5.6	Size Dependence of "ρ_μ".	126
5.7	Discussion of "$\rho_\mu - N_0$" relation.	131
5.8	Dependence of α on Shower Size.	135
5.9	The Mean Lateral Density Distribution of Muons.	137
5.10	Comparison with Other Work.	140
5.11	Variation of Lateral Distribution with Zenith Angle.	143
5.12	Variation of Lateral Distribution with Shower Size.	144
5.13	General Conclusions.	146

CHAPTER 6. FURTHER INVESTIGATIONS ON THE MUON COMPONENT OF EAS

6.1	Introduction.	148
6.2	The Ratio of the Response to EAS of Shielded and Unshielded Scintillators.	149
6.3	Comparison of Muon and Water Cherenkov Detector Response.	151
6.4	The Ratio of Muon to Cherenkov Response as a Function of Zenith Angle.	154
6.5	Further Study of the Lateral Distribution of Showers 2×10^7 Particles.	157
6.6	The Small EAS Arrays.	157
6.7	Energy of Muons.	159
6.8	Time Spread in Arrival of Secondary Particles.	160

CHAPTER 6. Continued. Page

6.9 Search for Anisotropy of "Muon-Rich" and "Muon-Less" Showers. 160

6.10 Large Array Extension. 161

6.11 General Conclusions. 161

APPENDIX 1. The Optical Design of the Detectors. 163

APPENDIX 2. Interpretation of Selected Showers. 169

ACKNOWLEDGEMENTS. 171

REFERENCES. 172

- - - - - - -

CHAPTER 1

THE STRUCTURE AND ORIGIN OF EXTENSIVE AIR SHOWERS

1.1 Introduction

Primary cosmic radiation is made up of high energy particles that continuously reach the vicinity of the earth from outer space. Studies of its composition, energy spectrum and variations with time and direction of motion are contributing to our understanding of the large scale processes that take place in the universe.

An extensive air shower (EAS) observed as the simultaneous arrival of a large number of secondary particles at the earth's surface, is seen whenever the earth's atmosphere lies in the path of a cosmic ray primary of energy greater than about 10^{14} eV. These very high energy primaries appear to arrive at the earth evenly from all directions. Mainly because of this isotropy in arrival direction the origin of these particles remains a field of speculation.

Data on cosmic rays of energy around 10^{12}-10^{13} eV from balloon-borne nuclear emulsions indicate that the majority of EAS primaries in the neighbourhood of the earth are probably protons. There is however some recent evidence

that heavier nuclei may be relatively more abundant within the energy range 10^{16}-10^{17} eV.

The flux of primary cosmic rays falls steeply with increasing energy. For energies greater than 10^{12} eV per particle the exponent of the integral energy spectrum lies in the range -1.5 to -2.2. Although direct detection of low energy primaries is possible using counters borne in satellites and balloons, for primaries above 10^{14} eV energy the flux is so low that investigations of their properties can only be carried out indirectly by making use of the lateral spreading of secondaries in EAS.

A shower, observed at sea-level or mountain altitudes, is the superposition of cascades of electromagnetic and nuclear interactions initiated by a primary cosmic ray particle on entering the earth's atmosphere, usually with an oxygen or a nitrogen nucleus. Deep in the atmosphere the result is detected as the simultaneous arrival of a large number of secondary particles spread over a large area.

At sea-level three separate components of secondaries can be distinguished. The nuclear-active (or N) component is concentrated close to the initial line of motion of the primary particle. The central, high energy region of the N- component forms the core of the shower. This is the remnant of the nucleon cascade and consists mainly of high

energy nucleons and pions.

The electron-photon component is spread out transversely over large distances from the core and represents about 90% of all the secondary particles in a shower at sea-level. The electrons, positrons and photons are mainly the products of electromagnetic cascades initiated by the decay, into two high energy photons, of the uncharged pions produced in the nucleon cascade.

The muon component also extends hundreds of metres from the core. It constitutes less than 10% of all secondary particles but because its radial distribution is not so steep as that of the electrons it becomes the dominant secondary component at distances greater than 1000 metres from the shower axis (i.e. the centre of the core). The main sources of the muon component are the charged pions produced in the nuclear interactions which decay into muons and neutrinos.

The arrival of a single energetic particle at the top of the atmosphere can thus be detected over a large area on the earth's surface. One or more detectors which record the simultaneous arrival of secondary particles are used to study such EAS. Inferences can then be made about the interaction processes taking place in the atmosphere and the nature and energy of the initiating cosmic ray particles. Indeed in addition to their importance for astrophysics, EAS are at

present the only means of studying nuclear interactions involving collision energies greater than 10^{14} eV.

1.2 Early Work

Extensive air showers were discovered in 1938 when coincidences between horizontally spaced geiger counters were obtained (Schmeiser and Bothe,1938;Auger et al.,1938). Cloud chamber studies by Janossy and Lovell (1938) showed that the particles involved were mainly electrons. The existence of nucleons and penetrating particles associated with the electrons was soon deduced (Auger et al.,1939). At that time these were thought to be secondary to electron-photon cascades initiated by high energy cosmic ray primary photons or electrons.

Evidence against this view came from a number of experiments. The "East-West" asymmetry gave evidence for positively charged primaries (Johnson,1938). Freier et al. (1948) discovered from balloon flights that the majority of low energy cosmic rays were protons. The existence of charged pions was demonstrated from nuclear emulsions exposed to primary cosmic radiation (Occhialini and Powell,1947) and the pion decay mode was observed (Lattes et al.,1947).

Results such as these, and more particularly the

discovery and production of neutral pions decaying almost instantaneously into two high energy photons (Steinberger, 1950) led to the development of a new model for EAS. By 1955 the main outlines of this model had been firmly established.

1.3 The Structure of EAS

The nucleonic cascade plays the dominant role in the development and structure of an EAS. A primary cosmic ray proton encountering the earth's atmosphere interacts after traversing a mean free path of about 80 grms/cm^2. (Mantano et al.,1963). The inelasticity of such interactions appears to remain approximately constant at 0.4 to 0.5 for energies above 10^{11}eV. This low value means that a nucleon emerges with a substantial fraction of the primary energy. Other nucleons of lower energy emerge together with a large number of secondary pions. The mean multiplicity appears to be about 40 at 10^{14}eV(Fowler,1963) and can be roughly represented by $3E_p^{\frac{1}{4}}$, where E_p is the primary energy in Gev (Cocconi,1965). McCusker and Peak (1963) conclude however that an energy variation proportional to log E_p fits the results more closely than $E_p^{\frac{1}{4}}$.

On average equal numbers of positive, negative and uncharged pions are produced. The neutral pions (mean

lifetime $\sim 10^{-15}$ sec.) decay very rapidly into two high energy photons. These initiate electron-photon cascades which develop by the repeated processes of pair production by photons and bremsstrahlung radiation by the created electrons. These cascades would die out well before sea-level is reached; a 10^{10} eV photon for example, produces a cascade of maximum development after about 200 grms/cm^2 (Butcher and Messel,1960). After maximum development the initial energy has become divided between so many particles that ionisation loss becomes dominant and the cascade is absorbed. However further interactions in the nucleon cascade create additional uncharged pions which on decay, make good the loss of the electron-photon component. The electron component spreads laterally away from the core over a wide area mainly because of Coulomb scattering.

The "primary" nucleon emerging from the first interaction, together with any other highly energetic nucleons and charged pions produced, continue along the original direction of the primary forming a sharply collimated beam, and on average interact after a further 80 grms/cm^2 of atmosphere. For a vertically falling shower the atmosphere presents about 13 interaction mean free paths, and the most energetic of the secondary nucleons will produce the nuclear-active component observed at sea-level. The lower energy

nucleons will be absorbed through ionisation loss in the atmosphere.

Charged pions produced near the top of the atmosphere with energy less than about 10 Gev are more likely to decay than interact, the decay products being muons and neutrinos. The majority of muons produced in the atmosphere reach sea-level because of their relatively long lifetimes and their low cross-section for all interactions apart from ionisation loss. The large lateral spread of the muons is due mainly to the emission angle of the parent pions, although Coulomb scattering and deflections in the earth's magnetic field play a small part.

The electron-photon component at observational level is produced mainly in the last one or two nuclear interaction lengths. The attenuation of this component low in the atmosphere thus reflects the absorption of the nucleons. On the other hand even those muons formed from pions produced in the first interaction will generally reach the earth's surface.

Other processes in addition to those above must also take place within an EAS:- heavy meson and hyperon production; muon decay into electrons; knock-on electrons; direct pair production of electrons, by electrons and muons; nuclear

reactions including photonuclear reactions with pion production. Such processes however will do little to affect the structure of a shower at sea-level and can be ignored in an initial analysis (Greisen,1960).

1.4 Investigations on the Lateral Distribution of Charged Secondaries

Study of EAS generally involves detecting the simultaneous arrival at the earth's surface of groups of particles at two or more horizontally spaced detectors. The spacing of the detectors normally determines the size of shower that is most efficiently detected. Showers of size greater than 10^{10} secondaries have been detected at the MIT Volcano Ranch Station, (Linsley,1963). Nineteen scintillation detectors are arranged with spacings of 1 kilometre between units, the area thus covered being 8 sq.kilometres. An even larger array covering 100 sq.kilometres is being developed (McCusker et al.,1963).

The method of analysis used by such arrays involves sampling the density of secondaries at various points on the shower front and building up an empirical function representing the lateral distribution of the density as a function of the distance from the axis. This then enables the complete

structure of any EAS front to be deduced from a sample of density measurements. The core position and total number of particles (or size), N can then be determined.

Greisen (1960) derived an empirical equation for the density distribution of charged secondaries which fitted the average experimental distributions obtained up to that date for showers with sizes ranging from 2×10^3 — 2×10^9 particles. At distances less than 100 metres from the shower axis his expression is a close approximation to a theoretical expression derived by Kamata and Nishimura (1958) for a pure electron-photon cascade with s put equal to 1.25. The age parameter, s, used in cascade theory indicates the stage of development of a shower. At the start of the cascade s = 0; then it increases to 1 at maximum development, and reaches the value 2 when only one particle of the cascade remains. At distances greater than 100 metres from the axis, deviation from the electron-photon cascade theory must be expected as the muon component becomes significant.

The lateral structure of the electron component is substantially independent of size or altitude although it shows wide fluctuations. The typical value of s is 1.25, but a value of s = 1.0 is found to be the best fit for the largest air showers ($N > 10^8$ particles) at sea-level (Linsley et al.,

1962) and also for showers of $N \approx 10^7$ particles at 4,200 m. altitude [630 grms/cm^2.], (Hersil et al.,1962).

1.5 Energy of Primary Particles

The relationship between the size of a shower and the energy of the primary particle must come either from theoretical models (Ueda,1960) or from empirical estimates based on a detailed accounting of the average energy dissipated by the various components. The energy content of the various components has been estimated by Zatsepin et al. (1963). Table 1.1 lists estimated values for a shower of 3×10^5 particles at an altitude of 4,200 m. above sea-level, i.e. near the maximum development of the shower.

Ionisation loss	$3.4(\pm 1) \times 10^{14}$eV
Electron component	$0.75(\pm 0.14) \times 10^{14}$eV
Nuclear component	$0.3(^{+0.3}_{-0.2}) \times 10^{14}$eV
Muon component	$0.9(^{+0.9}_{-0.2}) \times 10^{14}$eV
Total Energy	$5.4(^{+2}_{-1.6}) \times 10^{14}$eV

Table 1.1 Energy content of shower of 3×10^5 particles at maximum development.

Over the size range 10^6-10^9 particles Clark et al.

(1963) assumes the formula

$$E_o = 2x10^9 N_{max} eV.$$

where E_o is the primary energy, and N_{max} the maximum size of a shower. Greisen (1960) estimates a value for the mean primary energy of vertical showers of size $5x10^5$ at sea-level to be

$$E = 15(\pm 3)x10^9 \text{ per electron.}$$

1.6 The Size Spectrum

The size spectrum of showers is the rate of arrival of showers of size N on unit area as a function of N. Results have been obtained at sea-level and at mountain altitudes over the range of sizes 10^4—10^9 particles. If the size spectrum is represented by a simple power law, the exponent shows a definite fairly sharp change at around $5x10^5$ particles. The change in slope is from -1.65 to -2.2 at mountain altitude. Glencross (1963) in reviewing the large amount of experimental evidence for this change also points out other changes in EAS structure at this shower size. He attempts to account for this "kink" by suggesting a variation of inelasticity of nuclear interactions but has to use an extreme fluctuation model of shower development (Cranshaw and Hillas,1960) to explain the observations.

Muira and Hasegawa (1962) suggest that a break in the

energy spectrum of the primaries is more likely to explain the change in the size spectrum exponent. Evidence in favour of this view is accumulating, e.g. studies on the lateral distributions of the three shower components (Chatterjee et al.,1963); variation with size of the ratio of single to multicore showers as found by the Sydney group (Winn et al.,1965); altitude variation of the EAS density spectrum (Swinson et al.,1965). Although by no means conclusive the results tend to indicate that showers around 10^6 are produced mainly by multinucleon primaries.

If it is assumed that the size spectrum does reflect accurately the energy spectrum of the primaries, Figure 1.1, shows the composite primary energy spectrum over the whole energy range 10^{10}-10^{20} eV.

Figure 1.1 indicates also evidence for another change of slope of the energy spectrum around 10^{17}-10^{18} eV. (Linsley, 1963). It is suggested that the inflection in the region 10^{15}-10^{17} eV marks the crossover between galactic and metagalactic cosmic rays (Section 1.9).

1.7 The Longitudinal Development

Investigation of the longitudinal development of a shower is complicated by the extreme difficulty of observing

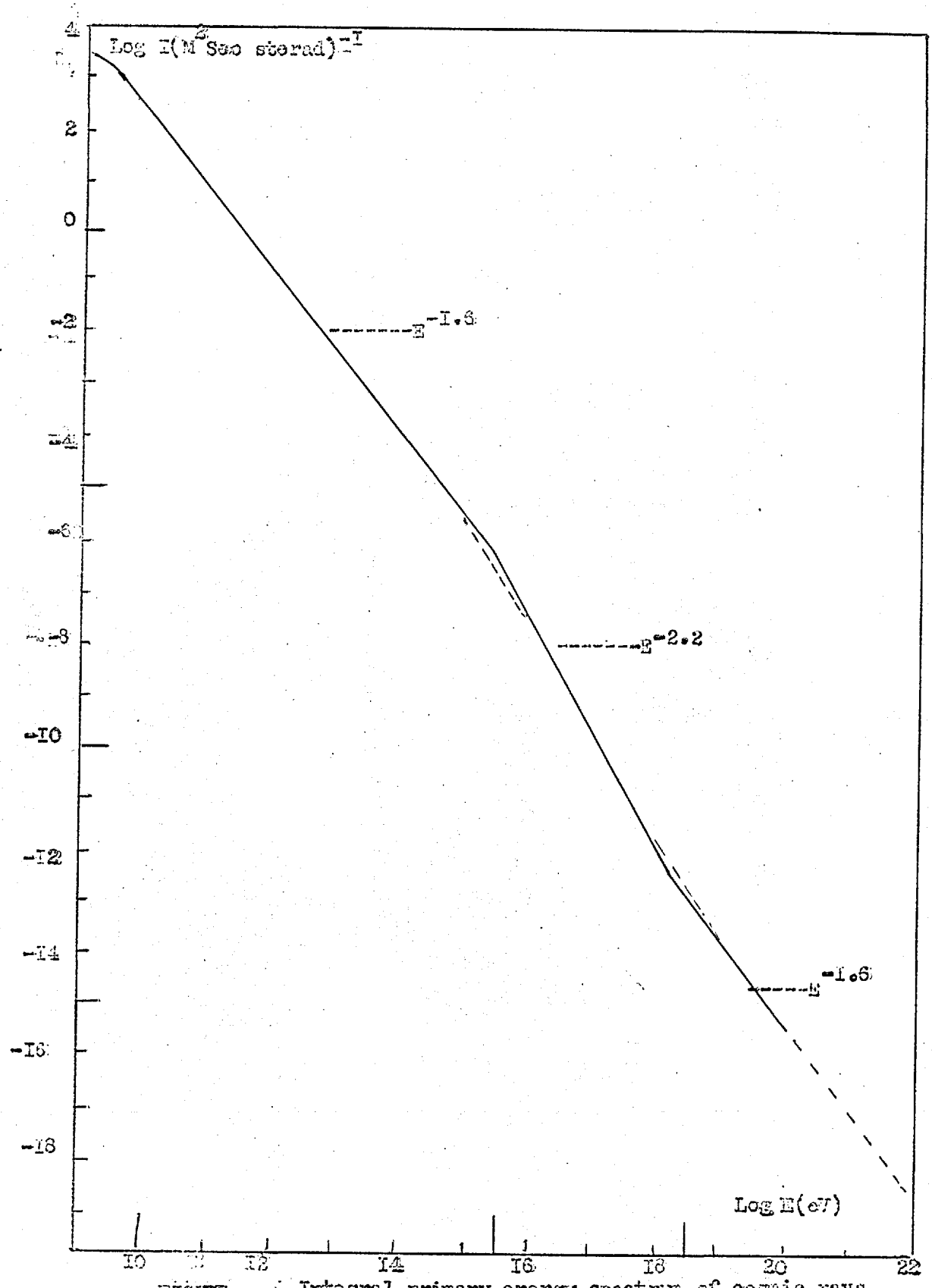


FIGURE I.1 Integral primary energy spectrum of cosmic rays

the same EAS at different stages of development. The study of the Cherenkov radiation produced by shower particles in the atmosphere provides one possible method. However results at optical wavelengths (e.g. Malos et al.,1962) are as yet rather imprecise.

The possibility of operating Cherenkov receivers in the ultra-violet regions of the spectrum is being investigated (Charman et al.,1965). In the spectral region 2,200—2,800Å the absorbing properties of the atmospheric ozone help to reduce undesirable stray light from the sources outside. Preliminary experiments are still being carried out.

More promising has been the discovery of radio pulses associated with EAS (Jelley et al.,1965). The study of radiation from EAS at radio wavelengths ($\lambda \sim 7$ metres) was stimulated by calculations of Askaryan (1962). He pointed out that a fractional excess of negative charge present in the shower may, at these longer wavelengths, give rise to a considerable enhancement of the intensity of the normal Cherenkov radiation because of mutual coherence, occuring when λ becomes comparable to the dimensions of the shower.

Radio pulses of short duration (< 0.15 μsec) have now been observed at Jodrell Bank at a frequency of 44 Mc/s ($\lambda = 6.8$ metres) in coincidence with EAS of size around 5×10^6 particles.

Although the mechanism for production of these radio pulses is by no means clear the discovery that the radiation is polarised dominantly East-West would suggest that the radiation is produced by charge separation in the Earth's magnetic field rather than by mutual coherence as proposed by Askaryan.

Experiments on radio Cherenkov pulses are continuing and an aerial array has now been set up at the British Universities Haverah Park array where more exact details of the EAS can be obtained than at Jodrell Bank.

A less ambitious way of investigating the longitudinal development of showers is by observing the change of mean shower rate at a given size with atmospheric depth. It is fairly well established that showers of size about 10^5 reach their maximum development at mountain altitudes ($\sim$ 600 grms/cm^2). The region of maximum will increase in depth with increasing shower size. At sea-level ($\sim$ 1000grms/cm^2) a shower around 10^9 particles will be at its full development.

The mean absorption length, Λ, of showers has been determined by observing the change in shower rate with atmospheric depth. Beyond the shower maximum the absorption can be defined as

$$\Lambda = \frac{-I dt}{dI}$$

where dI is the change in intensity of vertical showers in a given size range for a thickness dt of atmosphere.

It can be shown that the shower absorption length, Λ, is related to the average attenuation length of shower particles, λ, by the relation

$$\lambda = \gamma \Lambda$$

where γ is the exponent in the number spectrum of the EAS. This relation only holds if the fluctuations in shower development are not extreme. Bennett et al. (1962) have reviewed the values of λ derived by themselves and other workers as a function of size at sea-level. For $10^4 < N < 3 \times 10^6$ the particle absorption length is nearly constant, increasing slowly from about 180 to 220 grms/cm^2 and reflecting the dominating influence of the nuclear cascade ($\lambda_N \sim 200 \text{gm/cm}^2$).

For $10^7 < N < 10^{10}$ particles the value increases more rapidly with shower size as the region of maximum development is approached. The average attenuation length of the electron-photon cascade then becomes greater than that of the energy in the nuclear cascade.

A knowledge of the longitudinal development of individual showers would be very useful in assessing the importance of fluctuations in determining the features of the shower as detected on the earth's surface. It is hoped that either the

new radio technique or investigations of the optical Cherenkov radiation will enable such knowledge to be obtained.

1.8 Fluctuations in the Development of Showers

Various authors have examined the problem of fluctuations in the development of showers in detail (Miyake,1958;Ueda,1960; Clark et al.,1961;Linsley,1963A). The main factors contributing appear to be variations in the depth of the first few interactions and their dependance on the atomic weight of the primary. Statistical variations in the multiplicity, inelasticity, and angular distribution of particles produced in inter actions must also be considered. Such studies emphasise the difficulties of making accurate deductions about the primaries from observations on showers at a single depth in the atmosphere.

Experimentally it has been found that the fluctuations in the various components of the shower decrease with increase in shower size. A narrowing of the composition spectrum has been suggested as an explanation (Linsley and Scarsi,1962).

Since 1960 a great deal of attention has been devoted to utilising complex detector arrays to measure simultaneously several parameters of a single shower. The variation of these parameters between showers is yielding useful information about

shower development (e.g. Zatsepin et al.,1963;Chatterjee et al., 1963).

1.9 The Study of the Cores of EAS

The core of an extensive air shower contains the most energetic particles of the N-component and there is no doubt that these form the backbone of the EAS. The nucleonic component has been investigated experimentally using neutron counters, multiplate cloud chambers and ionisation chambers. Hodoscoped geiger counters under lead and scintillation transition chambers have also been used.

The small numbers of nucleons in a shower is such that results can only be obtained with large detectors and with results statistically averaged over many showers. For $N > 10^6$ particles experimental investigation of cores becomes extremely difficult. Study of the density and energy spectra of the nucleon component is however very important in building up a model of shower development.

The total number of N-particles in a shower as a function of shower size has been determined by a number of workers (Danilova and Nikolsky,1963;Chatterjee et al.,1963). It is found that

$$N_{n.a.}(>1\text{Gev}) \propto N^{0.7} \quad \text{at mountain altitudes}$$

Kameda et al.(1962) find that at sea-level

$$N_{n.a.}(>10\text{Gev}) \propto N^{1.0}$$

There is fairly general agreement among workers that the power exponent does rise with increase of minimum detection energy. Sitte (1963) points out that a non-linear relation is expected if it is assumed that the N-component originates in the nuclear interactions by a multiple production process.

The lateral distribution of nuclear-active particles is well represented by a function of the form

$$\rho_{n.a.} \sim e^{-r/r_0}$$

where r_0 varies from 1 to 3 metres in the size range 10^4-10^6 (Kameda et al.,1962). The N-component constitutes only about 1% of secondary particles near the core of a shower.

The composition of nuclear-active particles near air shower cores has not been determined at all accurately. Pete[s] (1963) points out that nucleons and antinucleons should occur with comparable frequency if it is generally true that a single energetic nucleon controls the nuclear cascade.

Evidence that such is the case comes from a study of the energy spectrum of the nuclear-active particles. The median energy of the most energetic nuclei in showers observed at 5,200 metres above sea-level is found to be about 2% of the primary energy. In one tenth of the cases it was as high as 20%. At sea-level the median energy is 0.1% and one tenth

have about 0.5% (Matano et al.,1963). Other workers obtain similar figures.

Several theories have been put forward to try to explain the general features of high energy nuclear collisions as inferred from interactions in balloon-borne emulsions and EAS. The theories must explain the following facts:-

1) The collision cross-section is very nearly constant at 40 mb. with variation of energy.
2) The average multiplicity increases very slowly with energy.
3) The energy and angular distributions of the secondaries suggest "fire-ball" formation; the secondaries seeming to emerge isotropically from two centres.
4) The inelasticity is less than 0.5.
5) The average transverse momentum of secondaries remains constant at around $\frac{1}{2}$ Gev/c.

Recent theoretical reviews have been made by Chernavsky and Feinberg (1963) and by Peters (1963A) but a comprehensive model to fit all the experimental facts has yet to be found.

The occurrence of multiple cores in showers has been observed by a number of workers. The most comprehensive investigation so far has been made by the Sydney group (Winn

et al.,1965). Using a 64 unit matrix of 0.41 sq.metre scintillators, used for a time as a 32 scintillator sandwich with lead absorber between, a detailed study of core structure was carried out.

In the size range $10^5 \leq N < 10^6$ particles the proportion of single cored to multiple cored showers observed fitted very closely that expected if it was assumed that single cores resulted from primary protons and multiple cores from multi-nucleon primaries. Above $N = 10^6$ particles however they observed only multiple cores. The suggestion is made that this is strong evidence for a change in composition of the primary radiation at an energy of about 3×10^{15} eV.

A 20 sq.metre spark chamber, with a much finer resolution than the Sydney scintillator matrix, has recently been set up in conjunction with the Tokyo EAS array to investigate the fine structure of cores (Shibata et al.,1965). Initial results indicate that a really detailed knowledge of the density structure of shower cores can now be obtained with such techniques.

1.10 The Muon Component of EAS

The study of the muon component in EAS is important for

a number of reasons. Although its mean density over the shower front is only 10% of the electron component it carries more of the total energy. The more energetic of the muons have undoubtedly been produced close to the initial interactions of the primary cosmic rays and should reflect the nature of the primary far more closely than the electron component seen at observation level.

The proportion of muons to electrons in showers should be dependent on the atomic number of the primary. In any case fluctuations in the ratio of the two components between showers is important in understanding the nature of the nuclear interactions. Showers with very few muons might be initiated by high energy primary gamma rays. A search for any anisotropy in arrival direction of these showers is being made.

The extensive lateral spreading of muons enable them to be detected over large distances from the core. Thus the extreme difficulty in detecting the nuclear-active component of showers of size greater than 10^7 particles is not encountered with the muon component.

1.10(a) The Lateral Density Distribution of Muons

The lateral distribution has been measured by a number

of workers both at sea-level and mountain altitudes for radial distances within 200 metres or so of the axis. The soft electron-photon component is generally absorbed out by a thickness of lead (or other efficient absorber), leaving the muon component to penetrate to the detector.

General agreement is obtained amongst the groups although the number of parameters involved, such as the minimum detection energy, the shower size range, and the altitude of observation often makes direct comparison difficult.

For distances greater than 200 metres from the core observations on muon density becomes more difficult. At these distances the density of particles becomes so low that large areas of shielded detector are necessary, and observation has to be confined to large showers ($>10^6$ particles).

The results obtained mainly by the MIT group (Clark et al.,1958) for distances over the range 10-1,000 metres from the axis were combined into an empirical equation by Greisen (1960):-

$$\rho_\mu(N,r) = 18\left(\frac{N}{10^6}\right)^{\frac{3}{4}} r^{-\frac{3}{4}}\left(1+\frac{r}{320}\right)^{-2.5} \quad \ldots\ldots 1.1$$

Here ρ_μ represents the number of muons per sq.metre of energy greater than 1 Gev at a distance r metres from the shower axis. Equation 1.1 indicates that only about half the muons lie within 300 metres of the core and that beyond 1,000 metres the density of muons becomes higher than that

of electrons.

Whilst equation 1.1 was based on fairly accurate experimental evidence below 200 metres from the core the amount of data available at larger distances was small and had rather large statistical errors present. Modifications might be expected in the light of further experimental results.

The spreading of the muons away from the core is primarily due to the ejection angle of the parent pions. The calculated mean deflections of muons arising from Coulomb scattering in the atmosphere are generally much smaller than the distance from the shower axis at observation level (Hillas,1965). The deflection of muons in showers by the earth's magnetic field has been calculated by a number of authors. An asymmetry in the radial distribution of muons is expected for showers approaching along the direction of the earth's field but the calculated effect is small. However a fairly large muon charge asymmetry should occur in certain regions of the shower front but this has not as yet been looked for.

Comparison of the experimental lateral distribution with theoretical cascade calculations (e.g.Hillas,1965) can bring light to bear on the relative roles of the competing

processes of interaction and decay of pions in the first few nuclear interactions. Although some pion decay occurs at all altitudes, muons will be mainly produced when the energy of the pions is sufficiently degraded for decay to compete successfully with interaction.

Calculations on the variation of the radius of curvature of the shower front with zenith angle (Dennis,1964) indicate that the mean height of production of muons is probably around 5 – 6 kilometres in close agreement with the theoretical calculations of Hillas. However earlier experiments attempting to measure the height of muon production by de Beer et al. (1962) indicate that quite a fraction are produced much higher than this.

1.10(b) Variation of N_μ with N

A number of workers have determined the way N_μ, the total number of muons in a shower varies with shower size, N. Agreement between different experiments is not very good, (see Table 5.1) but it is clear that the number of muons rises more slowly than the number of electrons. Greisen's equation 1.1 shows

$$N_\mu \propto N^{0.75}$$

The fact that the exponent is less than one indicates again the competition between pion interaction and decay. The higher the energy of the primary the longer it will take the product pions to be reduced to an energy necessary for decay to become dominant. Charged pions that interact rather than decay can be expected to produce roughly equal numbers of positive, negative and uncharged pions. The neutral pions will then decay initiating electron-photon cascades. Thus as the primary energy increases the pions at a given level have a higher chance of interacting rather than decaying into muons and therefore the proportion of muons falls.

Any sharp change in the muon/electron ratio with shower size should superimpose itself on the general trend discussed above. It should thus be possible by accurately measuring the variation of N_μ with N to observe any fairly sharp change in composition as is being suggested occurs around 3×10^{15} eV.

1.10(c) Energy Spectrum of Muons

The energy spectrum of muons in EAS has been determined by running large area shielded magnetic spectrographs in conjunction with detector arrays (Kazarov and Andronikashvili,

1957;Bennett et al.,1962;Rochester et al.,1965). At sea-level close to the core of a shower ($r \lesssim 100$ metres) there are very few muons with energy less than 5 Gev. The integral spectrum however sharply steepens as the energy increases beyond 10 Gev up to the highest energies measurable (~ 50 Gev).

As the core distance increases the muon mean energy decreases so that at 500 metres about half the muons have energy less than 2 Gev.

Bennett et al. (1962) find the mean energy of muons in EAS to be about 7 Gev and the total muon energy to be given by

$$E_\mu = 0.9 \times 10^{15} \left(\frac{N_e}{10^5}\right)^{0.75} \text{ eV}.$$

1.10(d) Charge Ratio of Muons in EAS

Although unassociated muons show a slight positive excess in numbers, muons in EAS appear to exhibit charge symmetry (Bennett et al.,1962;Rochester et al.,1965). The degree of charge symmetry among muons in showers might imply that muon production via K-meson decay is negligible in comparison with pion decay.

1.10(e) Fluctuations in Muon Density

The study of fluctuations in muon density is hindered by the large area of detector needed to obtain good statistical accuracy. However there is strong experimental evidence (Hasegawa et al.,1962;Chatterjee et al.,1963) that the number of muons does fluctuate considerably with respect to the total number of particles.

The causes of the fluctuations must be:-

(a) The fluctuations in the height of the first interaction.

(b) The mass spectrum of the primaries.

(c) Fluctuations in the shower development process arising from variation in the nuclear interaction processes.

The relative importance of these and how much one can infer about the primaries from a detailed study of fluctuations remains an open question.

1.10(f) Evidence for "Muon-Less" Showers

The existence of EAS containing very few muons (about 1/30th to 1/100th) of the mean has been established at Chacaltaya (Suga et al.,1963;Toyoda et al.,1965). The relative frequency appears to be about 0.02% for showers

in the energy range 10^{15}eV–10^{16}eV. It is suggested that these may be due to primary gamma rays. As gamma rays would not be affected by galactic magnetic fields, proof that these are genuine rather than the result of extreme fluctuations will come from establishing an anisotropy in their arrival directions. A significant peak in right ascension (between 200°-220°) is reported but the result is by no means conclusive.

1.10(g) "Muon-Rich" Showers

An attempt has also been made to look for anisotropy in muon-rich showers. Such a search was initiated on the assumption that these may be produced by multi-nucleon primaries. This is a consequence of the non-linear relationship between N_{μ} and N (see Chapter 5). An apparent variation in the distribution of the showers of size 10^6 in right ascension has been reported (Mantano et al.,1963) but again the results are not really statistically significant.

1.10(h) Conclusion

Studies of the muon component in recent years has greatly increased the detailed knowledge of EAS structure.

How much one can infer about the primary from the muon content of a shower is however far from clear.

1.11 The Composition of High Energy Primaries

Protons and the nuclei of heavier elements form the bulk of cosmic rays reaching the vicinity of the earth. Experimental investigations on the composition has been carried out chiefly using photographic emulsions borne in balloons at high altitude.

Although there is some scatter in the available data it appears that the chemical composition of the nuclear component is roughly as given in Table 1.2(p.31) up to energies at least around 10^{14} eV. Also shown is the average chemical composition of the universe as it is found in stars and meteorites. It is clear that the primary cosmic rays contain relatively more light nuclei (L) and heavy nuclei (H) than are present on the average in the universe.

A small fraction ($\sim$1%) of electrons have been detected amongst low energy cosmic rays (Meyer,1965). The primary radiation is also expected to contain fluxes of gamma rays and neutrinos but there is little experimental evidence to date on these components (e.g. Oda,1965).

GROUP OF NUCLEI	Z	% IN COSMIC RAYS	% IN UNIVERSE
p	1	93%	91%
He	2	6.6%	9%
L	3-5	0.13%	3×10^{-7}%
M	6-9	0.40%	0.09%
H	≥ 10	0.13%	0.03%
VH	≥ 20	0.05%	0.002%

Table 1.2 Composition of Cosmic Rays.

For energies above 10^{14} eV evidence for the composition spectrum is not very strong. From emulsion studies there is no indication at 10^{14} eV per particle that any change from lower energies might occur. Moreover comparison of theoretical cascade calculations and experimental results of intensity and momentum spectra at sea-level also indicate that heavy particles are present up to 10^{15} eV.

It is important to point out that in the energy range of extensive air showers the observed energy spectrum of the primary particles no longer relates to the energy per nucleon but to the total energy of the particles causing the showers. If the composition of EAS primaries remains unchanged from

that shown in Table 1.2 the relative content of protons with a given total nucleus energy is about 49%. The abundance of single nucleon and multi-nucleon primaries should then be almost the same in any primary energy interval.

There is fairly strong evidence from the studies of the Sydney group on multi-cored showers (Winn et al.,1965) that very few protons exist in the primary energy range around 10^{16} eV. Several other features of air showers in this range tend to add weight to this conclusion.

Observations on EAS produced by primaries of around 10^{18} eV energy suggest that protons may again dominate at this energy (Linsley,1963).

It is necessary to study in detail a parameter of showers which is sensitive to the nature of the primary producing it. However it is not certain as yet whether the muon component, core structure or degree of fluctuations are true indications or are influenced more by variations in shower development.

1.12 Time Variations and Isotropy of EAS Primaries

Many types of variation in the intensity of cosmic rays are observed at low energies ($\sim 10^{9}$ eV), associated in

particular with activity on the sun. However at higher energies ($>10^{14}$ eV) the intensity of cosmic radiation is remarkable for its constancy.

Two methods are used to try to detect preferential arrival directions of primaries. At lower energies, around 10^{14}-10^{15} eV, the flux of EAS on small detector arrays is quite high ($\sim$50 per hour). This enables the rate of recording of showers to be analysed with respect to sidereal time with a high degree of statistical accuracy. However the high rate is offset by the low directional resolution achieved and the large corrections needed to eliminate atmospheric effects (e.g. Jones,1965).

For higher energies ($>10^{15}$ eV) it is possible to pin-point the direction of arrival of the primary by determining accurately the direction of the axis of the EAS produced. These can then be plotted on celestial co-ordinates to search for clustering.

If the anisotropy is defined as

$$A = \frac{I_{max} - I_{min}}{I_{max} + I_{min}}$$

where I_{max} is the maximum intensity recorded and I_{min} the minimum, upper limits can be placed on A for various primary energies;

$$A \leq 0.1\% \text{ for } E \sim 10^{14} \text{ eV}.$$

$A \leq 1\%$ for $E \sim 10^{16}$ eV.

$A \leq 3\%$ for $E \sim 10^{17}$ eV.

This extreme isotropy, even for the highest energy primaries makes the problem of the origin of these particles very difficult to solve. A general stirring up in the turbulent magnetic fields in galactic space is thought to be the main reason for the high degree of isotropy observed.

An asymmetry in the arrival directions of primary gamma-rays of energy around 10^{14} – 10^{16} eV might be expected. These could be produced by neutral pions from the collisions of charged cosmic rays and the hydrogen in the universe, the distribution of which might not be uniform. However statistics on the anisotropy of "muon-less" showers (Section 1.10(f) are not yet good enough to come to any conclusion.

Evidence in favour of an anisotropy in "muon-rich" showers is also not very strong /Section 1.10(g)/

Recent attempts have been made to find evidence for some anisotropy of primaries of energy greater than 10^{17} eV (Dennis and Wilson,1963;Linsley,1963). No significant effect has yet been found but results are still accumulating.

1.13 The Origin of Cosmic Rays

Theories of the origin of cosmic rays must account for the fact that the total energy density in the neighbourhood of the earth is about 1 eV per c.c, If this is the same throughout the whole Galaxy the total cosmic ray energy in the Galaxy is about 10^{56} ergs. If a mean lifetime for cosmic rays of around 3×10^{8} years is assumed then the total power output from the sources must be around 10^{40} ergs/sec. In addition meteoritic data indicate that the cosmic ray intensity has not changed appreciably over the last few hundred million years.

Any theory of the origin which suggests that the cosmic rays are confined by magnetic fields to a smaller region than the Galaxy, e.g. the solar system, falls down on power output as the containment time would be far less than 10^{8} years. Moreover direct observations of solar cosmic rays show that they have neither the energy spectrum of chemical composition of the galactic cosmic radiation. In addition very high energy particles ($>10^{14}$ eV) could not be contained inside such a region for sufficient time to render them isotropic.

The total power output of ordinary stars, magnetic stars or even high power stars like T Tauri, falls far short of what is required. However supernovae and probably the

more numerous, but much less powerful, novae appear to be quite capable of producing at least 10^{40} ergs/sec, the required output. Moreover it seems possible that particles of energy as high as 10^{17} eV/nucleon could be produced inside the shells of the supernovae.

Ginzburg and Syrovatskii (1964) have therefore proposed that the original cosmic rays are formed basically in supernovae shells in which they are accelerated to high energies. They are ejected from the source in such a way that the original cosmic rays are preponderantly heavy nuclei. They then execute a random walk from their source to the earth, being scattered by the magnetic fields of the interstellar gas.

In traversing space the nuclei will lose energy by ionisation and nuclear interactions. Heavy nuclei are split to lighter particles by collision with the interstellar hydrogen changing the chemical composition to that of the observed primary radiation.

Scattering of the particles by inhomogeneities in the galactic magnetic fields has a mean free path of a few parsecs (1 parsec = 3.3 light years). As the nearest supernova is several hundred parsecs from the earth isotropy in arrival directions is understandable on the supernovae theory.

There is a general diffusion of cosmic rays out of the Galaxy caused by scattering leading to the mean lifetime of around 3×10^8 years assumed above.

Cosmic ray acceleration in interstellar space, for example by the Fermi mechanism, cannot account for more than a factor of ten up on the energy of a primary at its source. Any galactic theory of cosmic rays cannot therefore explain the presence of protons with energy above 10^{18} eV. They can neither be accelerated to such energies in supernovae, nor be contained inside the Galaxy long enough for a measureable intensity to be built up. The Larmor radius for a relativistic particle of energy E and charge Ze in a field of H gauss is given by

$$r = \frac{E}{300HZ} \qquad \ldots . \quad 1.2$$

For a proton with $E = 10^{18}$ eV and assuming a galactic magnetic field of around 10^{-6} gauss, $r = 3 \times 10^{21}$ cm. (cf. $\sim 10^{21}$ cm. for radius of Galaxy).

Morrison et al.(1954) conclude that a marked fall off in the number of particles in the radiation should occur at an energy of about 10^{15}-10^{16} eV owing to escape from the Galaxy. It seems that metagalactic sources must be responsible for the production of the highest energy primaries.

Certain optical galaxies appear to be in violent eruption. Burbidge (1963) calculates the cosmic ray energy density one might expect from such events in metagalactic space and arrives at a figure of around 10^{-13} ergs/cm^3 (cf. 10^{-12} ergs/cm^3 inside the Galaxy).

The recent discovery of quasi-stellar radio sources and quasi-stellar galaxies opens up the field considerably (Burbidge and Burbidge, 1965). There is without doubt enough power output from these objects for them to constitute strong sources of cosmic radiation. Until more is known about their sources of energy and general properties, their position in the overall solution of the origin of cosmic rays must remain open.

The theory that the region of primary energy 10^{15}-10^{17}eV is a transition region from galatic cosmic rays to metagalactic particles has received some support during the last two years or so. There seems to be a fair amount of evidence for an unusually high ratio of heavy nuclei in this region. It has been suggested that above 10^{15} eV per nucleon the galactic magnetic folds can no longer contain the cosmic rays so that as the total energy of the primary increases the light elements successively escape from the Galaxy. The escape energy is charge dependent (equation 1.2) so that heavy multicharged nuclei would be most abundant inside the

Galaxy in the energy range 10^{16}-10^{17} eV.

The presence of protons around 10^{18} eV could indicate the merging of the galactic and metagalactic fluxes with the latter dominating above 10^{18} eV per particle. However this simple picture will probably need considerable adjustment in the light of future work.

1.14 Scope of the Present Work

The Haverah Park EAS array of detectors is at present detecting showers produced by primaries of energy around 10^{17} eV. The results presented in this thesis are initial results obtained by running muon density detectors in conjunction with this array. It is hoped that the variation of muon content of showers, in particular with size, around this primary energy will give a clear indication of the composition of the primaries. Also construction of the lateral distribution of the muon component is undertaken in order to learn more about the detailed development of EAS in the atmosphere.

CHAPTER 2

THE DESIGN OF MUON DETECTORS AT HAVERAH PARK

2.1 The Haverah Park EAS Array

The Joint Universities' Extensive Air Shower Array was set up in 1962 for the purpose of studying primary cosmic rays of energy around 10^{17}-10^{18} eV by means of the EAS they produce near sea-level. The site chosen for the experiment is at Haverah Park, Yorkshire, and at the time of writing, the Universities of Leeds and Durham, and Imperial College, London, are in active collaboration there. The main experimental set-up has been described in detail (Lillicrap,1963; Turver,1963;Dennis,1964).

The principal array of detectors consists of four large area water Cherenkov detectors spaced in a triangular arrangement with the central station at the centroid of the other three (Figure 2.1). Each of the outside stations lies 500 metres from the central detector. The 34 sq.metres of detector area at each station are made up of 15 units. Each unit is self-contained consisting of a galvanised iron tank, 4'x6' in cross-sectional area, and 4' deep, lined inside with sheets of white diffusing P.V.C. (I.C.I.,Darvic) and filled with water. A photomultiplier dipping into the water

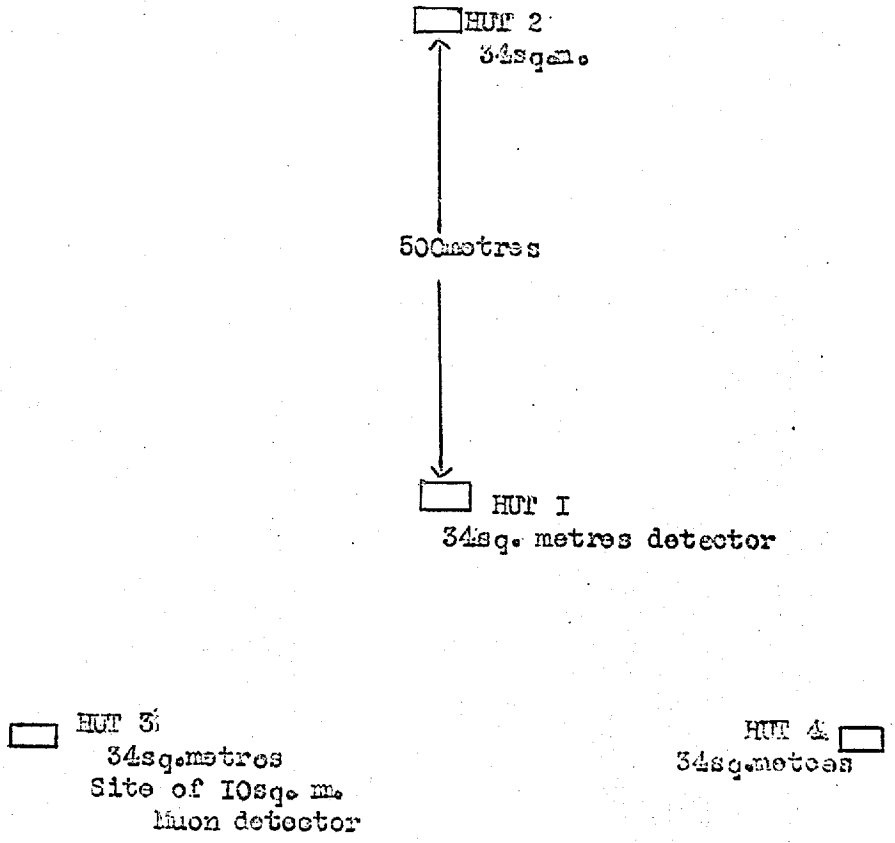


FIGURE 2.I. Plan of 500m. array at Haverah Park

converts some of the Cherenkov radiation emitted by relativistic charged particles traversing the detector into electrical pulses. The pulses from the fifteen units at each outside station are added together and then transmitted through underground cables to the central station. Here the pulses from each station are displayed separately on the cathode ray tubes of a four-fold oscilloscope.

The common time-base circuit of the four tubes is only triggered when densities greater than ten particles per station are detected in coincidence at the central station and two of the outer stations. The pulse heights from the four stations are then recorded on film. The pulse heights are related to an equivalent number of vertical muons through the detector by a standard calibration procedure. Blanking pulses exactly 6 microsecs. apart on each time-base enable the small time differences in arrival of the shower front at the four stations to be measured.

Under the chosen triggering conditions the array records about forty events in every twenty-four hours. From these the arrival of large EAS on the array can be observed and in the majority of cases their size, core position and direction of arrival can be determined to a fair degree of accuracy, (Dennis,1964). The distribution in size of showers triggering the system is shown in Figure 2.2.

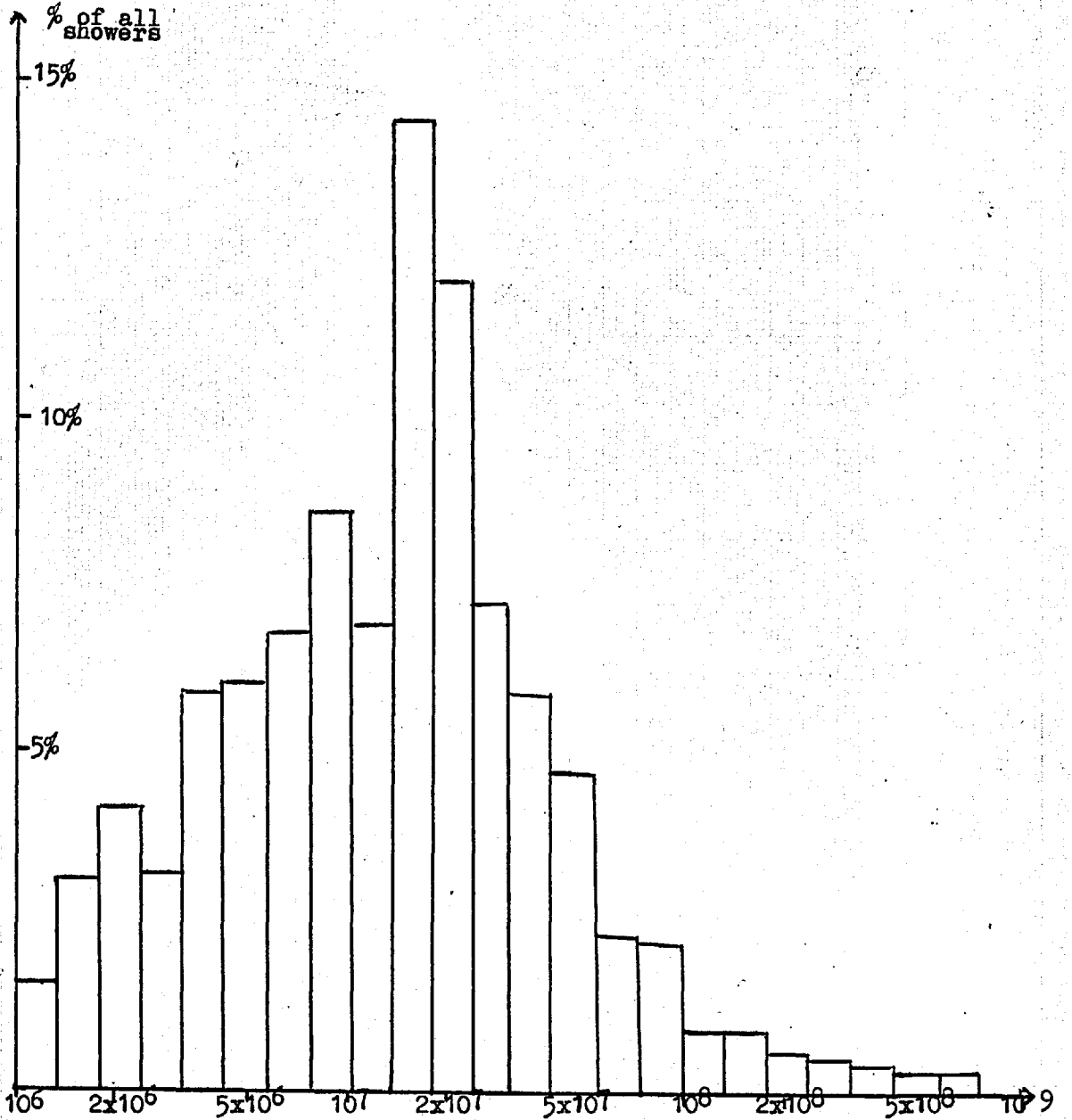


FIGURE 2.2. Relative frequency of showers of size N triggering main array at Haverah Park.

2.2 Muon Density Detectors

The Cherenkov water tanks are sensitive to all types of relativistic charged particles. To study the muon component in detail it is necessary to absorb out completely the "soft" electron-photon component from the EAS. As only about a tenth of all shower particles are muons it would require prohibitively large areas of shielded detector to determine the gross features of a shower from its muons alone. Invariably unshielded detectors are relied on to determine the size, position and direction of a shower and the muon component is then sampled at one or more points on the shower front.

The purpose of the present work is to investigate the muon lateral density distribution in showers of size 10^7-10^8 particles. To do this a large area shielded detector was constructed. Lead blocks with their high density and high atomic number (radiation length for electrons in lead is about 5.8 grms/cm^2.) are used as an efficient and convenient means of shielding.

2.3 The Siting of the Detector

Previous workers have shown that the proportion of muons to all particles in showers increases with distance from the core, ranging, at sea-level, from a few per cent. close in,

to 50% or so at 1,000 metres from the axis (Greisen,1956). Considering this variation and also the availability of space on site the muon detector was placed in one of the outlying stations. The range of core distances covered and the relative frequency of occurence of events at these distances is shown in Figure 2.3.

A lateral density distribution in the range 300-1,000 m. from the shower axis could be expected. This range covers the region where the muons make an increasingly significant contribution to the density of all secondary particles.

Because of accessibility by a tarmac road Hut 3 of the site was chosen for the experiment.

2.4 Area Considerations

To reduce statistical errors it was desirable to have the largest possible area of muon density detector. On the other hand the high cost of lead absorber and the amount of space available at the station meant a compromise had to be made. The criterion taken was the area of detector needed to record on average at least one muon per shower. Over the range 300-1,000 metres about one in three of the secondary particles are muons. At least two-thirds of all showers triggering the array give greater than ten particles at Hut 3. Such an event comes from a density of three particles per

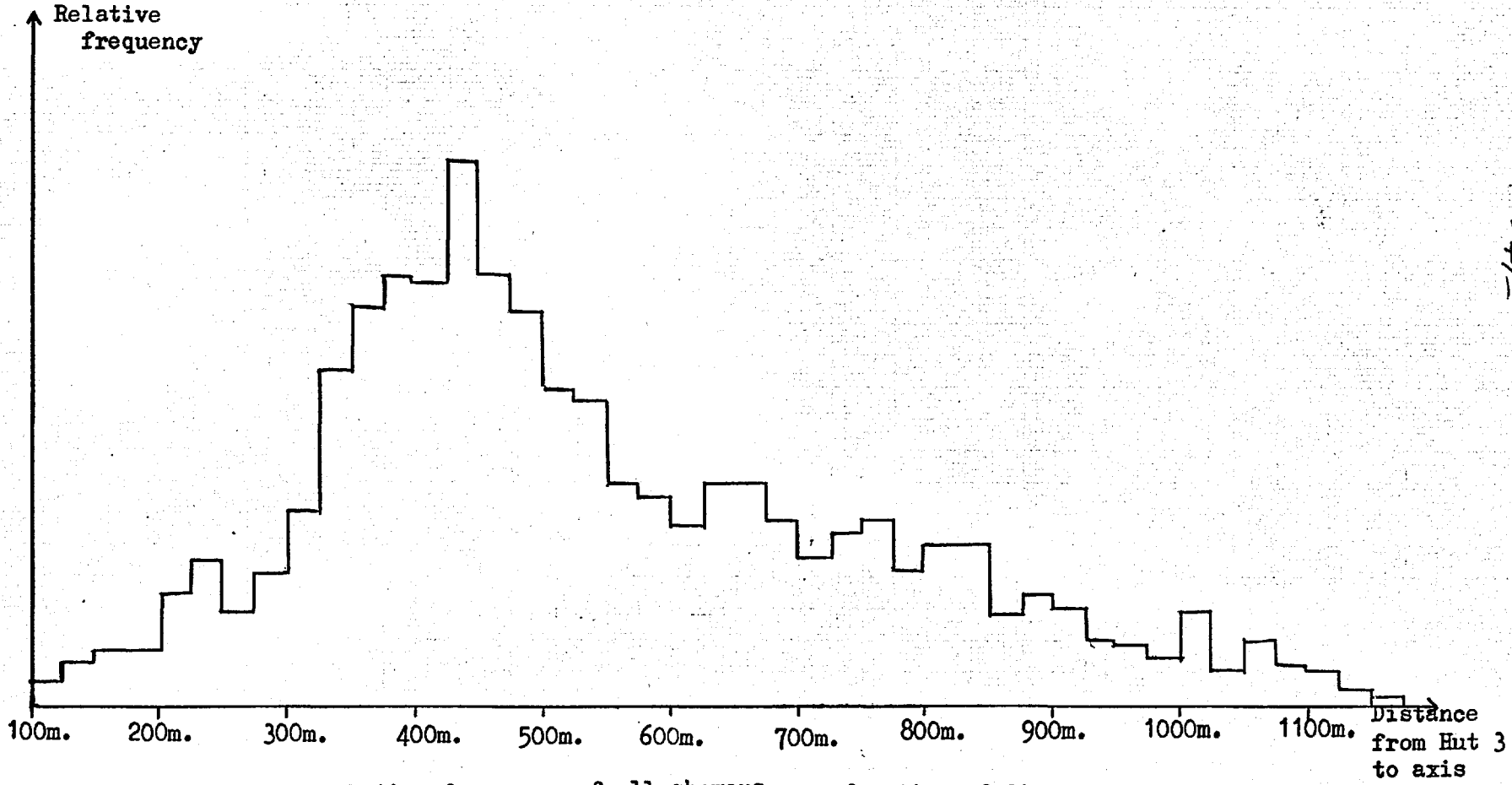


FIGURE 2.3. Plot of relative frequency of all showers as a function of distance of axis from Hut 3

10 sq. metres of which generally one is a muon. Ten sq. mtrs. of muon detector would therefore be a workable area.

2.5 Detector Details

The muon detector now in use consists of four units, each having 2.5 sq.metres of active area. Each unit is based on the design of large area liquid scintillator detectors developed by Dr. J. C. Barton for his work on muon interaction underground at Holborn in London (Barton et al.,1962).

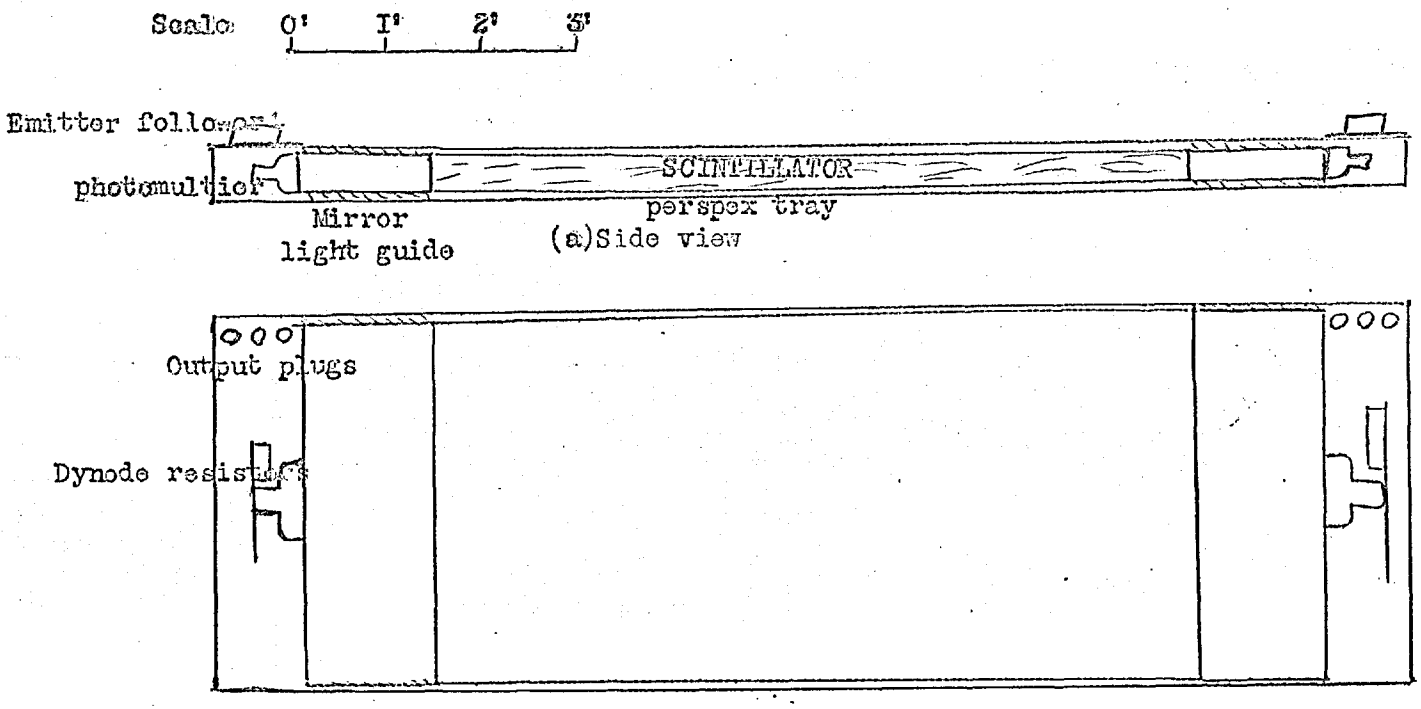
Medicinal liquid paraffin (B.P.) with 0.6 grms/litre of p-terphenyl and 0.006 grms/litre of POPOP as solutes is used as a scintillator.

In each unit approximately 60 gallons of scintillator mixture are contained in an open perspex tray 8'x3'6" in area by 4" deep. This is supported horizontally on ten $\frac{1}{4}$" diameter duralumin rods (to ensure a perspex to air interface for total internal reflection of the scintillation light), inside a light tight wooden box 12'6" long by 7" high. The inside of the box is painted black to reduce spurious reflections.

The tray is extended at both ends by a hollow rectangular mirror light guides, 16" long. The mirrors are thin, back silvered, and are supported on a wooden framework.

The lid of the box leaves the last 11" at each end open for insertion of the photomultiplier and associated

FIGURE 2.4. Liquid paraffin scintillator detector; 2.5 sq. metres



head unit. The photomultipliers used are E.M.I. 9530A with 5" diameter photocathodes. These are positioned, one at either end of the detector looking horizontally along the centre of the detector in contact with the light guides. The photomultipliers are mounted on duralumin plates extending the full width of the detector. The pulses from the anode of the photomultiplier are fed into an emitter follower on top of the plate and matched into a 68 ohm cable (Uniradio 39) through a co-axial plug. Supply E.H.T. and L.T. (-20v) are also fed in through plugs in the plate.

The dynode chain series resistor and emitter follower circuit, shown in Figure 2.5, is a direct copy of that used in the Cherenkov detectors. The emitter follower's overall gain of 0.5 is stable against normal temperature variations and linear from a few millivolts up to voltages in excess of one volt output.

The response of each unit was taken as the added pulse from the two photomultiplier tubes after their gains had been carefully balanced by suitably adjusting the E.H.T. voltage applied to each tube.

2.6 Design Considerations

The reasons for adopting the above design can be discussed under separate headings:-

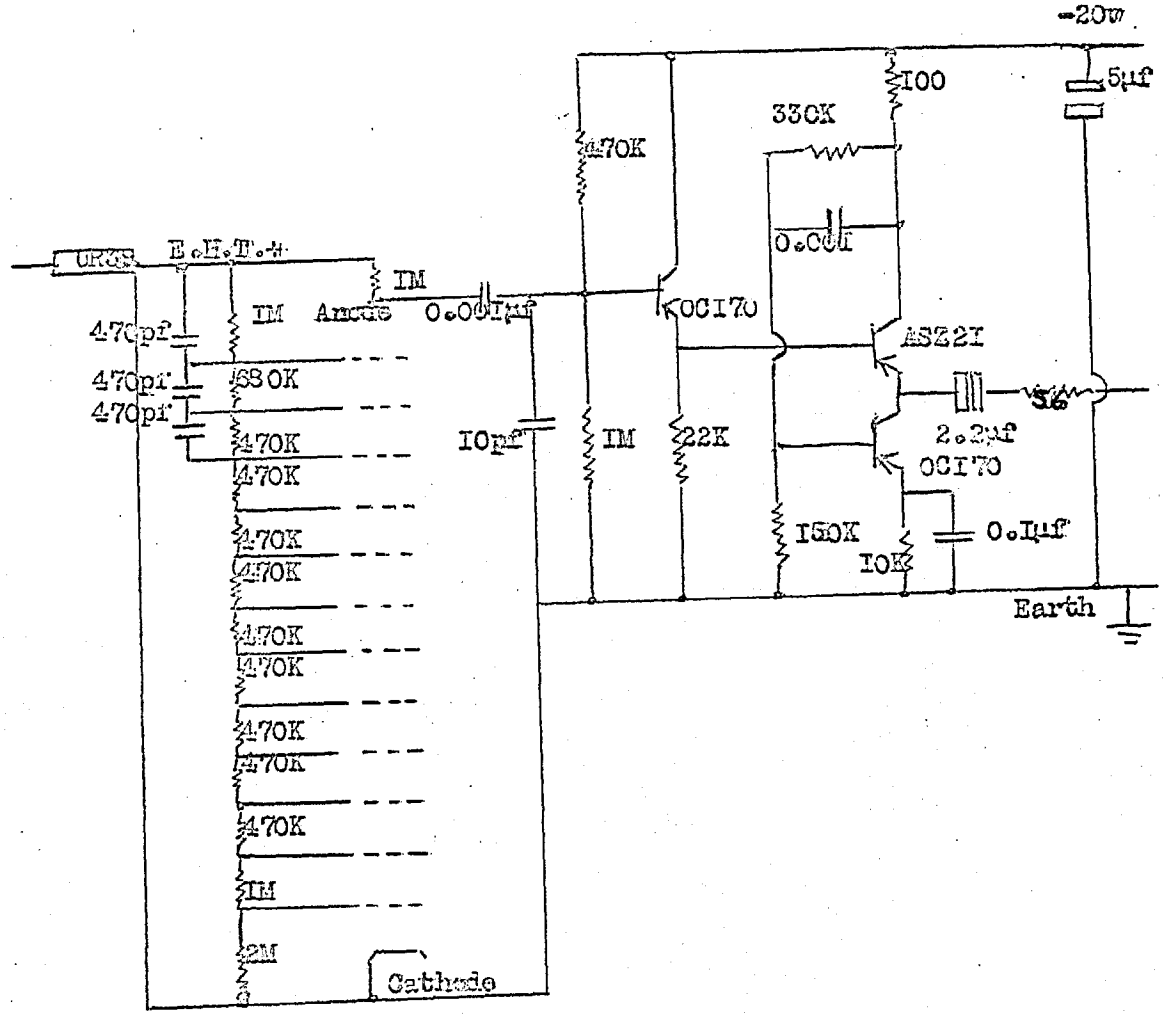


FIGURE 2.5 The head unit circuit

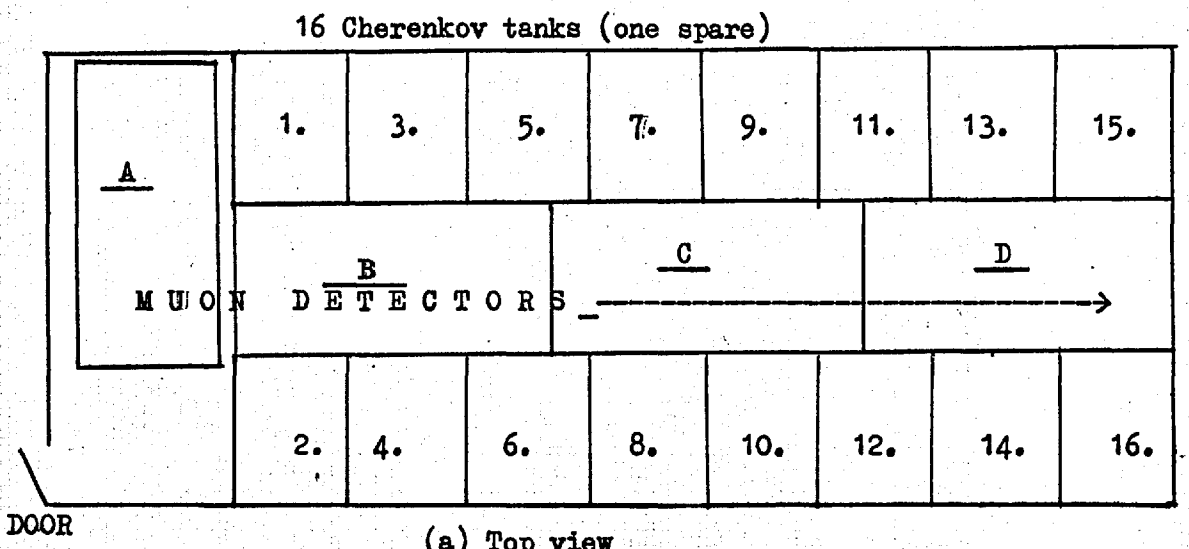
(a) Geometry:

Figure 2.6 shows a plan of Hut 3, the site of the detectors. To introduce muon detectors with their accompanying shielding down the centre of the shed without causing a significant scattering of the secondary particles into the main array tanks, required a particle detector of extremely thin geometry. With the present design the overall height of detector plus shielding is kept below 1'6".

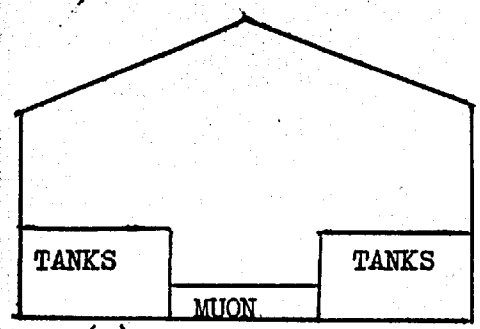
The mean response of Hut 3 to events triggering the array during the first six months after installation of the muon detector has been calculated. Within the accuracy of calibration the mean density at Hut 3 was found to be the same as the other two outside stations. This is taken as sufficient proof that any scattering occuring is tolerably small.

(b) Optics and Uniformity of Response:

The arrangement with a large rectangular slab of scintillator, viewed from its shortest sides, relies on total internal reflection at the perspex to air, and paraffin to air, interfaces. Perspex and liquid paraffin have very nearly the same refractive index (1.49) and can thus be regarded as an optically homogeneous block. Brini et al.(1955) show that this is the best arrangement for uniformity over a



(a) Top view



(B) End view

Scale 0' 3' 6' 9' 12'

FIGURE 2.6. Plan of Hut 3

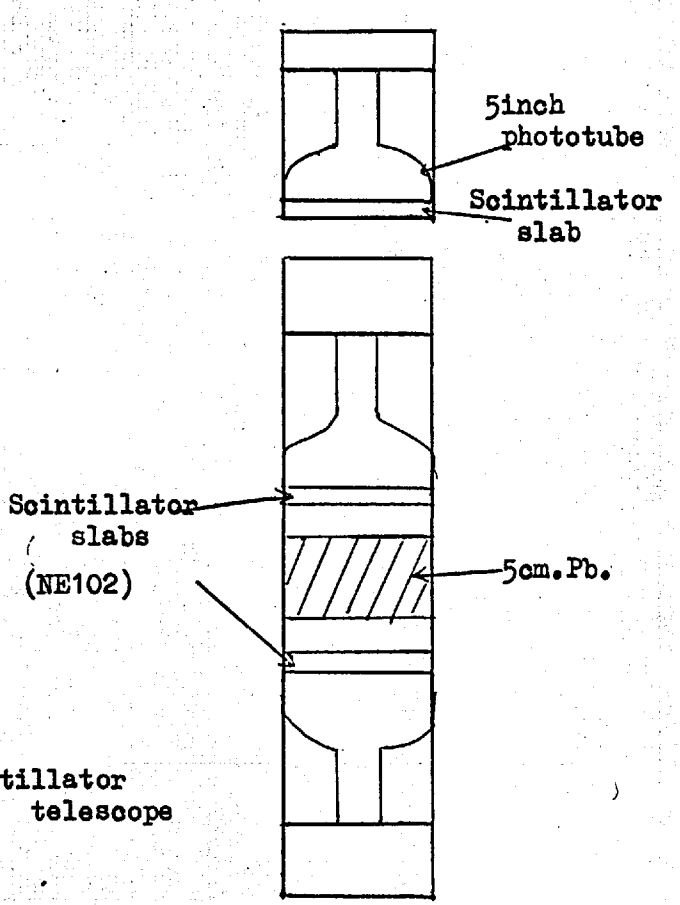


FIGURE 2.7. Scintillator telescope

large area as well as producing a good light collection efficiency (Appendix I).

The plane mirror rectangular light guides were adopted for their simplicity of construction. They replace the perspex tray extension guides filled with pure medicinal paraffin and eliminate the difficult optical coupling and leak-proof gasket seals of the original design (Barnaby and Barton,1960). To ensure good uniformity their length should be comparable with the width of the tray. The 16" long guides used were the longest convenient to the space available. The use of mirror light guides sacrifices little resolution for simplicity of design. They also eliminate any spurious pulses of Cherenkov radiation due to passage of particles through the liquid light guides.

The active area of each unit, 2.5 sq. metres, is a factor of two up on any other detector previously built of a similar design. The reason for going to such a large area per unit were:-

1) The average cost per sq. metre of detector becomes much less.
2) The amount of lead shielding necessary per sq.m. is considerably reduced.
3) It was necessary to make full use of the available space in Hut 3.

4) Considerable reduction is achieved in the amount of associated electronic circuits.

The increased size does not interfere too much with the uniformity of response over the detector. This was to be expected from some recent measurements by Barton et al.(1964) which showed the effective attenuation length of scintillation light in such a mixture to be 195 cm. Tests on uniformity are described in 2.8.

(c) Choice of Scintillator:

Medicinal liquid paraffin (B.P.) containing p-terphenyl and POPOP as solutes was used as the scintillator following the work of Barton (Barton et al.,1962;1964). Although paraffin is less efficient than the more usual organic liquid scintillators such as toluene (about $\frac{1}{8}$th response) the advantages of cheapness and high flash point (229°C) are most important, particularly in view of the large quantities to be used. Its advantages over plastic scintillator slabs are mainly those of cost. Also it had become known that several workers have found distinct discolouring of plastic scintillators with age. In view of the long path lengths involved this could produce a serious loss of uniformity in such a large area scintillator.

The concentration of 0.6 grms/litre of p-terphenyl was used because of the trouble that could be caused on cold nights when a greater concentration might become oversaturated and crystallise out. The loss of efficiency (light output/cm. track length) from the original recipe of 0.8 grms/litre is about 20%.

Several workers have succeeded in improving the efficiency of cheap scintillators. Shellsol A and Dekalin have both been added to liquid paraffin with good effect (Wilson et al.,1963;Barton et al.,1964). Meyer et al.(1963) have added PPO and naphthalene. Although efficiency is increased in these cases the effective attenuation length of light invariably goes down, in some cases considerably. Also the stability of such mixtures has not yet been proven. In view of the importance of the latter two properties it was decided to use the original mixture for the muon detector.

(d) Liquid paraffin as a Scintillator:

The scintillation process that takes place may be briefly described as follows. A charged particle passing through the scintillator will excite the solvent molecules along its path by raising their less energetically bound electrons above the ground state. Some of the excitation

energy is transferred to the primary solute (p-terphenyl) molecules by collisions and becomes "trapped". Emission then occurs. POPOP as secondary solute or spectrum shifter absorbs the emission and/or trapped energy from the p-terphenyl and emits its own characteristic, longer wavelength spectrum. The advantages of the secondary solute are to bring the emission spectrum more closely into the spectral sensitivity of the photomultiplier and also increase the mean free path of transmission through the scintillator (Brooks,1956).

The scintillation pulses from the detector have very fast rise times ($\lesssim 10^{-8}$sec.) and decay times of around 8 microsecs. determined by the emitter follower circuit. A high energy muon passing through the detector will lose about 2 Mev/grm.cm^{-2} by ionisation. The phosphor will therefore absorb about 16 Mev from a vertical penetrating muon. About 1% of this will reach the photocathode surface in the form of photons.

2.7 Calibration and Single Particle Pulse Height Distribution

Calibration of the detector in terms of mV/particle output was carried out in the standard manner of finding the mean response to vertical cosmic ray muons. It was essential first to adjust the E.H.T. on the two photomultipliers so

that the gain of each was the same. This was done by feeding each into a discriminator and counting the rate of pulses from cosmic ray secondaries above a fixed discrimination level. This level was equivalent to about two particles passing simultaneously through the detector leading to count rates of about 1,000 per minute with good statistical accuracy over a few minutes. The E.H.T. voltages were adjusted until the counting rates were within 5%, showing the gains to be within 2%. As a check the rates were also compared at a higher discrimination level.

Nearly vertical cosmic ray muons were selected by placing a muon telescope over the centre of the detector. The telescope was made in two units (Fig.2.7). One contained two slabs of plastic scintillator (6" diameter by $\frac{1}{4}$" thick) separated by 5 cm. of lead. The slabs were viewed by 5" photomultipliers. The other unit contained a single slab and photomultiplier.

Initially one unit was placed below the detector and the other above to ensure that muons went right through. When a muon passed through the telescope the three-fold coincidence obtained triggered an oscilloscope time-base. The added photomultiplier output pulses were applied to the Y-plates through a suitable delay. The mean pulse height in millivolts was taken as the mean pulse height per vertical muon through the detector, with corrections applied due to non-uniformity

and angular spread of the particles.

Placing both units on top of the detector showed no appreciable change in the mean. This was an essential arrangement when the detector was laid on the floor under lead shielding.

The detector could also be calibrated by using the telescope coincidence trigger to gate a multichannel pulse height analyser to which the detector output was connected. A single particle pulse height distribution from the detector using the scintillator telescope and multichannel analyser is shown in Figure 2.8.

Also shown is a Poisson distribution with a mean of 8 fitted to the peak of the distribution. This can be regarded as the "effective" mean number of photoelectrons emitted from the photocathode. The effective number will not be the same as the true number because of factors which contribute to the spread of the distribution, such as:-

1) The finite angle of the muon telescope, about 20° acceptance.
2) The Landau contribution due to the statistical variation in the energy absorbed from the muons by the phosphor.
3) Unbalance of the two photomultipliers.

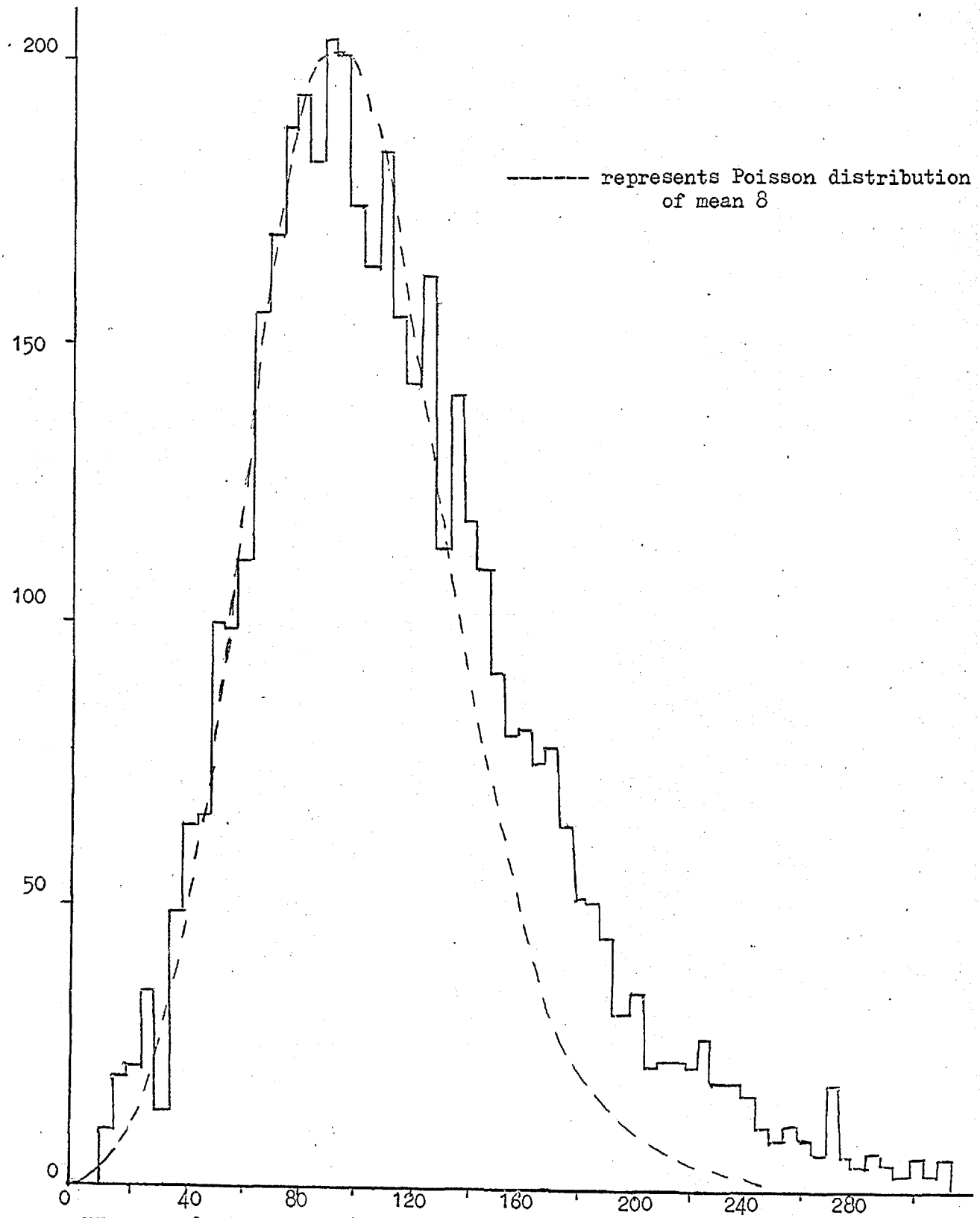


FIGURE 2.8. Single particle pulse height distribution using scintillator telescope above detector, close up.

4) Statistical variation in the multiplication of the first few dynodes of the photomultiplier

The mean number of photo-electrons actually emitted from the photocathode per muon is probably about 20.

Figure 2.9 shows the differential pulse height distribution of secondary cosmic radiation in the scintillator, with the photomultipliers added but not put in coincidence. The single muon peak appears superimposed on the photomultiplier noise.

2.8 Uniformity of Response

A check on the uniformity of response over the area of the detector was made by placing the scintillator telescope over a variety of positions on top of the detector and finding the mean pulse height for vertical muons in each position.

Figure 2.10 shows a plot of the response against position for a line down the centre of the detector. The response rises about 25% above its mid-point value when close up to the light guides. Provided the phototubes are well balanced complete symmetry holds.

For positions midway between the photomultipliers, off the central axis, the response is not significantly different

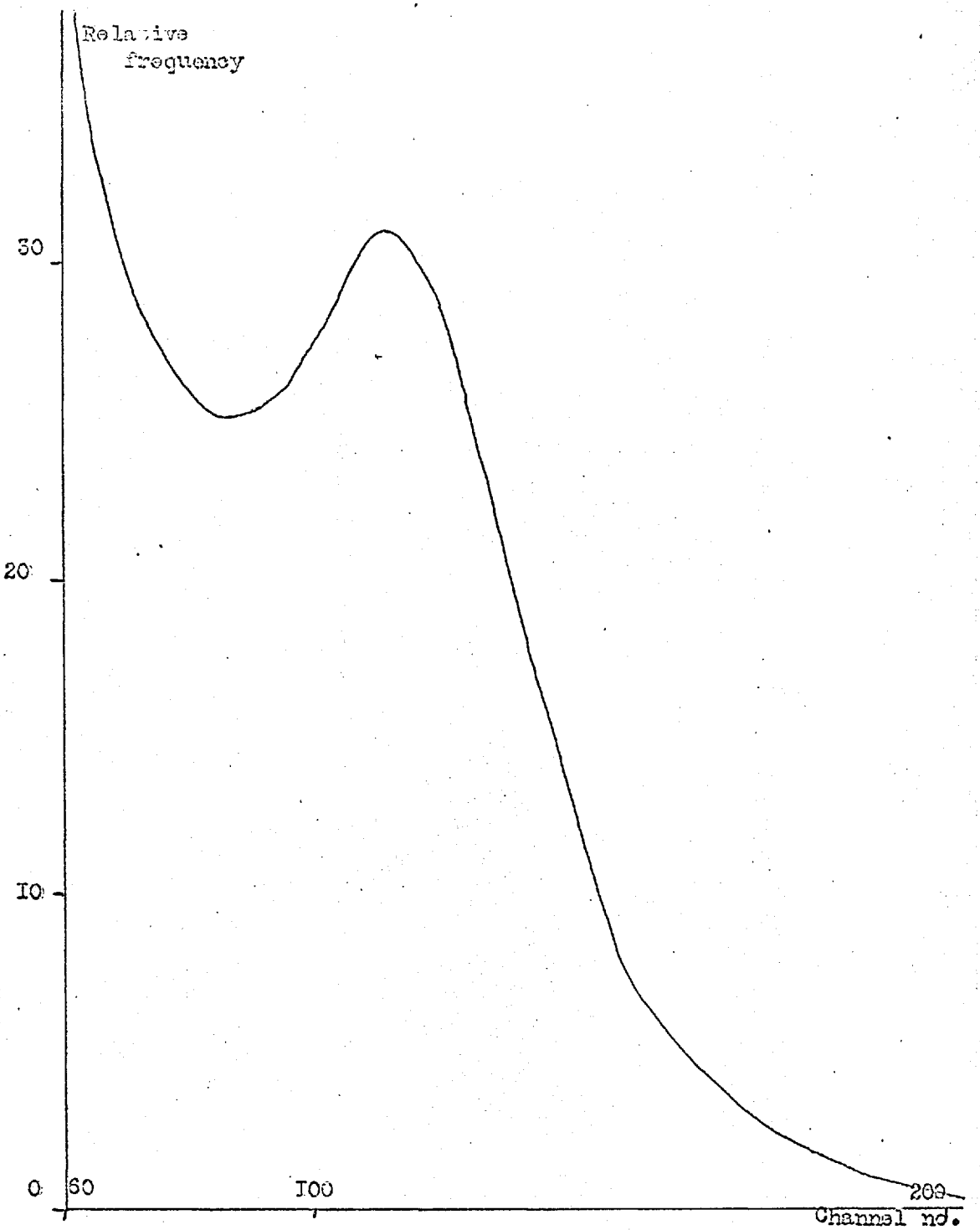


FIGURE 2.9 Differential pulse height distribution of secondary cosmic rays.

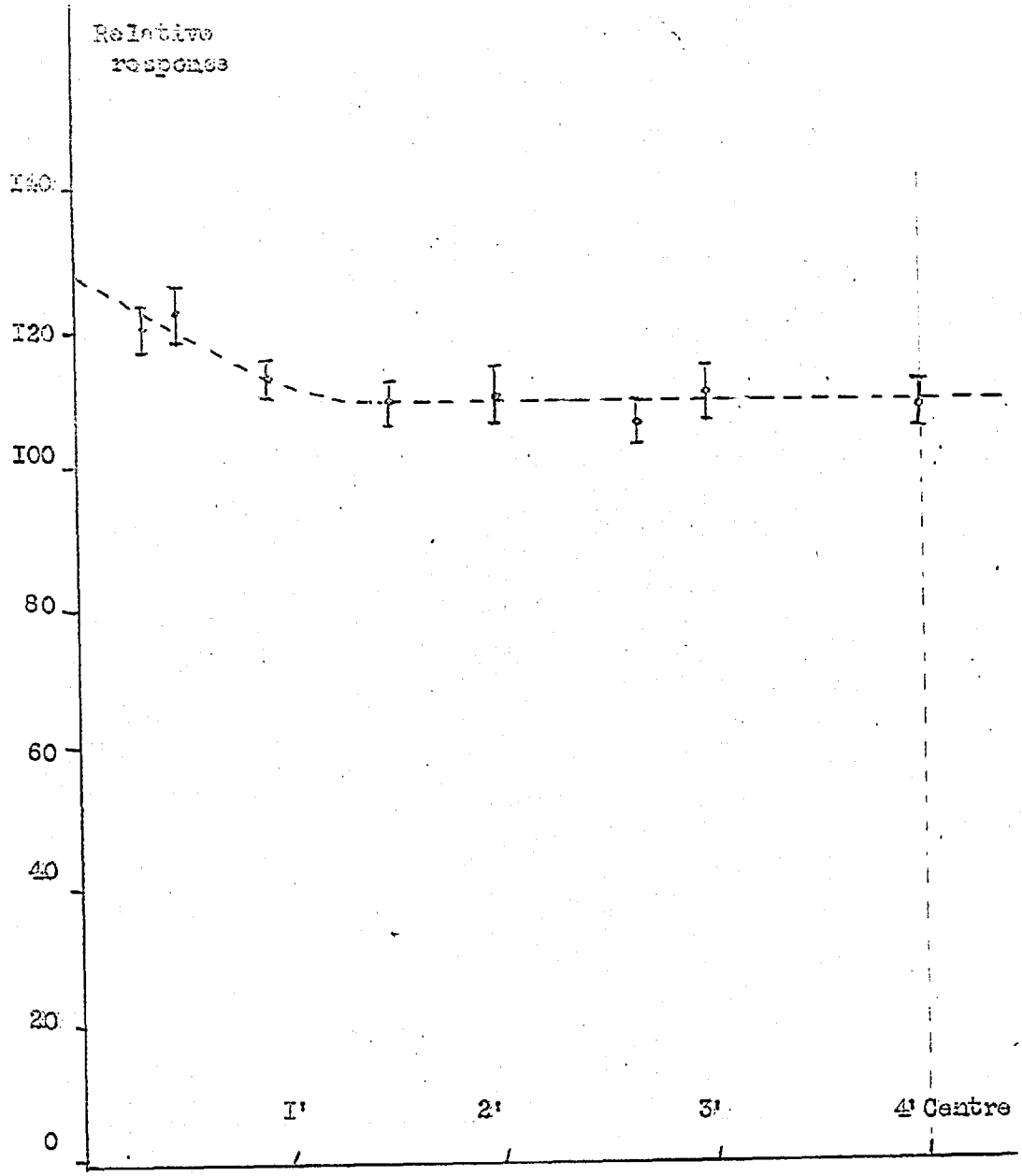


FIGURE 2.10. Uniformity of response down central axis of detector

from the central position. Moreover the response along one side of the detector rises less towards the photomultipliers than it does along the central axis.

The mean response for the whole detector was calculated to be about 5% above the value at the centre.

Tests with an inclined telescope showed that within statistical error the response went up directly with sec Z, where Z was the angle between the axis of the telescope and the zenith. Thus the response of the detector is proportional to the path length of a penetrating particle through it.

2.9 Stability

There has been no indication after some twelve months running of any deterioration either in response or uniformity of the detector unit. An advantage of medicinal paraffin is that it is relatively inert and has no deleterious effect on perspex. Nor does it readily absorb oxygen which could lead to quenching of the scintillation energy (Barton et al.,1962).

The mains power supply to each station is stabilised and the photomultipliers are run off additionally stabilised E.H.T. units.

The main short term instability is the temperature coefficient of the photocathode efficiency, about -1% per ^{o}C.

As the temperature of the Hut is kept constant within a few degrees this is not serious and averages out over a period of time. Also the calibration runs generally lasted a full temperature cycle (i.e. 24 hours).

2.10 Shielding

The shielding of the detectors from the electron-photon component of the shower is done by 12,000 lead blocks, 6" x 2" x 2" (supplied by British Lead Mills). Lead walls, 8" high, enable the detector units to be bridged by 1" thick steel plates, 5'9" long by 6" wide. Twenty of these covered each detector providing adequate (12") overlap at each end to trap high zenith angle particles. The steel plates support the overlying layers of lead.

Chapter 3 describes an experiment to determine the thickness of lead necessary to ensure complete absorption of the electron-photon component.

CHAPTER 3

THE ABSORPTION IN LEAD OF THE ELECTRON-PHOTON COMPONENT OF EAS

3.1 Introduction

Early study of cosmic rays at sea-level showed that Geiger counters under increasing thickness of lead shield reached an almost constant counting rate beyond 10 to 15 cm. thickness (Clay,1927; Auger,1938). Rossi (1933) found that the rate of coincidences by a three-fold counter arrangement under lead, plotted against thickness of lead absorber above it, first increases, reaches a maximum at about 2 cm. of lead and then decreases for larger thicknesses. Above 10 cm. of lead however this Rossi transition curve showed no further decrease. Rossi interpreted the sharp maximum as due to a "soft" radiation producing easily absorbed cascade showers while the level tail was due to a "hard" radiation.

Auger et al.(1939) showed that EAS also consisted of soft and hard components. The soft component was identified as electron-photon cascades in the atmosphere. Many experiments were then undertaken to establish that the penetrating component consisted of muons. Cocconi et al.(1949) measured R(t), the fractional number of shower particles capable of penetrating

a thickness, t, of absorber. Coincident rates between an unshielded array of Geiger counters and a shielded stack were investigated. They established that at sea-level the plateau of the Rossi curve for EAS started at around 15 cm. of lead, whereas at 3,260 metres altitude at least 20 cm. of lead were needed to eliminate all the soft component. Other researchers have carried out similar experiments at sea-level with the same type of technique and with different amounts of lead (e.g.Broadbent and Janossy,1947;McCusker and Millar, 1951).

Results show that, for thickness above 15 cm. of lead, coincidence rates between shielded and unshielded arrays of counters, due to EAS, remain almost constant for increasing thickness of absorber. This rate is about 2.5% of the coincidence rate of unshielded detectors only. This has been interpreted as the proportion of penetrating particles in showers.

No attempt had been made to sort out how the thickness of absorber needed depended on distance from the core and most experiments had sampled EAS within a few metres of their axes.

In the present work, it was decided to carry the investigation further and determine the amount of lead needed as shielding to study the muon density distribution in large

EAS. An absorption experiment using the scintillator units was therefore carried out.

3.2 Experimental Details

In order to investigate the absorption by lead of the secondary particles of EAS a two-fold detector was set up. One 2.5 sq.metres detector unit was supported directly above another with a gap of two feet between them. The responses of the two detectors were initially equalised on counting rates. The output from the top detector was fixed at 20 mV. per vertical muon and both detectors were calibrated absolutely by the muon telescope.

A block diagram of the electronics system is shown in Figure 3.1. The pulses from the two photomultipliers of the top detector were added through an amplifier. The amplified pulses were matched into 1 microsec. of delay cable (Hackethal, HH2500) and then into a mixing circuit. The pulses from the bottom unit were likewise amplified, given 4 microsecs. of delay and fed into the mixer. The output was displayed on a Solartron CD 1012 oscilloscope.

The two-fold detector arrangement was placed in "Hut 3", one of the outer stations of the Haverah Park 500 metre air shower array (Figure 3.2). To get a simple but useful in-

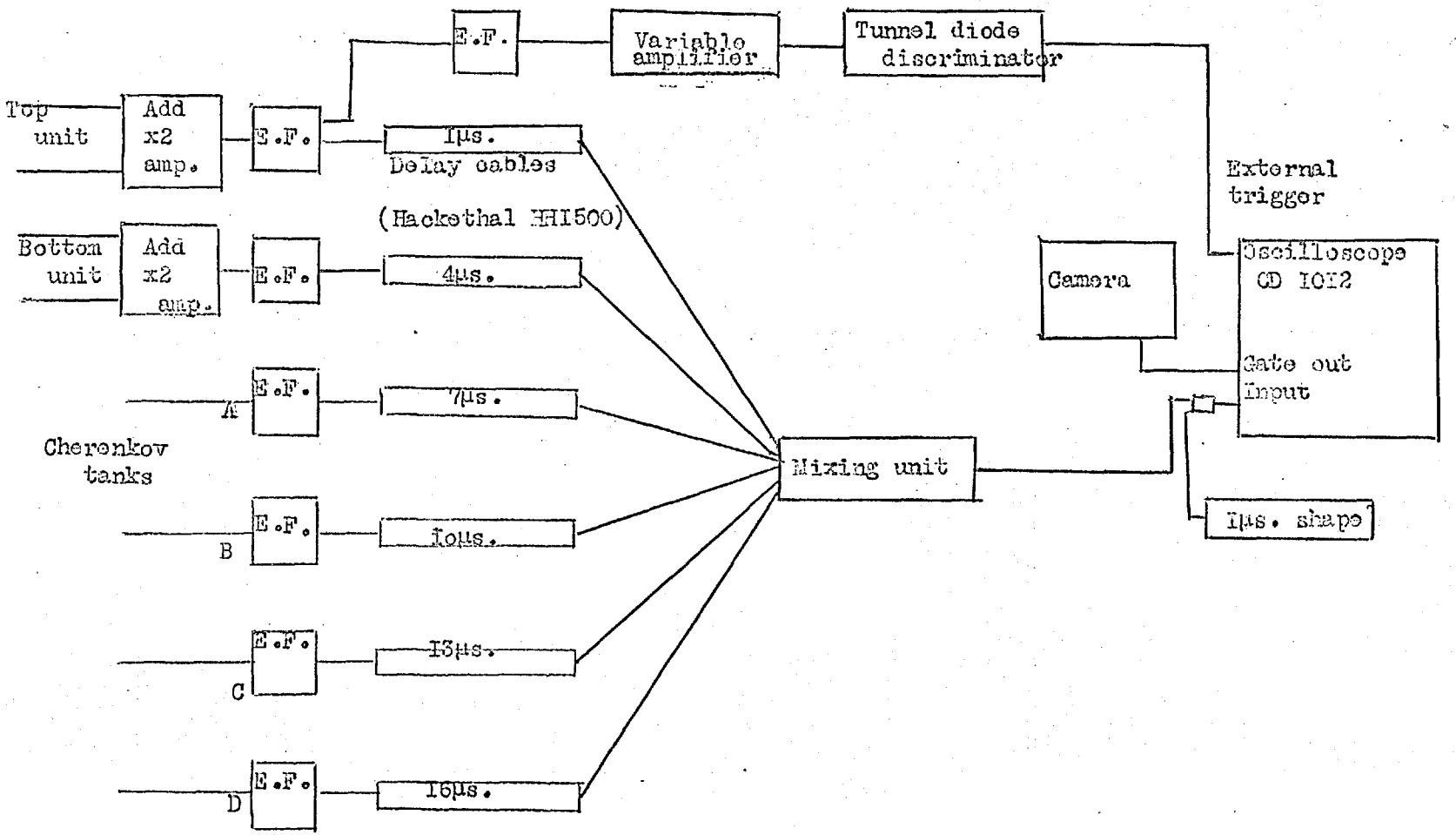


FIGURE 5.I. Block diagram of recording system for the absorption experiment

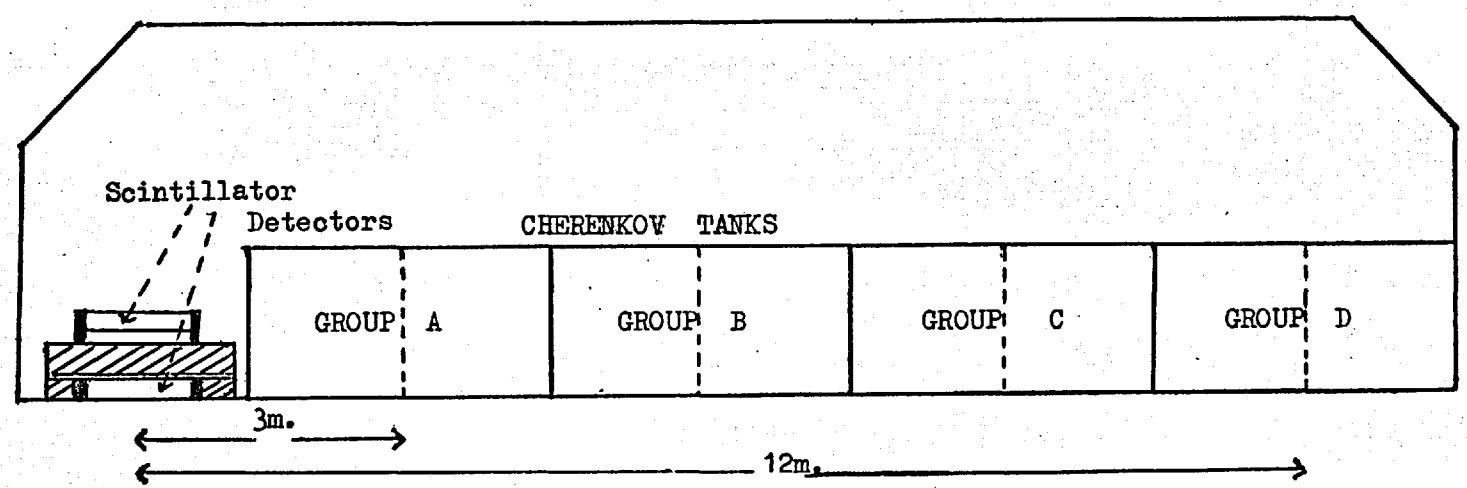


FIGURE 3.2 LAYOUT OF HUT 3 FOR THE ABSORPTION EXPERIMENT.

dication of EAS falling on the station pulses from four groups of Cherenkov tanks in it were displayed separately, on the same oscilloscope.

Pulses from each group of tanks were extracted from the main electronics system at the station and fed by small lengths of co-axial cable to emitter followers in the subsidiary adding unit. With relative delays the pulses were then fed into the mixing circuit. One hundred metres of co-axial cable (UR39), shorted at one end, clipped the pulses to 1 microsec. width, allowing the six pulses to be displayed side by side on a 20 microsec. time-base.

A second output from the top detector was amplified and fed into a tunnel diode discriminator which gave a 5 volt negative square pulse output. The amplifier had a variable gain which effectively varied the discriminating level. The output from the discriminator triggered the time-base circuit of the oscilloscope. The display could be photographed by a Shackman Mark III recording camera.

3.3 Experimental Procedure

Once both detectors had been calibrated in terms of mV. output per vertical muon, the gains were kept constant by checking counting rates at regular intervals.

The first stage of the experiment was to measure the ratio of the output responses of the two scintillators with 1" of steel plate plus the top detector and its supports (2" of wood) shielding the bottom unit.

The recording oscilloscope was triggered whenever the output response from the top detector was equivalent to 40 or more particles (800 mV. discrimination). Standard voltage pulses were photographed on each film as calibration.

The recorded pulse heights gave directly the ratio of the shielded to unshielded responses. They also gave details from the Cherenkov detectors of the kind of shower that caused the event. The method of classifying events is described in section 3.4.

A series of measurements was made, with an additional 5 cm. (2") layer of lead at each stage. At each layer two or three days' operation provided 1,000 to 1,500 events. Of these about 20% were selected according to the criteria below. As the shielding increased, the gain of the bottom unit was raised on two occasions to bring the output response into the range of the oscilloscope.

The experiment was discontinued after the effect of 30 cm. of lead had been studied.

3.4 Identification of Core Positions

The Cherenkov detectors were grouped in fours along the length of the station away from the scintillator arrangement.

Two types of event were selected:-

(a) "Near" showers - those EAS which produced a large pulse in the nearest group of tanks, a fall off down the shed and a pulse in the furthest set less than 20% in magnitude of the nearest group.

(b) "Distant" showers - those EAS which produced the largest pulse in the furthest group of tanks and a fall off along the shed.

These two types were chosen as being the easiest interpretable events and represented about 20% of all events. Although other types did lend themselves to analysis the above two classes gave adequate information about the absorption curves.

It is shown in Appendix II that "Near" showers have cores falling within 5 metres of the detector and that "Distant" showers must fall with their axes at least 10 m. from the scintillators. The shower sizes covered were those containing 10^4-10^6 particles.

3.5 Results

Figure 3.3 shows plots of the results. The ratio of shielded to unshielded response is shown as a function of the thickness of the absorber. The ratios were obtained by summing up the shielded response for all the selected events and dividing by the sum of the unshielded pulse heights The errors indicated are calculated on the total number of events and the broadness of the distribution of ratios of individual events.

The gain of the bottom unit was increased on two occasions by increasing the photomultiplier E.H.T. voltages. These changes introduce a probable 2% error in absolute calibration between the three ranges of absorber thickness:- 0 to 10 cm; 15 to 25 cm; 30 cm. of lead.

Both types of EAS show a Rossi type transition curve. Electrons and photons incident upon the absorber multiply into showers by the repeated process of bremsstrahlung and pair production. These showers reach their maximum development at a thickness of a few radiation lengths and are then absorbed. Apart from ionisation loss the majority of the muon component passes straight through without interacting. In the case of "Near" showers in particular, nuclear-active particles from the core of the shower will fall on the detector. These may cause nuclear interactions in the

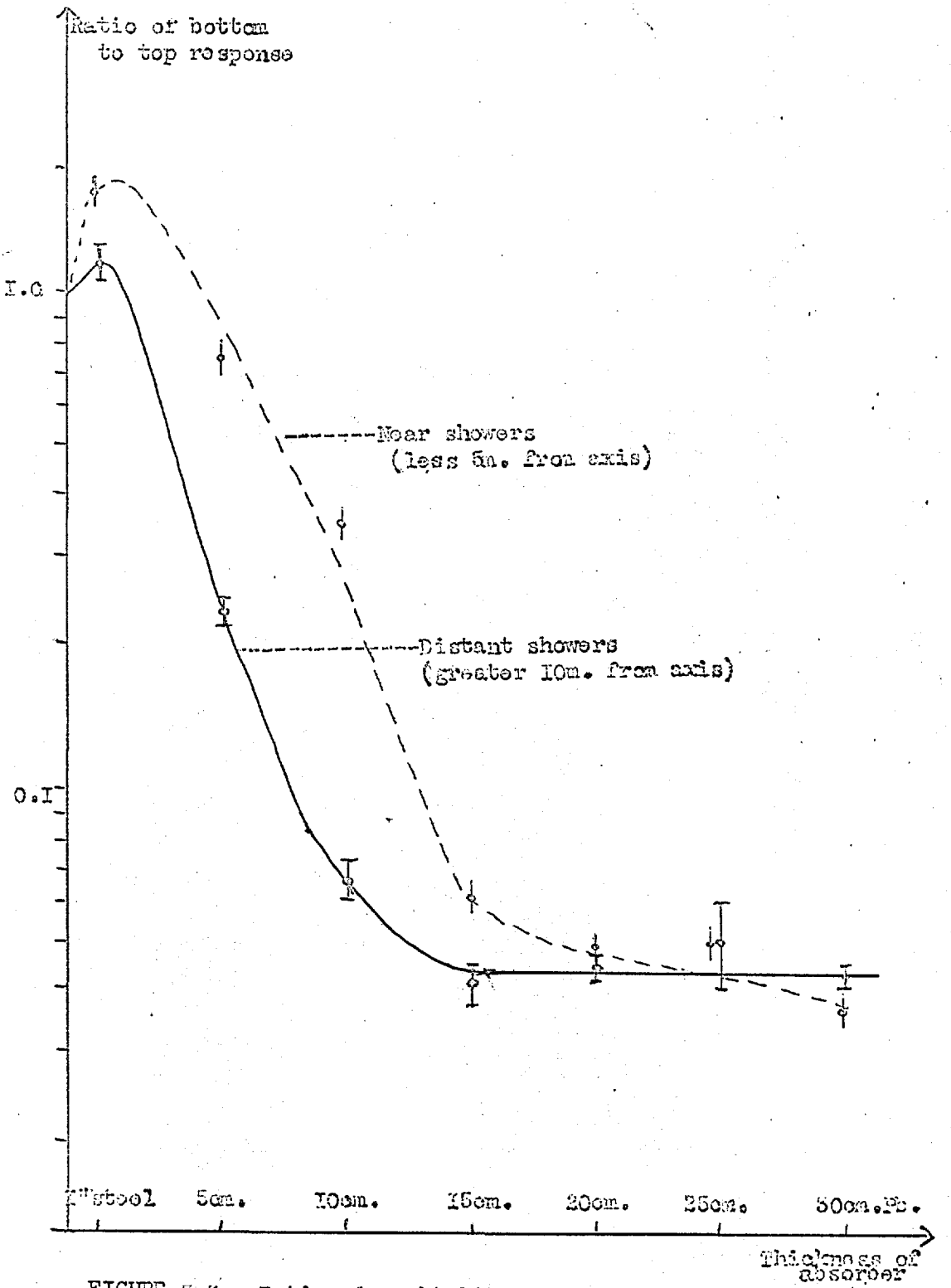


FIGURE 5.3. Ratio of unshielded to shielded response under increasing thickness of lead absorber for EAS.

	Thickness	Bottom/Top Response 5metres	12metres
	No absorber	1.00	1.00
1 GAIN CALIBRATION (±2%)	1"steel	1.62(±5%)	1.16(±10%)
	5cm Pb	0.74(±4%)	0.23(±7%)
	10cm Pb	0.41(±4%)	0.066(±10%)
2 GAIN CALIBRATION (±2%)	15cm Pb	0.062(±5%)	0.041(±10%)
	20cm Pb	0.048(±5%)	0.046(±7%)
	25cm Pb	0.044(±10%)	0.050(±20%)
3 CALIBRATION (±2%)	30cm Pb	0.036(±3%)	0.043(±4%)

GAIN OF TOP DETECTOR ±2%

GAIN OF BOTTOM DETECTOR CHANGED AT 15cm. & 30cm. LEVELS

CALIBRATION TO ±2%

Relative gains 1 B/T 1

2 B/T 3

3 B/T 10

lead with subsequent multiplication.

The results for "Distant" showers indicate that, provided observations are carried out at distances greater than 10 m. from the core of a shower, detectors under 15 cm. of lead respond only to a slowly absorbed penetrating component. This can be regarded as consisting predominantly, if not entirely, of muons. A more detailed interpretation of the results is attempted in the following sections.

3.6 Absorption of the Electron-Photon Component

Much theoretical work has been done on the propagation of electromagnetic cascades. Rossi (1952) reviews in detail the theoretical approach to the study of shower cascades produced by high energy electrons and photons incident on matter. Diffusion equations are set up representing the growth in numbers of electrons and photons in a cascade as a function of energy and depth in the material. The processes that are of importance in the transfer of energy are:- bremsstrahlung; pair production; Compton effect; ionisation loss.

The radiation length is defined as the mean free path for bremsstrahlung production by an electron. The critical energy, e_0, is that for which the rate of loss of energy by

collision is equal to that by radiation. By collision loss is meant the energy lost in excitation and ionisation of the electrons in the atoms of the propagating medium. The values of both the radiation length and critical energy depend on the nature of the material.

Solutions of the diffusion equations are difficult to obtain and approximations must be used for the various theoretical cross-sections. Analytical solutions under Approximations A and B are derived. Approximation A neglects both Compton effect and ionisation loss and applies only for energies well in excess of the critical energy. Under Approximation B, the Compton effect is still neglected but collision loss is described by asymptotic formulae for complete screening of the nucleons by the atomic electrons. These approximations only lead to reliable solutions for energies above the critical energy, e_o. At energies near e_o the asymptotic formulae break down and below the critical energy Compton effect and ionisation processes contribute considerably both to the absorption and production of shower particles. Solutions of the diffusion equations taking all the contributing processes accurately into account have not been obtained.

Recently, with the aid of computers, accurate calculations have been carried out by Monte Carlo methods. Results of

random interactions over small intervals of thickness using accurate theoretical cross-sections can be summed up and the probability of a particular end result calculated.

Butcher and Messel (1960) have carried out detailed calculations of electron number distribution in various absorbers. Accurate theoretical cross-sections at low energies were used and collision losses and Compton effect taken into account. Results were tabulated for a wide range of electron and photon primary energies.

(a) Energy of Electrons and Photons in EAS at Sea-level:

Several attempts have been made to determine experimentally the energy of the electrons and photons in EAS as a function of distance from the axis (Vernov et al.,1960; Hasegawa et al.,1962;Lillicrap et al.,1963). General agreement is obtained.

Figure 3.4 shows the variation of the mean energy per electron in the range 1-100 metres from the core. The measurements have been carried out on EAS of various sizes (10^5 to 10^7) and the average energy found to be independent of size.

Theoretical calculations by Kamata and Nishimura (1958) are in general agreement, although for distances close to the axis the experimental results are somewhat lower than

theory predicts since the theory assumes a primary particle of infinite energy.

The experimental curve of Figure 3.4 (Hasegawa et al.,1962) only gives the energy for the total electron-photon component per electron. To interpret the absorption curves something must be known of the division of energy between the individual electrons and photons.

Electrons at large distances from the core ($\sim$100 m.) are mostly Compton recoil electrons of low energy (about 10 Mev) produced by the numerous photons in that region of the shower (Kamata and Nishimura,1958). The individual electron energies do not differ greatly from those of the photons. At these distances there are up to ten photons to each electron.

Close to the axis however, in the region where pair production and radiation play the dominant role, the numbers of electrons and photons are comparable.

Experimental evidence in accordance with these considerations comes from work on Cherenkov water detectors (Allan et al.,1960;1962;Lillicrap et al.,1963). Lillicrap et al. show that a value of n , the photon-electron number ratio which increases to 2 or 3 at distances of about 10 m. from the core leads to reasonable agreement between theory and experimental results.

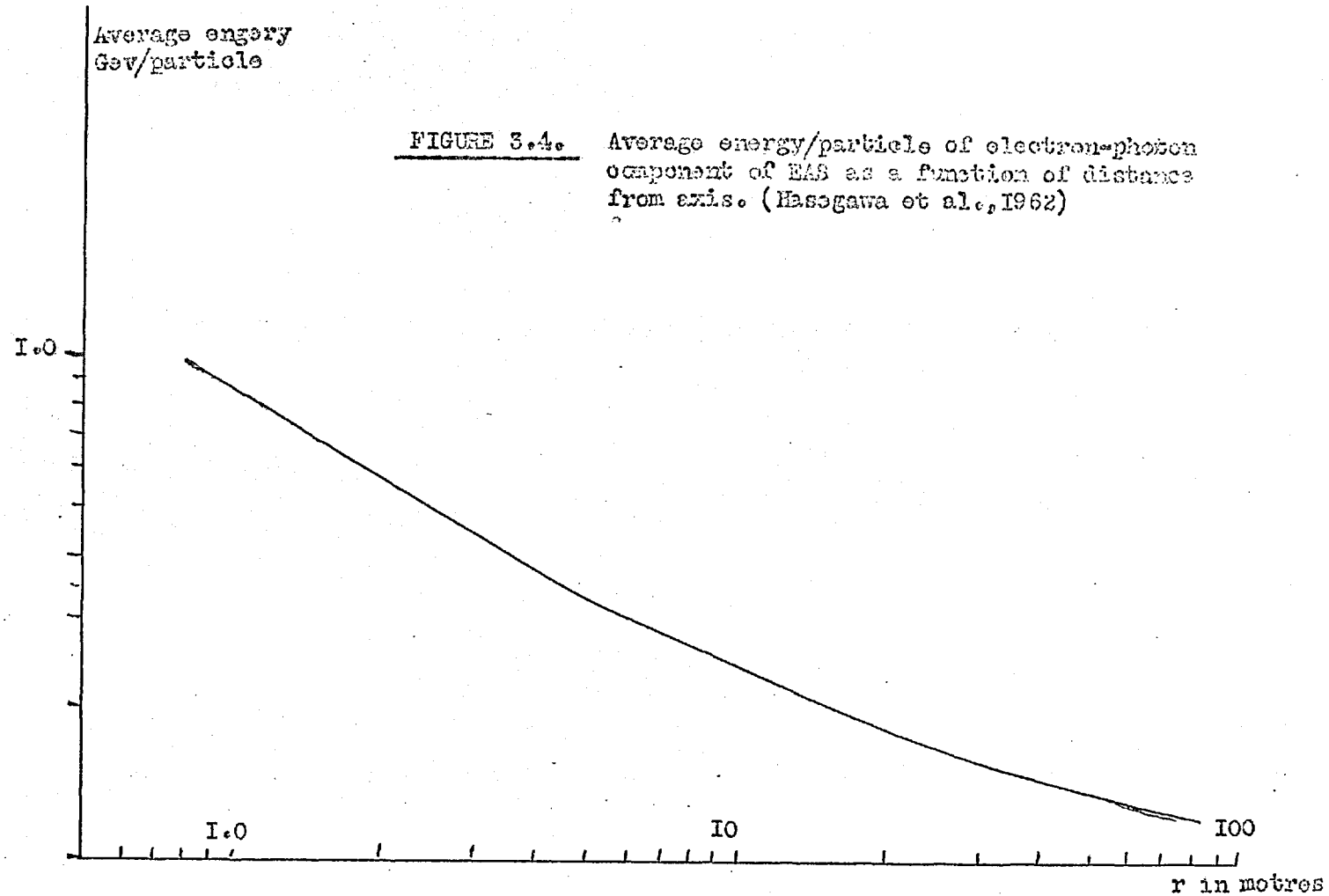


FIGURE 3.4. Average energy/particle of electron-photon component of EAS as a function of distance from axis. (Hasegawa et al., 1962)

The above considerations of the radial distribution of the photon-electron ratio were used together with Figure 3.4 to estimate the energies of the individual secondaries incident on the scintillator in the two categories of showers. In the following discussion the mean energy of the electrons and photons in "Near" showers will therefore be taken as:-

$$\frac{500 \text{ Mev}}{n_\gamma + 1} (r < 5\text{m}) = 250 \text{ Mev/particle}$$

and for "Distant" showers:-

$$\frac{250 \text{ Mev}}{n_\gamma + 1} (r > 10\text{m}) = 250 \text{ Mev/particle}.$$

(b) Absorption Calculations:

Table 3.1 shows figures derived from Butcher and Messel (1960) who tabulate calculations for air and aluminium. Their tables can be applied to all materials of low atomic number provided primary and secondary energies are expressed in terms of critical energy, e_o.

Table 3.1 lists the expected mean number of secondary electrons of energy in excess of 2.5 Mev and 5 Mev emerging from 1.5 radiation lengths (about 1") of steel. The critical energy, e_o, for steel is about 24 Mev. Each electron will be accompanied by several photons.

With absorbers of high atomic number, such as

SECONDARY ENERGY GREATER THAN	PRIMARY ELECTRON		PRIMARY PHOTON	
	100Mev	250Mev	100Mev	250Mev
2.5Mev	0.82	1.81	0.72	1.36
5.0Mev	0.65	1.53	0.61	1.20

Table 3.1 Mean number of electrons and photons emerging from 1.5 radiation lengths of steel due to incident electron and photon as a function of primary energy. (Butcher and Messel,1960).

THICKNESS OF ABSORBER	Radiation Length	"NEAR" SHOWERS		"DISTANT"SHOWERS	
		E.M. Theory	Experi-mental	E.M Theory	Experi-mental
2.5cm St	1.5	1.6	1.62	1.0	1.16
5 cm Pb	10	0.80	0.74	0.30	0.23
10 cm Pb	20	0.07	0.41	0.017	0.066
15 cm Pb	30	0.004	0.062	0.001	0.041
20 cm Pb	40	0.001	0.048	0	0.046
25 cm Pb	50	0.000	0.049	0	0.050
30 cm Pb	60	0.000	0.036	0	0.043

Table 3.2 Comparison of experimental points with e.m. theory.

lead, scattering becomes important at low energies. Mossel et al.(1962) have carried out calculations for 1 Gev primaries incident on lead up to depths of 10 radiation lengths (5 cm. of lead). Woischnig and Burmeister (1964) have taken these calculations up to depths of 25 radiation lengths for a range of primary energies (Figure 3.5).

An attempt is made in Figure 3.5 to extend the published curves up to 40 radiation lengths. Such a procedure is justified since the dominant propagation process at these depths will be Compton loss by low energy photons. At minimum absorption, the photon absorption length in lead is almost constant over a range 1-10 Mev at 35 grms/cm^2. At minimum ionisation (1-10 Mev energy range) electrons in lead lose 1 Mev/grm.cm^{-2}. Photons with their longer absorption length will be several times more abundant.

The curves of Figure 3.5 represent statistical averages. Thus when the number of particles is indicated to be less than one, the curves describe the probability of finding such a particle in a shower.

Although the curves are plotted for incident electrons only, for depths in excess of one radiation length, they also hold for photons of the same energy.

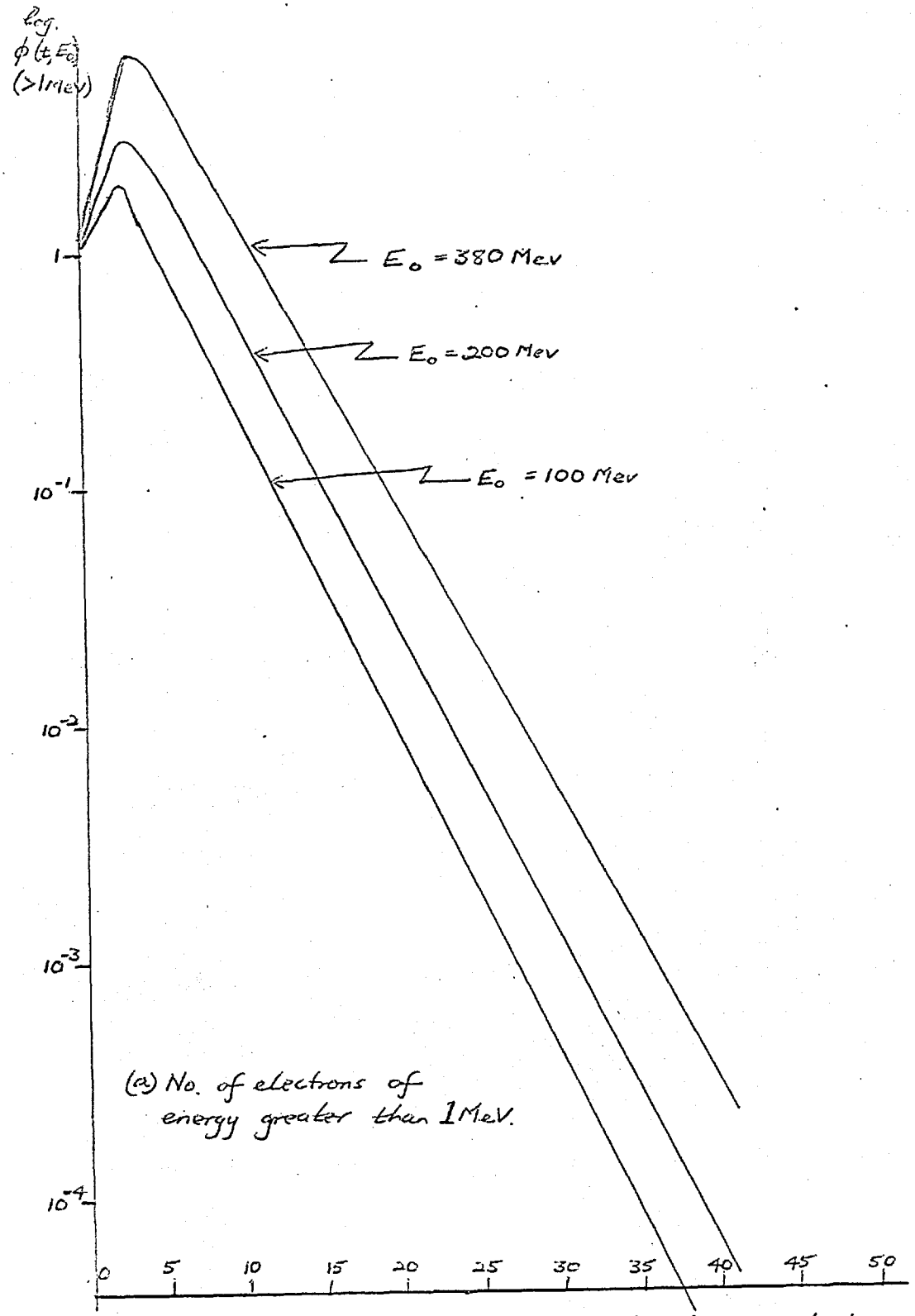


FIGURE 3.5 No. of electrons as a function of depth in radiation lengths produced by electrons of various primary energies

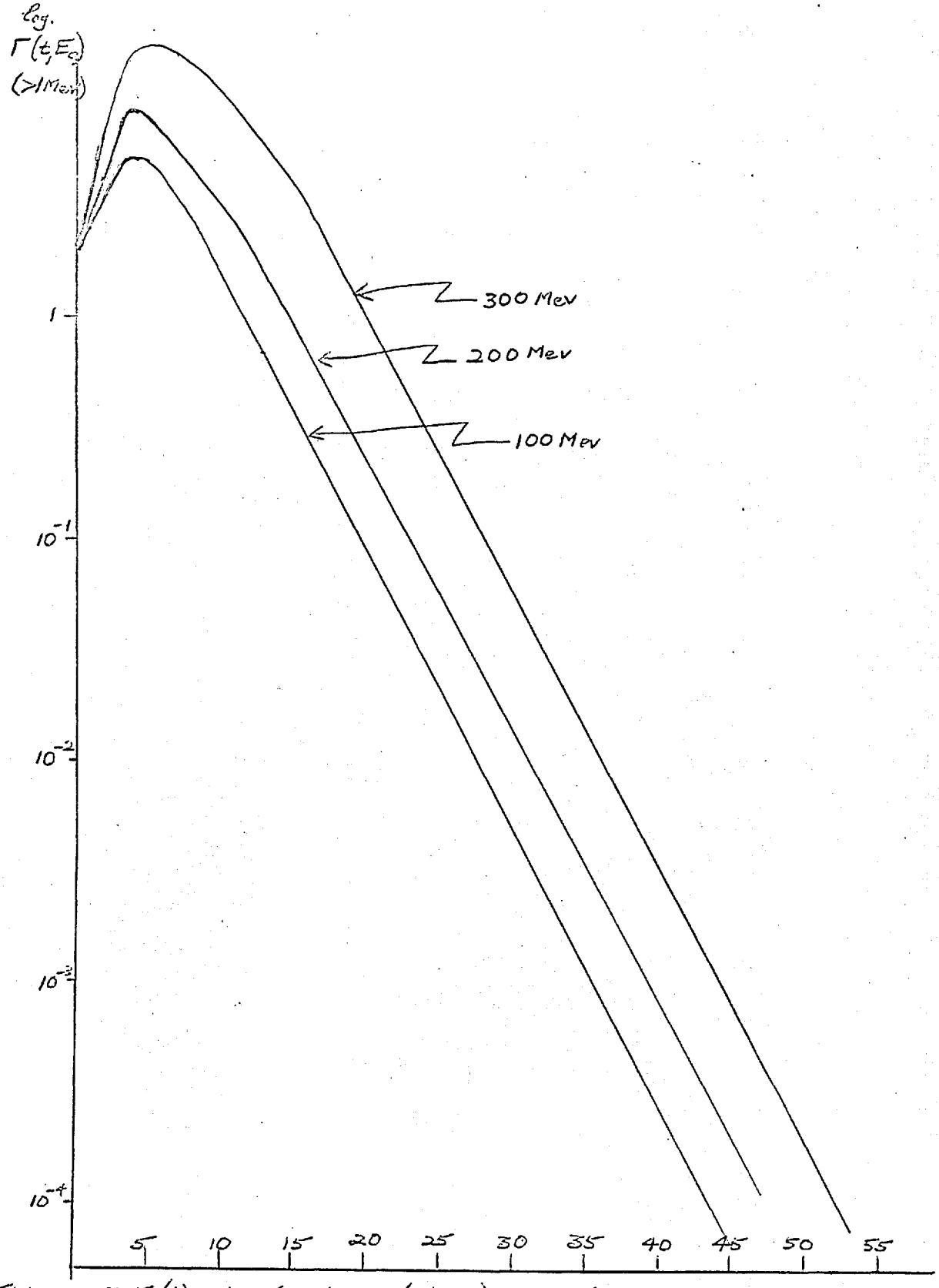


FIGURE 3.5 (b) No. of photons (>1 Mev) as a function of depth in radiation lengths produced by electrons of various primary energies.

(c) Interpretation of the Absorption Curves:

In Table 3.2 p87 the experimental results are compared with the mean multiplicities of response as expected from the Monte Carlo calculations. The figures are based on the curves of Figure 3.5 together with the estimated detector response to low energy secondaries.

In correlating the experimental points with the theoretical absorption of electron-photon cascades the following considerations must be taken into account:-

1) The secondary energies under discussion cover the region near the critical energy where some of the theoretical cross-sections become difficult to apply.
2) Absolute multiplicities are difficult to determine from the experimental curves as a particle penetrating the absorber needs to give up 16 Mev of ionisation energy in the scintillator to be recorded as a single particle.
3) There is a spread of particle energies incident on the absorber.
4) A significant flux of nuclear active particles is present near the cores of EAS (Section 3.8). Nuclear interactions at varying depths of absorber cause nuclear and electromagnetic cascades to

develop. By-products of such interactions may emerge from the absorber.

Plots of the distribution of shielded to unshielded response for individual events (Figure 3.6) confirm experimentally the importance of 3) and 4) above. The distributions are much broader for "Near" showers than "Distant" showers. This reflects the steep variation of the energy per particle with radial distance, in the region covered by the "Near" showers and the higher probability of nuclear interactions occuring. The fall off of density with distance from the axis is such that the nucleon conponent is only important for "Near" showers.

5) Poisson's Distribution cannot be used for the calculation of fluctuations as the particles of a cascade are not genetically independent. Any deviation from the average behaviour occuring in the early development of the shower influences the successive generations. This must increase the statistical fluctuations in the number of particles observed at a given depth (Ross, 1952)

Calculations have been carried out using Furry and Polya distributions derived from statistical models of shower processes, by Furry (1937),

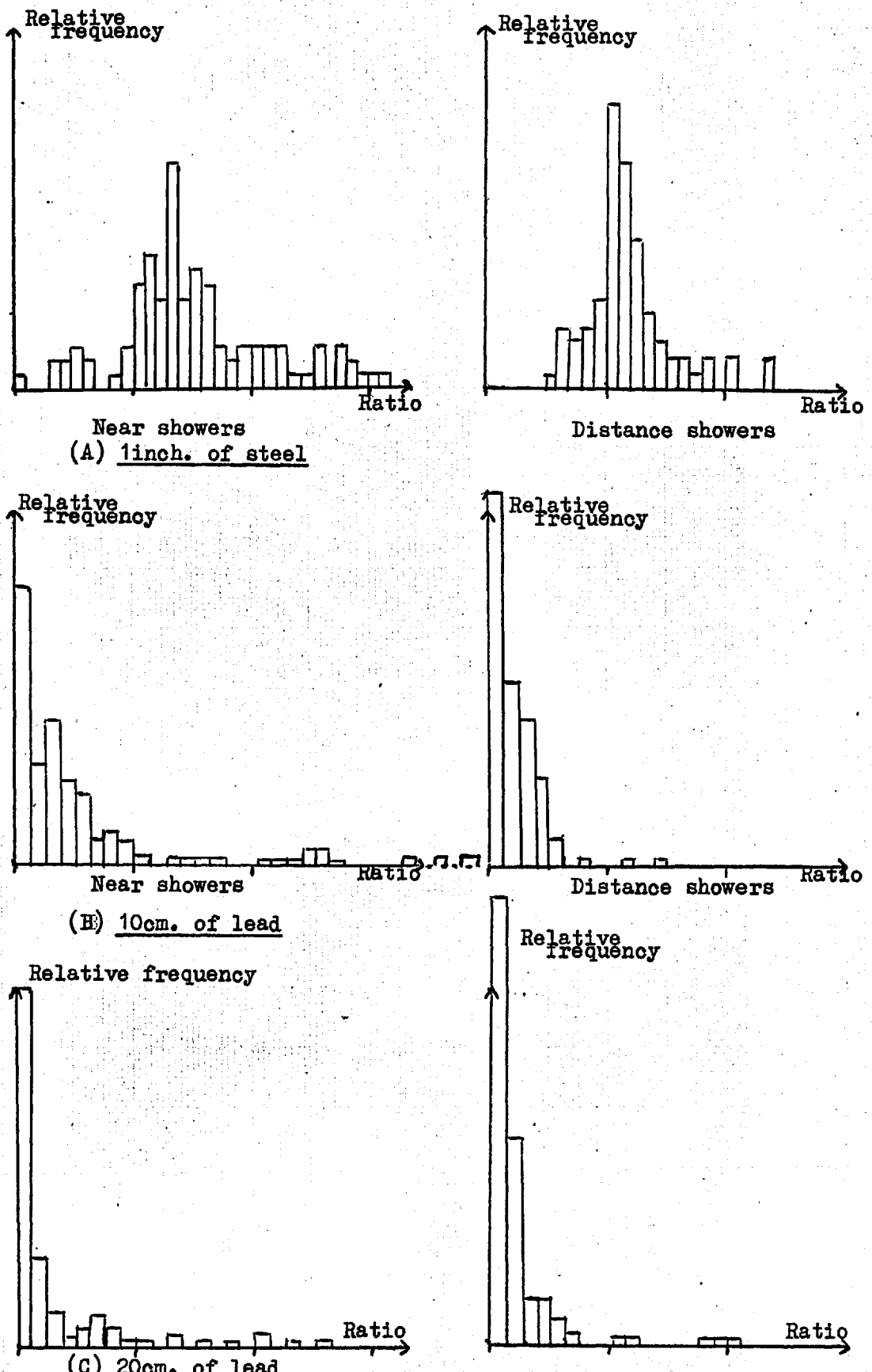


FIGURE 3.6 PLOTS OF FREQUENCY OF RATIO OF SHIELDED TO UNSHIELDED DETECTOR RESPONSE FOR INDIVIDUAL SHOWERS.

Bertanza and Martelli (1954) and Arley (1948) Rather drastic simplifications have to be made to obtain numerical values. The Monte Carlo method however does enable accurate probabilities to be calculated. In any case at large depths (> 10 radiation lengths) Poisson's distribution closely applies.

With these considerations in mind a fairly quantitative agreement between the experimental curves and electromagnetic cascade theory is obtained. For "Distant" showers the electron and photon initiated cascades develop quickly reaching their maximum after about 1.5 radiation lengths of absorber. They are then rapidly absorbed so that the probability of detection after 10 cm. of lead (20 radiation lengths) has been added is very small. The plateau from 15 cm. onwards must consist almost entirely of muons.

For "Near" showers the electron-photon cascades reach their maximum somewhat later than 1.5 radiation lengths. The secondaries are quickly absorbed so that after about 15 cm of lead the probability of detection is negligible. The slowly absorbed remnant must then consist of the nuclear-active component and its secondary products as well as the muon component.

3.7 Interaction and Absorption of the Muon Component

Nearly all of the energy loss of muons on traversing an absorber can be accounted for in terms of electromagnetic interactions. Collision processes are the dominant mechanism of energy loss for energies less than 100 Gev. At higher energies bremsstrahlung and pair production become important (Cousins and Nash,1962;Hayman et al.,1963).

The energy of muons in EAS at sea-level has been determined by shielded magnetic spectrographs run in conjunction with arrays. Bennett et al.(1962) have calculated the mean energy of muons in EAS from experimental curves to be 7 Gev. The majority of muons lie in the range 2-10 Gev.

As in most measurements the spectrometer had a low energy cut-off near 1 Gev. This lower limit is unimportant close to the shower axis (less than 100 m.) where nearly all the muons have energy in excess of 1 Gev. Further out from the core (around 500 m.) however the integral spectrum is still quite steep near 1 Gev indicating a significant proportion of muons with energies less then this.

The main sources of energy loss of 10 Gev muons are shown in Table 3.3 with their mean energy loss per grms/cm^2. The total rate of loss of energy is almost independent of energy in the range 0.5-100 Gev.

The differential cross-section for ionisation loss varies

PROCESS	Mev/grm.cm^2	LOSS IN 20cm.of Pb.
Ionisation & Excitation.	1.1	250 Mev
Direct pair production.	0.008	2
Bremsstrahlung.	0.010	2
Nuclear interactions.	0.006	1.5
Total	1.12	255 Mev

Table 3.3 Main sources of energy loss of 10 Gev muons with their mean energy loss per grm/cm^2. (Rossi,1952;Hayman et al.,1963).

as $1/v^2$, where v is the fraction of energy transferred to an electron. Generally, therefore, ionisation is an almost continuous process of small energy losses. Occasionally a high energy knock-on electron ($\geqslant$ 1 Mev) is produced. Lloyd and Wolfendale (1959) showed experimentally that the probability of a muon emerging from a lead plate accompanied by a single knock-on electron is 5.8% in the momentum range 0.5 $\rightarrow$ 200 Gev/c. Stoker et al.(1961) have plotted the mean number of knock-on electrons as a function of lead thickness. The curve rises rapidly to about 6% at 1 cm. and flattens off. The number of knock-on electrons emerging with energy above 10 Mev is about 1% of the muon flux (Walker,1953;Stoker et al., 1961). The mean effect of knock-on electrons on the response of the shielded detector will be to increase the effective muon density by less than 1%.

The probabilities of direct pair production, bremsstrahlung and nuclear interactions by a muon are so small that the effect of any energetic secondary emerging is negligible when averaged over all showers. Also the probability of a 1 Gev muon decaying in 15 inch thickness (shielding plus detector) is extremely small ($<10^{-6}$).

Muons require about 250 Mev of energy to penetrate 20 cm. of lead because of ionisation loss. The absorption curves

of "Distant" showers at thicknesses above 20 cm. of lead should then reflect the integral energy spectrum of muons above 250 Mev. As this is exceedingly flat for a shower falling within 25 metres of the detector the levelling off of the experimental curve is in agreement (Bennett et al., 1962). For "Near" showers the muons also do not contribute to the absorption.

3.8 The Effect of the Nuclear Active Component

The mean energy and density of the nuclear-active particles in EAS decrease with distance from the core to such an extent that beyond 10 metres the muon component is much the more important component of the two (Kameda et al., 1962;Cocconi,1961). Within 5 metres of the axis the nucleon density is greater than the muons and can be expected to make a significant contribution to the absorption curves of "Near" showers. Close to the core they represent about 2% of all secondary particles.

The interaction mean free path of nucleons in lead is 160 grms/cm^2. (cf. 80 grms/cm^2. for air)(Sitte,1961). The longer interaction length in the dense medium can be accounted for by consideration of the "self-shielding" effect of the closely packed nucleons.

For the highly energetic nucleons (10^{11}-10^{12} eV) close to the shower axis, pions will be the most abundant secondary products in nuclear interactions. In a dense material like lead the charged pions produced will have a large proability of interacting before decaying and will thus contribute to the propagation of a nucleon cascade. The attenuation length in lead is about 400 grms/cm^2. (cf.120 grms/cm^2. in air).

The multiplicity of a nuclear interaction is energy dependent ($\sim E^{\frac{1}{4}}$). For energies above 10^{10} eV several pions will be produced in an interaction. Neutral pions will decay into two high energy photons initiating electromagnetic cascades.

For shielding thicknesses up to 5 cm. of lead the nucleons will have little probability of interacting. For increasing thickness the nucleon component will play a significant part in the absorption of "Near" showers. Large fluctuations in multiplicity below the lead shield are to be expected. This is borne out by the histograms of Figure 3.6.

The absorption of the "Near" showers observed experimentally beyond 15 cm. of shield can then be accounted for by the attenuation of the nucleon component and its secondary products. A component with an attenuation length of 400 grms/cm^{-2}.(35 cm. of lead) could fit the experimental points for "Near" showers in Figure 3.3 quite closely beyond

15 cm. thickness if the estimated muon component is first subtracted.

The absence of a significant contribution of nuclear-active particles in "Distant" showers is clear from the extreme flatness of the experimental curve after the absorption of the electron-photon has taken place.

3.9 The Proportion of Penetrating Particles

For "Distant" showers (>10 metres) the proportion of penetrating particles is 4.5 (±0.5)% of all secondary particles (Fig.3.3). This agrees well with other workers who have selected showers at these distances.

The curve for "Near" showers also appears to flatten off at around 4%. This is significantly higher than earlier workers have obtained with counter techniques. Results of coincidences between unshielded and shielded counters have yielded consistently a value of about 2.5% (Broadbent and Janossy,1947;Cocconi et al.,1949;McCusker and Millar,1951). The most likely explanation is the effect on the detector response of nuclear interactions in the liquid scintillator. The depth of the scintillator is about 0.1 of an interaction mean free path. Therefore about 10% of the nucleons penetrating the lead can be expected to interact in the

scintillator. Secondary products may cause a large response in the detector.

The histogram in Figure 3.6(c) indicates that a few large pulses due to the above cause could easily explain the discrepancy in the mean response of the shielded detector.

3.10 Conclusions

The conclusions in regard to showers in the size range 10^4-10^6 is fairly clear cut. To study the muon density at distances greater than 10 metres from the core of such showers a shield of 20 cm. of lead around the detector is sufficient to absorb out completely the unwanted secondaries. Muons of energy greater than 250 Mev, arriving vertically, will penetrate to the detector. There is a small probability of an energetic knock-on electron accompanying an emerging muon.

Extrapolation of this conclusion to the study of muons in showers of size greater than 10^7 is also justifiable since:-

(a) The average energy per particle in the electron-photon component changes very little with shower size (Hasegawa et al.,1962).

(b) The extent of the energetic nucleon component does

not change with shower size, and is certainly negligible for distances greater than about 100 m. from the core (Greisen,1960).

The experiment described in this Chapter therefore confirms that 20 cm. of lead shield is adequate to study the lateral distribution of density of muons in showers of size $> 10^7$ for distances greater than 1.0 metres from the core. With this thickness above the detector a vertical muon will lose on average slightly less than 250 Mev of energy by ionisation in the absorber. The detector will therefore respond to all muons of energy greater than 250 Mev incident vertically on the detector. For inclined showers this lower limit will be slightly greater due to the increased thickness of absorber that must be traversed.

CHAPTER 4

THE PULSE HEIGHT SPECTRUM PRODUCED BY SECONDARY COSMIC RAYS

4.1 Introduction

Comparison of the integral pulse height spectrum obtained with the different cosmic ray detectors at present in use at Haverah Park has raised a number of questions that have made a thorough investigation necessary. The problems have arisen as a consequence of the monitoring procedures whereby any change in the counting rate from a single detector at a fixed discrimination level has been used to give an indication of a change in gain. This fixed discrimination level is generally set at a response equivalent to 2 or 3 vertical penetrating cosmic ray muons.

This Chapter describes experiments performed on the liquid scintillator detector and compares the results with the spectrum obtained from other types of detector.

4.2 Apparatus

A detailed description of the detector units is given in Chapter 2. For the purpose of the present experiment one unit, 2.5 sq.metres in area, was used. The scintillator's

depth of 10 cm. amounts to an absorption depth of about 8 grms/cm^2.

The added output from the two photomultipliers was taken as the detector's response. The unit was calibrated by using a narrow angle telescope to select muons which go vertically through the detector (section 2.7).

The detector unit could be covered with lead absorber up to a height of 30 cm. with one inch of steel as support.

To obtain the pulse height spectrum the output of the detector was fed into a single channel pulse height analyser (Nuclear Enterprises, NE5103) and into a scaler. For low counting rates a 400 channel pulse height analyser (Victoreen 400M) was used.

Calibration of the analysers was carried out using a pulse generator giving a standard 1 volt pulse output and a variable attenuator. A constant check was kept on the gain of the detectors during experimental runs and the barometric pressure was also recorded.

4.3 The Integral Spectrum Obtained from the Liquid Scintillator

Figure 4.1 shows a plot of the integral pulse height spectrum obtained from the liquid scintillator. Also shown are the spectra obtained under 1 inch of steel, 5 cm. of lead,

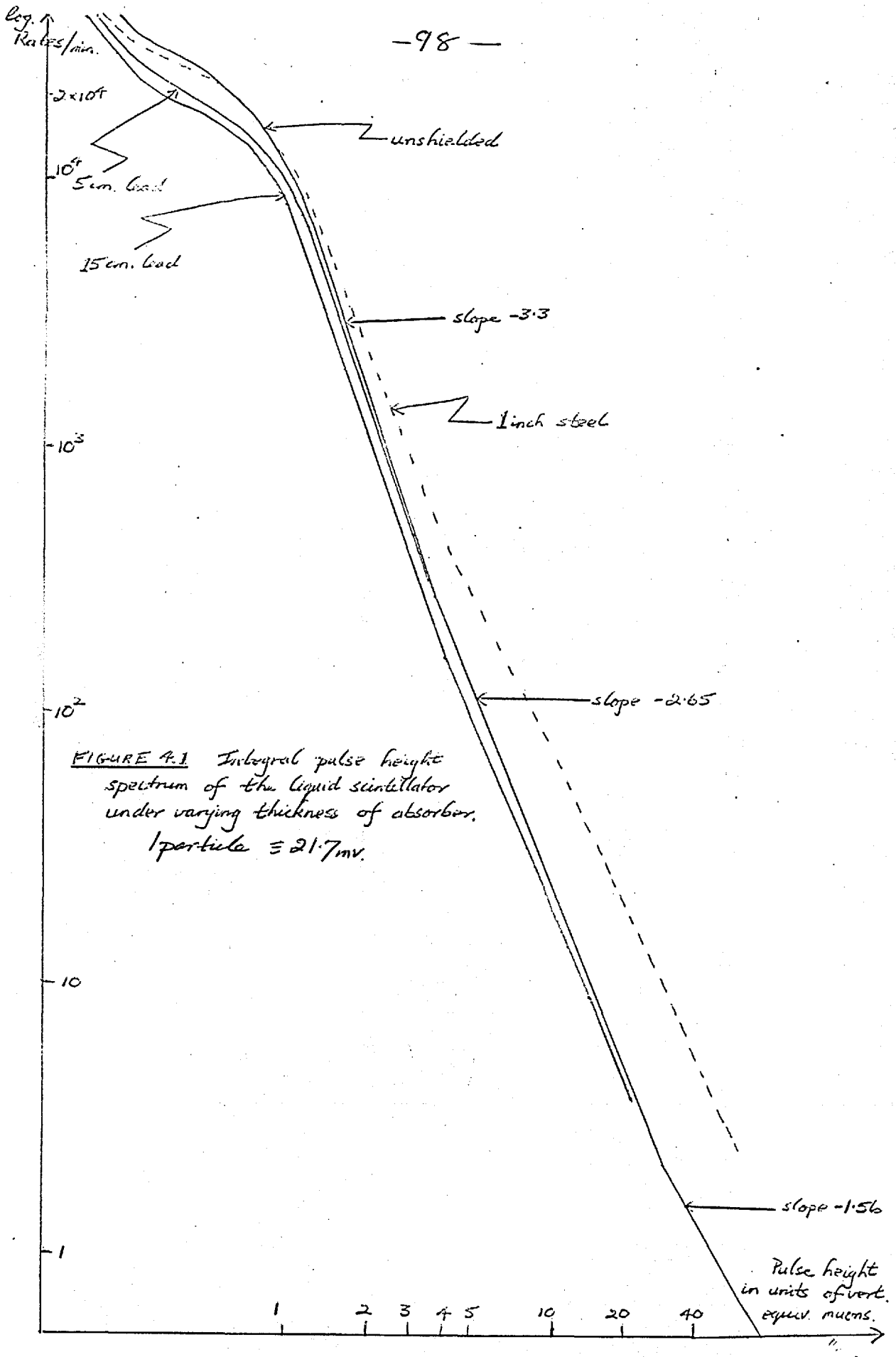


FIGURE 4.1 Integral pulse height spectrum of the liquid scintillator under varying thickness of absorber. 1 particle ≡ 21·7 mv.

and 15 cm. of lead shield.

The uncovered spectrum below 10 mV is interpreted as due mainly to thermal noise in the photocathode of the photomultipliers. Between 10 and 50 mV the spectrum is due to the distribution in response of the detector to the large number of single unassociated cosmic ray secondaries (mainly muons) passing through the detector. The rate of 2×10^4 corresponds closely to what is expected from the results of other workers at sea-level.

Between a pulse height equivalent to 2 vertical muons and 200 muons the unshielded spectrum can be accurately represented by a power law of the form

$$R(> n) = An^{\gamma}$$

where n is the number of equivalent vertical muons. The exponent, γ, has a constant value within three well defined regions

(a) for $2 < n < 4$ $\quad \gamma = -3.3(\pm .1)$

(b) for $5 < n < 20$ $\quad \gamma = -2.7(\pm .1)$

(c) for $40 < n < 200$ $\quad \gamma = -1.56(\pm .15)$

4.4 Single Particles

Region (a) can be regarded as determined predominantly by the distribution of pulse heights of single muons passing

through the detector. The two contributing factors are the statistical distribution of response per unit track length in the scintillator, and the variation of total track length per particle with zenith angle.

The contribution of the latter effect can be calculated if it is assumed that the intensity at a zenith angle, θ, is given by

$$I(\theta) = I_0 \cos^2\theta \qquad \ldots . 4.1$$

This relation appears to apply fairly accurately for $\theta < 80^\circ$ (Wolfendale, 1963).

The intensity of particles per sq.metre of detector with a zenith angle, θ within $d\theta$ will then be proportional to $\cos^3\theta \sin\theta \, d\theta$.

Integration yields for the rate of particles, with zenith greater than θ:-

$$R(>\theta) \propto \sec^{-4}\theta$$

the track length inside a flat detector of infinite area, for a zenith angle θ, will be proportional to $\sec\theta$. Hence the rate of track lengths greater than d for fully penetrating particles is of the form

$$R(>d) = R(>\sec\theta) = C\sec^{-4}\theta$$

where C is independent of θ.

Thus due to the zenith angle distribution, the integral spectrum due to single muons should have an exponent of

about -4. The slight flattening observed (-3.3) is probably due to the statistical broadening of the response per unit track length and the inaccuracy of equation 4.1.

The "kink" in the spectrum in the 4 to 5 particle region must indicate a fairly sharp cut off of the angular effect because of the finite dimensions of the detector. Although the maximum track length would yield a response equal to about 10 vertical muons, beyond 4 to 5 equivalent particles the proportion of the detector unit in which longer path lengths are possible rapidly diminishes.

4.5 The Contribution of Extensive Air Showers

In the region beyond 40 equivalent muons the curve assumes a slope of about -1.6 up to densities as high as it is practicable to measure. This region is interpreted as due entirely to the effects of EAS.

To a first approximation the density spectrum is simply related to the number spectrum of showers if the integral number spectrum for EAS near sea-level is represented by a power law of the form:-

$$F(>N) = KN^{-\gamma'} \qquad \ldots . 4.2$$

In order to contribute to a density of n at a particular point the axis of a shower of size N must fall at a distance r.

The differential density spectrum due to EAS is then

$$R(n)dn = \int_0^\infty \int_0^\infty 2\pi r F(N) dN dr \qquad \ldots\ldots 4.3$$

where from equation 4.2

$$F(N)dN = KN^{-\gamma-1/2}dN.$$

If f(r) is the structure function for charged particles in EAS, then

$$n = Nf(r).$$

If this structure function is assumed to be independent of shower size N, equation 4.3 can be integrated.

Then $R(n)dn = \text{const. } n^{-\gamma'-1}dn.$

from which $R(>n) = \text{const. } n^{-\gamma'}$.

The exponent, γ', of the integral number spectrum for showers is thus the same as that of the density spectrum.

The value of γ obtained from figure 4.1 agrees closely with that of other workers.

4.6 Local Showers

Below a response equivalent to about 40 particles the effect of EAS is smothered by a contribution of much greater intensity. The observed intensity of response in this region has been found to be independent of area. The sources of the pulses must be confined to a narrow region and these pulses have therefore been called local showers

(Green and Barcus,1959;Miyake,1962). These authors have suggested that the local showers can be attributed to incident nucleons.

In their response to ionisation, scintillation counters are quite similar to pulse ionisation chambers. A detailed study of the "burst" spectrum in such ion chambers has been made by Carmichael and Steljes (1955).

A single muon traversing 10 cm. thickness of scintillation gives up about 20 MeV in energy of ionisation. In the same thickness a slow proton can lose 100Mev, while if it travels horizontally it can lose considerably more. The flux of nucleons at sea-level is about 1% of the total muon flux (Brooke and Wolfendale,1964). Thus it is reasonable to expect pulses of ionisation five times larger than for a single muon at a rate 10^{-2} that of the muons. Moreover, there is an approximately 10% chance of an incident nucleon interacting in the scintillator e.g. with a carbon nucleus, leading to the production of two or more outgoing protons with similar energy. Pulses equivalent to ten muons at a rate 10^{-3} of the muon rate could thus also be explained.

If it could be assumed that the scintillation light output is proportional to ionisation independently of whether the ionisation is produced by muons or protons, the observed pulse distribution would thus be fully accounted for.

However, a more realistic estimate is that in the scintillator liquid, the scintillator efficiency is about 10 times less for protons than for muons (Barton,1965). The interpretation in terms of nucleons therefore remains in doubt.

Measurements have been made of the spectrum when increasing thicknesses of absorber are placed over the scintillation detector. A 1" thick steel plate gave an increase in the number of large pulses presumably due to cascades from the soft component. However there is very little difference in the pulse spectra for no shielding; 5 cm. of lead; and 15 cm. of lead. One would expect nucleons to be reduced in number by a factor of two or so by absorption in the lead, and the observed attenuation is more consistent with a muon origin of the pulses.

The barometer coefficient for the ionisation of counting rate with pressure was measured with a scintillation counter under lead, at a discrimination level equivalent to about six vertical muons. The result, 4% per cm. of Hg, is in closer agreement with the known barometer coefficient for the muon component rather than the nucleons.

4.7 The Spectrum from a Plastic Scintillator

The integral pulse height spectrum was also determined

for a 1.1 sq.metre area plastic scintillator detector, of 7.5 cm. depth. The scintillator was viewed with a 5" photomultiplier by diffuse reflection (Dufresne, 1965).

The density of the plastic (NE102) is 1.03 grms/cm^2. so that the absorption depth of 7.7 grms/cm^2. was little different from the liquid scintillator used previously.

The integral spectrum is shown in Figure 4.2 where the response has been normalised to give the same rate as the 2.5 sq.metres of liquid scintillator above a level corresponding to about 1/3rd. of a vertical muon. This means that the rates recorded by the plastic scintillator have been increased by the ratio of the areas of the two detectors.

The discrepancy at the EAS end of the spectrum is easily explained as due to the difference in area of the two detectors. Although the rates have been increased in the ratio of areas (2.3) a shower producing a density equivalent to a response of n particles the plastic will produce a response of 2.3n particles in the liquid scintillator. The rates of these different responses should be the same.

A more significant difference between the two spectra is the disappearance of a "kink" at around five equivalent muons. This might be explained as a difference in the form

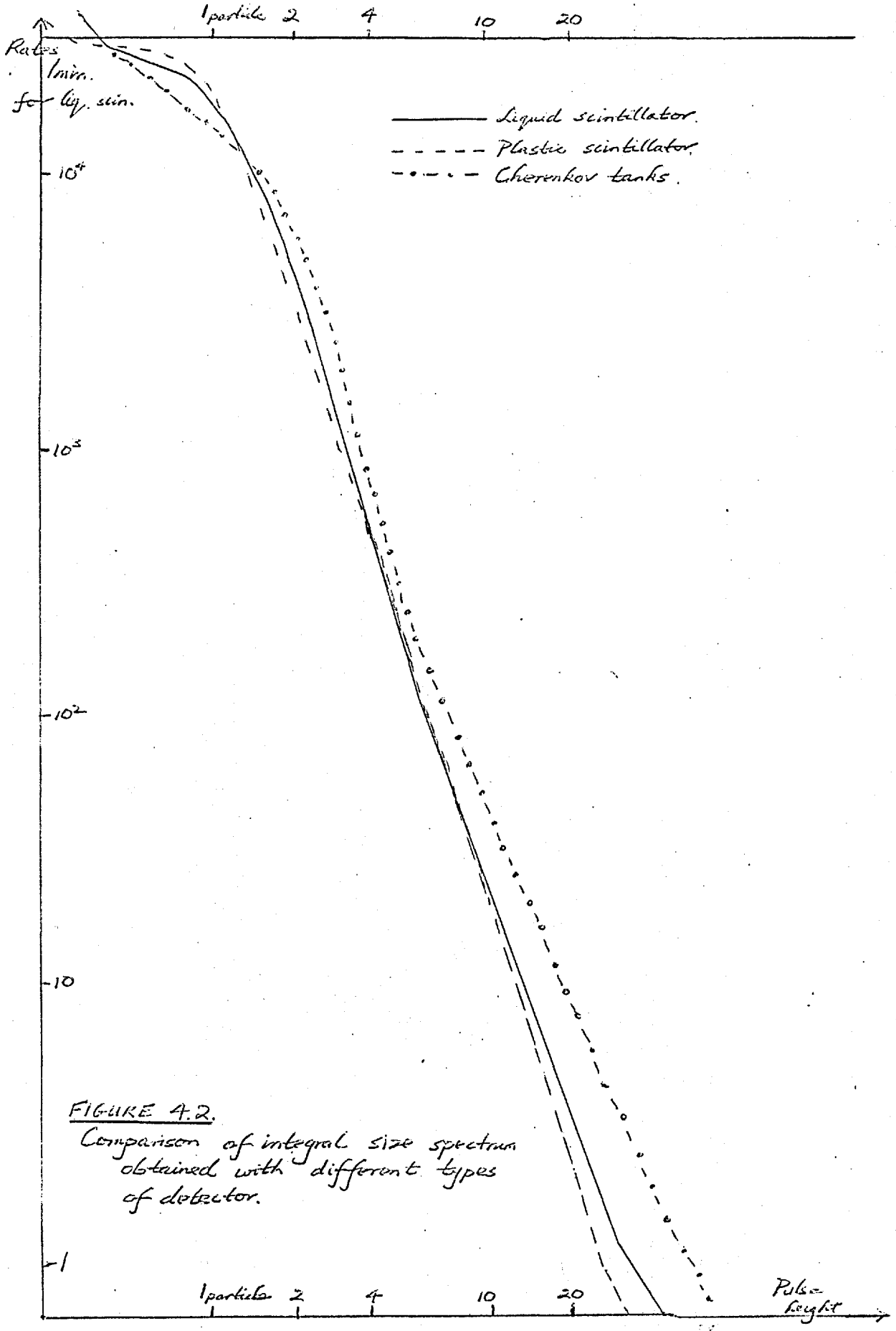


FIGURE 4.2.
Comparison of integral size spectrum obtained with different types of detector.

of the "local shower" response in the plastic causing the spectrum to run smoothly into the single particles. Since both types of detector represent approximately the same thickness of matter (8 grms/cm^2.) it is difficult to see how the observed effect could be so great on this explanation.

A more likely reason appears to lie in the different optical set-up of the detectors and in particular their different distribution in uniformity of response (Figure 4.3).

In the case of the liquid scintillator the mean of the response curve lies above the mode, leading to a broadening of the single particle response towards higher pulse heights. The effect of this broadening is to raise the single muon region of the spectrum above the local shower curve leading to enhancement of the change-over at around five particles.

For the plastic scintillator arrangement the mean lies below the mode, broadening the single particle response towards lower pulse heights. This broadening merges the single particle region into a smooth spectrum with the local showers.

Experimental evidence in favour of such an explanation was obtained by introducing a large non-uniformity into the plastic response by reducing the light reaching the photo-multiplier from about $\frac{3}{4}$ of the detector by a factor of about 2, leaving a region of normal response. An integral spectrum

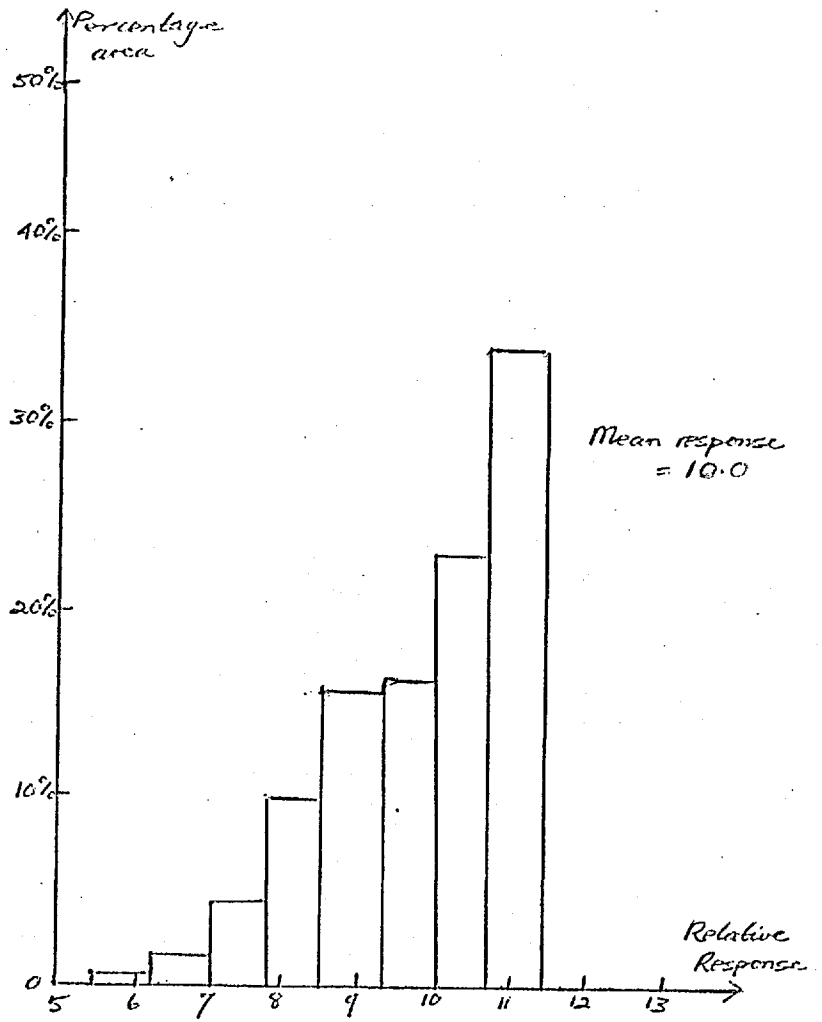
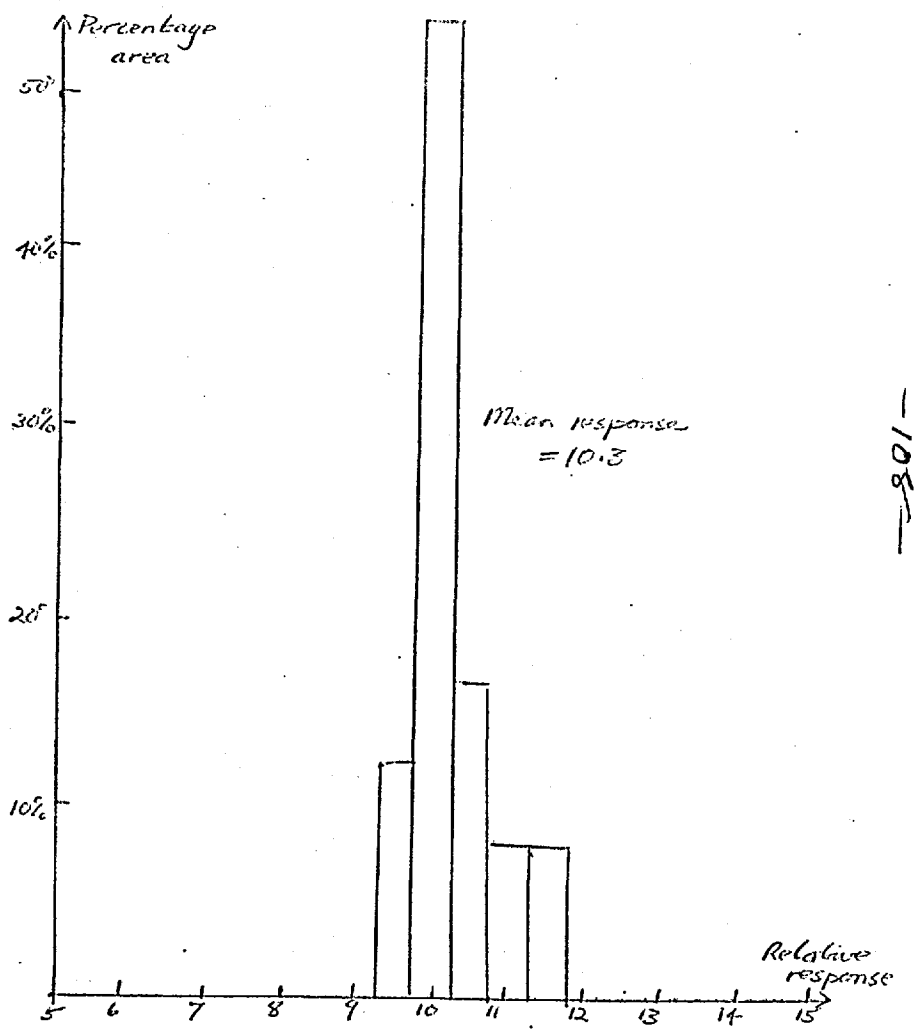


FIGURE 4.3. (a) Uniformity response of plastic scintillator.



(b) Uniformity response of liquid scintillator.

taken with such an arrangement showed a slight change of slope at around the 5 particle level.

4.8 The Pulse Height Spectrum from a Cherenkov Tank

Also shown in Figure 4.2 is the integral pulse height spectrum obtained from a large Cherenkov water detector, 2.25 sq.metres in area and about 1.2 metres deep. The spectrum shows distinct differences from that obtained from the scintillators.

The most important result however, is the continued presence of "local showers" in the region 4 to 40 equivalent vertical muons. Since the Cherenkov tank responds only to relativistic particles ($v/c \sim 0.7$), processes involving slow protons must now be disregarded.

A possible cause of these local showers is the production of electron-photon cascades in the water due to single incident high energy electrons and photons. Cascades produced in the air a few radiation lengths above the tank are spread laterally to an extent which greatly reduces their effectiveness for generating Cherenkov light in the tank. However to explain the high flux of local showers it is necessary to assume that the flux of unassociated high energy electrons and photons at sea-level is considerably greater than the published values.

An alternative interpretation of large responses from the Cherenkov detector in the region around 10 equivalent muons can be sought in the optical properties of the detector. Single particles with large zenith angles ($>40^{o}$) traversing the water near the photomultiplier could be expected to emit a relatively large amount of Cherenkov light straight onto the photocathode of the tube. Calculations indicate this might well explain the presence of local showers.

In order to clarify this problem a detailed set of experiments has been undertaken on the Cherenkov detectors (Allan et al.,1965). The experiments so far performed, both at sea-level and underground (60 m.w.e.), lead to the conclusion that the "local showers" are muon induced. However the explanation offered above in terms of direct light onto the photocathode cannot hold since with a black bottomed tank (i.e. non-reflecting) the phenomenon of "local showers" largely disappears.

4.9 Conclusion

The detailed mechanism by which "local showers" are produced is still not clear. It seems impossible that an explanation of the pulses in the Cherenkov tanks can be made in terms of incident nucleons. It does however seem likely

that the source of these pulses is the same for both types of detector and experiments to date indicate that their origin should be sought for in muons.

It maybe that the local showers really represent a combination of a number of effects and a further series of experiments is planned to help solve the problem.

CHAPTER 5

THE MEAN LATERAL DENSITY DISTRIBUTION OF MUONS IN SHOWERS OF SIZE $5 \times 10^6 - 10^8$

5.1 Introduction

The lateral spreading of muons to distances in excess of one kilometre from the core of an EAS indicates that the angular spread of the parent pions must play the dominant role in determining the lateral distribution in showers observed at sea-level. Coulomb scattering by atmospheric nuclei and deflections in the earth's magnetic field also contribute to a smaller extent ($\sim$100 m.).

The low interaction cross-section of the muons and their relatively long mean lifetime enable a large proportion of those created high in the atmosphere to reach the earth's surface. Thus a small angular divergence of muons from the shower axis at their production level leads to a large radial spread at sea-level.

The density distribution of muons in a shower as a function of the distance from the axis can thus be expected to contain information both on the character of the early nuclear interactions and on the nature of the primary

particle. The density distribution integrated over the whole shower front allows the total number of muons as a function of shower size to be determined.

For showers of size around 10^6 particles the lateral distribution has been accurately measured out to distances of several hundred metres from the core. Greisen (1960) using results obtained by the M.I.T. Group (Clark et al., 1958) derives an empirical structure function for muons

$$\rho_\mu(N,r) = 18(N/10^6)^{\frac{3}{4}} r^{-\frac{3}{4}} [1+(r/320)]^{-2.5} \quad \ldots\ldots 5.1$$

where ρ_μ represents the number of muons of energy greater than 1 Gev per sq.metre at a distance r metres from the shower axis. Greisen also concludes from experimental points that the lateral distribution is not a strong function of the shower size, N.

In recent years intensive effort has gone into looking at the muon content in individual showers in the size range around 10^5- 10^6 particles. This work has been undertaken largely with the view to picking out "muon-less" and"muon-rich' showers and studying their distribution of arrival directions. EAS arrays in Bolivia, Moscow, and Tokyo incorporate large shielded detectors for this purpose. Correlations in the fluctuations of the muon numbers with fluctuations in the other secondary components are also being investigated (Chatterjee et al.,1963).

On the other hand, little work has been done on establishing the muon density distribution in showers of size $> 10^7$ particles at distances exceeding 300 metres from the core. In view of the importance at present being attached to the question of the composition of the primary particles of energy greater than 10^{16} eV an accurate determination of the mean muon lateral distribution is important.

The present experiment was set up with this aim in mind. The experimental details and initial results are presented in this Chapter.

5.2 Experimental Details

A detailed description of the detector units is given in Chapter 2. Considerations of minimum useful area, cost and available space led to the construction of 10 sq.metres of liquid scintillator shielded with lead. This consists of four separate units arranged in one of the outer stations of the 500 metre array as shown in Figure 2.6.

Twelve thousand lead blocks (6"x 2"x 2") are used to shield the detectors from the electromagnetic component. The lay-out of the shielding of one of the units is shown in Figure 5.2. A 20 cm. (8") thickness of lead covers the long sides and top of the detector. The overlap (9") of the

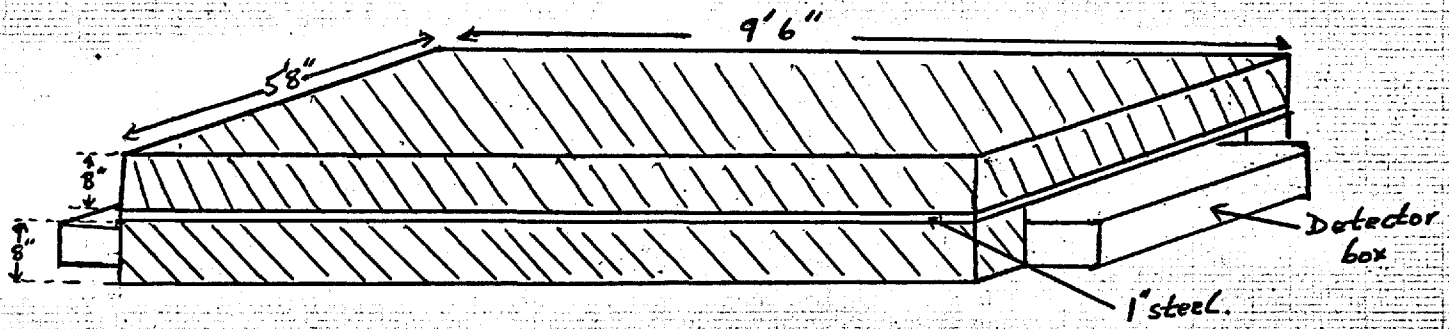


FIGURE 5.2 Sketch showing layout of shielding over a 2.5 sq. metre detector unit.

shielding at the photomultiplier ends of the detector ensures that only particles from showers having both a zenith angle above 60° and an azimuthal angle within a small range can reach the active area of the detector without passing through at least 10 cm. of lead. Such showers can be rejected in the analysis.

Figure 5.3 shows a block diagram of the recording system. Pulses from the photo-tubes are first added in pairs, allowing the total response of each detector unit to be sampled and the responses of the four units are then added. The output pulses are clipped to 1 microsec. width by a shorted cable and fed into 10 microseconds of delay cable. The output from the cable was fed into the Y-amplifier of a cathode ray oscilloscope. The oscilloscope was set to give a time-base length of about 20 microseconds and a maximum Y deflection equivalent to the response of 10 particles.

Whenever an air shower causes the main 500 m. array to record, a coincidence pulse is sent back to the outer station through an underground cable. This coincidence pulse triggers the time-base circuit of the oscilloscope so that a pulse due to the passage through the shielded scintillator of any muons associated with the EAS is observed. The time-base output from the oscilloscope triggers an automatic camera

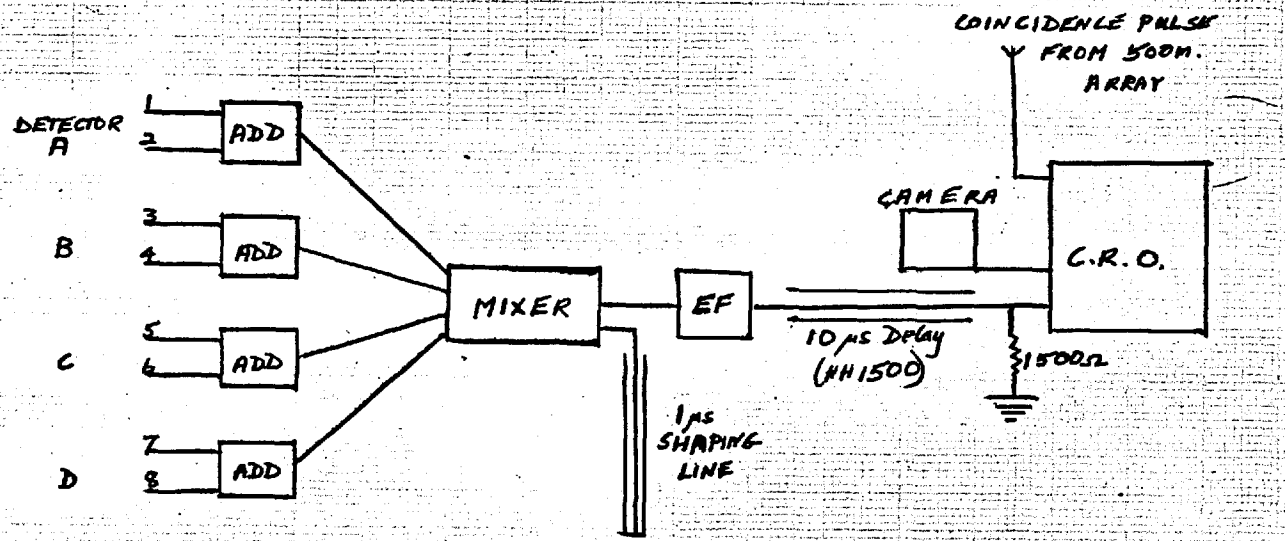


FIGURE 5.3. Block diagram of recording system

which records the muon pulse height on film. A message register number which is advanced every $\frac{1}{2}$ minute is also recorded on each frame. This allows the event to be easily correlated with the corresponding event on the main array film record and enables the time of its occurence (in GMT) to be determined.

A delay of 10 microseconds in the recording circuit is essential. This delay allows time for the Cherenkov pulses produced in the outer station by the shower to be transmitted to the central station (2.33 microseconds) to be recorded there as a coincidence between three stations (within 4 microseconds) and for the master coincidence pulse to be sent back to the outer Hut (2.33 microseconds).

Recently it has been found more convenient to have the recording oscilloscope at the central station, sending the detector pulses there by underground cable (Aerialite 363). This has enabled a considerable reduction to be made in the amount of delay cable used with a consequent improvement in the sharpness of the rise-times of the pulses.

A twelve position switch enables the output pulses from each tube and the added pulses from each detector to be monitored separately. By passing these pulses through a discriminator and into a scaler, a convenient check on the gains of the photomultipliers is obtained (Section 5.3).

5.3 Calibration and Checks on Response

Calibration of the detector units was carried out using the procedure outlined in Chapter 2 for finding the mean response to single vertical muons. Due to the layout of the detectors the three units of the telescope had to be placed above the lead shield. Such an arrangement yields a mean pulse height not appreciably different from an arrangement that ensures that the vertical muons pass right through the detector.

During calibration a coincidence from the telescope, placed over the centre of a detector unit, was used to trigger the time-base of the recording oscilloscope. Conditions were otherwise the same as during the main running of the experiment. This ensured that errors such as mis-matching did not creep in during calibration. The mean pulse height, with a 5% correction to allow for non-uniformity and a small correction for the finite angle of the telescope, was taken as the mean response for a vertical muon.

A mercury contact relay pulse generator set at 1 volt output was used to supply pulses to calibrate the film. These "standard" pulses were fed into the recording system instead of one of the tubes and recorded on the beginning and end of each film. The same pulse generator and procedure

was used in putting calibration pulses onto the films recording the muon densities in EAS. The stability of the pulse generator was checked at intervals with a standard AVO meter.

Initially one unit was calibrated accurately to within 2% so that its output response was about 75 mV/particle. The other three units were aligned with this by adjusting the E.H.T. applied to the tubes till the counting rates above a fixed discriminating level (equivalent to about 2 vertical muons) were the same for each detector unit. During adjustment the pairs of tubes in each detector were kept closely balanced.

The calibration of all four detectors was then checked using the scintillator telescope and the multichannel pulse height analyser.

For vertical showers the active area of total shielded detector is 10 sq.metres. The thin geometry of the detector units means that the projected area of the detector in the plane of an inclined shower is very closely a linear function of sec θ, where θ is the zenith angle of the shower axis.

Because of the small angular deflections of muons in EAS it is safe to assume that within the limits of accuracy of calibration the muons arrive with the same direction as the axis of the shower. Hence the path length of the muons

in the detector will increase in proportion to sec θ.

Tests with an inclined telescope have shown that the response of the photomultiplier is directly proportional to the path length. Thus the reduction in area of the detector in the plane of the shower front (with θ greater than zero) is exactly offset by the increased path length inside the detector. In practice this means that the response of the detector to showers of any zenith angle, in units of vertical muon response, is accurately the density per 10 sq.metres in the shower front.

Confidence in the calibration procedure was obtained by plotting histograms of the response of the detector to showers for different zenith angles. The histograms show that the output pulses are broadly distributed into units of integer vertical muons with the unit increasing for large zenith angles in keeping with the increase in path length.

Checks on the response of the detector were made as often as possible, at least several times a week. For this purpose the counting rates from the separate tubes were recorded through a discriminator set at a fixed voltage level. Recalibration of the detector units was undertaken whenever the normal running of the detector had been upset, for example by a power-cut.

5.4 Shower Analysis

A brief description is given in Chapter 2 of the operation of the 500 metre array. The film record for each event yields nine quantities for use in calculating the main parameters of the shower. These are:- the relative times of arrival of the shower front at the four stations; the nominal particle density at each station in units of equivalent vertical muons per sq.metre; and the time of occurence of the event, in GMT, to the nearest $\frac{1}{2}$ minute.

During the running of the muon experiment analysis has been carried out using an IBM 7090 computer at Imperial College. Although to a certain extent this has duplicated the analysis performed by the Leeds University Group on an English Electric KDF9, the facilities of the 7090 have been very useful in extracting the information most relevant to the muon experiment.

The programme procedure has been to calculate first the arrival direction of each shower with respect to a horizontal plane. The times of arrival at the three outside stations are generally used for this, on the assumption of a plane shower front. The zenith angle, θ, and azimuthal angle, ϕ, (measured eastwards from north) are determined for the

direction of arrival of the shower axis. Small corrections have to be applied since the four detectors do not lie in a horizontal plane. The time of occurence of the event together with θ and ϕ then enable the right ascension and declination, on the assumption that the direction of the shower axis is identical to this. An attempt is also made to determine the radius of curvature of the shower front from the relative times.

The core position and shower size are calculated from the "nominal densities". A structure function of the form;-

$$D = kNr^{-n} \qquad \ldots\ldots 5.2$$

is assumed, where D is the nominal density, k a normalisation constant, N the shower size, r the distance from the axis, and n an empirically derived structure function exponent.

Using equation 5.2 an initial core position is found for each shower. This involves solving three simultaneous equations containing the ratio of the nominal densities and the three unknowns, X and Y (the co-ordinates of the core position) and the structure function exponent n. The exponent n is varied within defined limits to give the best fit.

The next stage is to adopt an empirically derived mean value of n (dependent on zenith angle) and use this to determine the best position of the axis by the method of least squares fitting. This involves minimising the function

$$\chi^2 = \sum_{i=1}^{4} W_i (D_i^{obs.} - D_i^{calc.})^2$$

where the weights, W_i, are equal to the square of the standard error in the observed density, $D_i^{obs.}$.

The calculated nominal densities, $D_i^{calc.}$, are obtained from equation 5.2 by using a best fit value of kN at each of the trial core positions.

In order to calculate the normalisation constant, k, assumptions have to be made concerning the absorption of EAS secondaries in the Cherenkov detectors. An equation expressing k as a function of θ has been derived by Dennis (1964) for a 10^7 particle shower at sea-level.

The shower size, N, is then determined from the calculated best fit value of kN at the final core position.

Using computed results from artificial showers Dennis has estimated that there is a probable error in core location of about 60 metres and that in the arrival direction determination there is an average total angular error of 6-7°.

5.5 Treatment of the Muon Density Measurements

During the running of the muon experiment some 5,000 events were recorded by the array up to August 1965. Accurate size and core positions were obtained for about 60% of these showers. The others were rejected either because they fell

in positions which rendered as unacceptable the probable error in the density measurements at one of the stations, or because the empirical structure function could not be fitted closely enough to the densities.

An average of just over 2 muons were recorded per shower, although in only 50% of the events was more than one muon recorded. In order to obtain sufficient statistical accuracy it has been necessary to average a particular parameter over a large number of showers. This means that various assumptions have had to be made during the analysis.

It became obvious from the results that the density of muons in a given distance interval from the axis does not increase directly in proportion to the shower size, N. It is important in normalising the range of shower sizes to a particular shower size to determine the appropriate power law dependence.

On the assumption that the density of muons as a function of size and distance, $\rho_\mu(N,r)$, is given by an expression of the form:-

$$\rho_\mu(N,r) = CN^{\alpha} f(r) \qquad \ldots\ldots 5.3$$

it is necessary to determine α before statistically significant curves for f(r), the lateral distribution function, can be obtained by normalisation over a wide size range. For this purpose it must be assumed, in the first instance, that

the form of f(r) is independent of shower size.

5.6 Size Dependence of "ρ_μ"

Initially showers in a narrow size range, $1x10^7$-$2x10^7$ particles, were selected. A "log-log" plot of the mean ρ_μ against distance for these showers yielded a best straight line slope of -2.1 between r = 300 metres and 1,000 metres. This slope is almost the same as that given by Greisen's equation 5.1 for the same distance range. This supported other experimental evidence that the exponent of the lateral distribution is independent of the size in the size range 10^6-10^8particles.

On this assumption the points at varying distances within a size range can be normalised to a particular distance without introducing a bias dependent on the size interval chosen.

In order to make use of such a procedure the showers were divided up into eleven size intervals from 10^6-10^8 particles and eight distance intervals from 300-1,200 metres. In each size range the muon densities were "normalised" to a distance of 550 metres using a -2.1 exponent law and weighted by the total number of muons in the interval range.

Showers in two zenith angle ranges were selected.

Figure 5.4 shows the results for zenith angles $\theta < 40^{\circ}$ and $40^{\circ} < \theta < 65^{\circ}$. Best straight lines are fitted to the points.

Two important results are evident from the graphs:-

(a) The exponent α increases with increase of zenith angle. This is to be expected at high zenith since the secondary particles in a shower become mainly muons due to the large thickness of atmosphere traversed.

(b) The mean number of muons, in the distance interval 300-1,200 metres from the core, varies with shower size as:-

$$\rho_{\mu}(550\text{m.}) = AN^{0.56}(\pm.05) \qquad \ldots\ldots 5.4$$

where A is independent of N.

It should be pointed out that N here represents the size of the shower as determined by the Cherenkov detectors on the assumption that equation 5.2 holds. If the size dependence of ρ_{μ} given by equation 5.4 is correct than the assumption that the shower size varies directly proportional with the Cherenkov response at a fixed distance from the axis, no longer holds.

The water Cherenkov detectors, although sensitive to all relativistic charged particles, respond differently to the incident electromagnetic and muon components because of their large depths (3.4 radiation lengths).

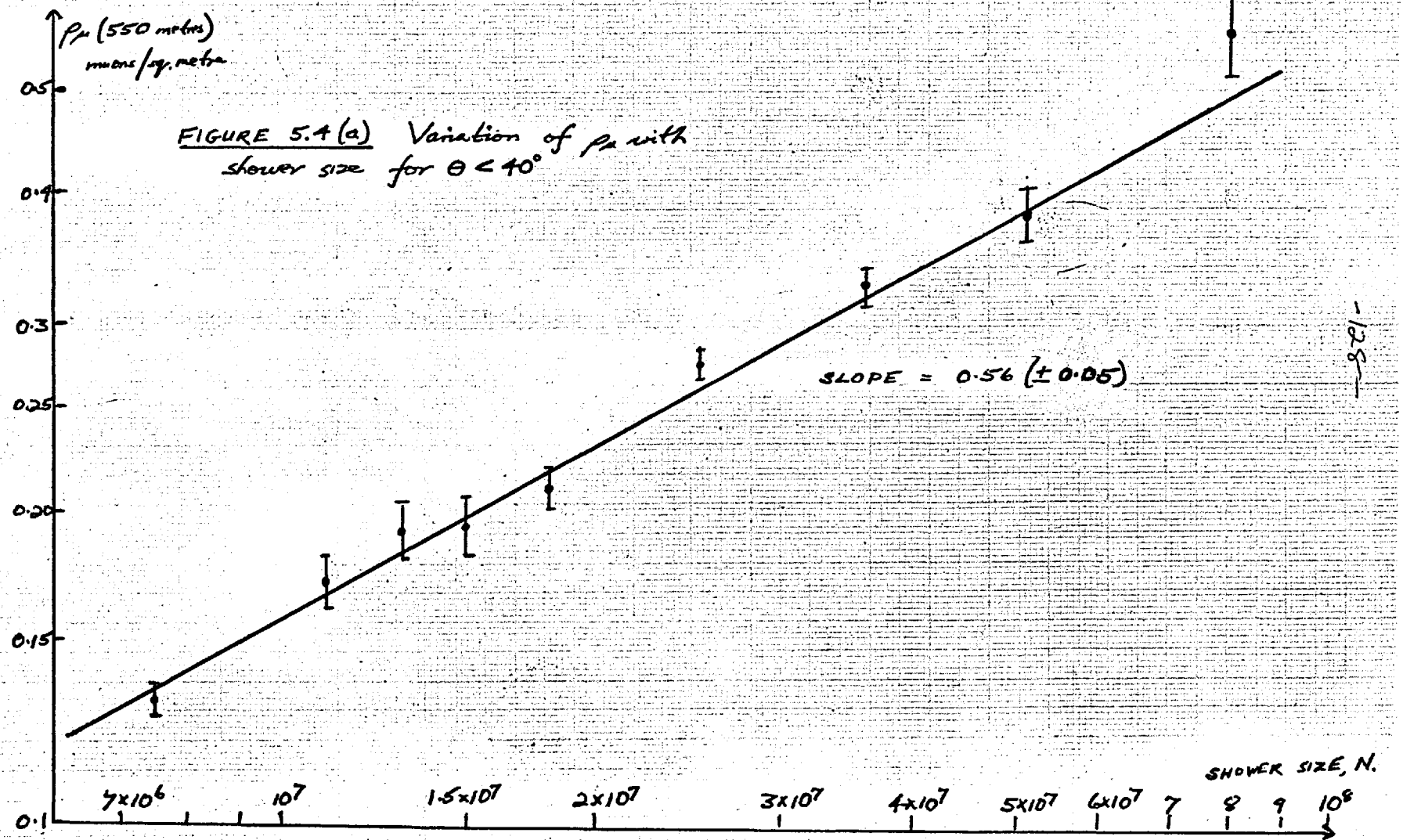


FIGURE 5.4 (a) Variation of ρ_μ with shower size for $\theta < 40°$

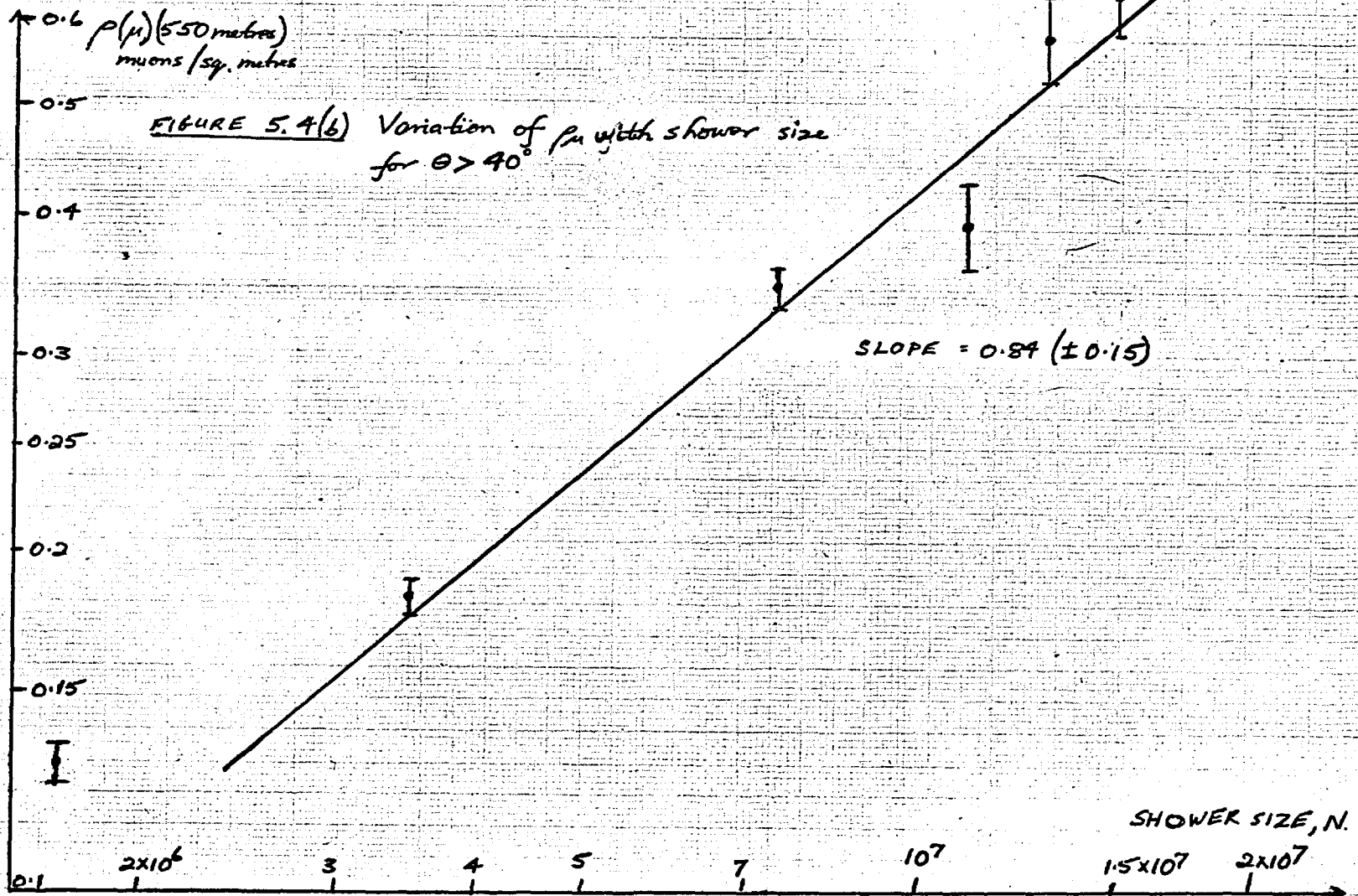


FIGURE 5.4(b) Variation of ρ_μ with shower size for $\theta > 40^\circ$

Calculations on the effect of cascading and absorption yield a value of 0.42 equivalent vertical muons per incident electron as the response of a Cherenkov detector to the electron-photon component. The "nominal density" as detected by the Cherenkov tanks is thus more dependent on the behaviour of the muon component than direct density detectors.

The effect that this "muon sensitivity" has on shower size determination is difficult to calculate exactly. However a quantitative indication of what is involved can be derived.

The proportion of muons to electrons increases from about 1% near the axis to 50% or so at 1,000 metres. Typically at 500 metres the proportion is about 35%. Assuming the 0.42 factor given above the "nominal density" as determined by the tanks at this distance is about 45% due to the electron-photon component and 55% to the muons.

As the number of muons is not proportional to shower size neither therefore will be the nominal density at 500 m. The normalisation constant in equation 5.2, k, will not then be independent of size. The shower size determined using this equation must result in showers greater than the "normalisation size" of 10^7 being underestimated in size, since the proportion of muons decreases.

If a power law of the form:-

$$N = N_o^{\beta}$$

is assumed where N is the Cherenkov determined size and N_o represents the actual total number of secondary particles, β will be less than 1.

To determine β , a typical distance from the axis was taken as 500 metres and the effect over the range 10^7-10^8 particles calculated. Over this size range it then appears that,

$$N = N_o^{0.90}(\text{approx.}) \qquad \ldots\ldots 5.5$$

This indicates that at a shower size of 10^8 particles the size is underestimated by about 20%.

The effect of this underestimation on the size spectrum as obtained at Haverah Park can be easily calculated. Dennis (1964) obtained a spectrum of the form,

$$I(>N) = K\left(\frac{N}{2\times10^7}\right)^{\gamma} \qquad \ldots\ldots 5.6$$

at sea-level where $\gamma = -2.2 \pm 0.1$ in the size range $2\times10^7 \rightarrow 2\times10^8$.

Assuming that N as calculated from the Cherenkov tanks varies as given by equation 5.5 the size spectrum, equation 5.6, should be corrected to

$$I(>N) = K\left(\frac{N_o}{2\times10^7}\right)^{-2.0\pm0.1} \qquad \ldots\ldots 5.7$$

This value of γ is in far closer agreement with the value obtained by other researchers at sea-level (Muira and Hasegawa,1962;Delvaille et al.,1962;Clark et al.,1961).

Equation 5.4 must also be modified to give the relation between "ρ_μ" and N_o. Applying equation 5.5, equation 5.4 now becomes,

$$\rho_\mu(550\text{m.}) = N_o^{0.50} \qquad \ldots . 5.8$$

5.7 Discussion on "ρ_μ — N_o" relation

The fact that α is less than 1 is consistent with simple theoretical ideas applied to the model of shower development outlined in Chapter 1.

A large number of the muons reaching sea-level are produced by pion decay near the top of the atmosphere. Charged pions formed in the nuclear cascade lower in the atmosphere tend to interact rather than decay because of the higher density of air nuclei encountered.

The number of charged pions formed at the top of the atmosphere increases only slightly with a higher primary energy. The pions that are produced are therefore more energetic and collimated. They will then have an increased probability of interacting rather than decaying, since the

number of grms/cm.^{2} of air encountered within their mean lifetime will increase. The proportion of muons in the shower as a whole therefore decreases with respect to the electron component.

Table 5.1 compares the value of α obtained in this experiment with that obtained by other workers.

Greisen's formula, equation 5.1, is based largely on results presented by Clark et al.(1958). Linsley et al. (1962) used only a limited shielding of 10 cm. of lead. The results of Hasegawa et al. represent only the upper edge of their $N_r N$ plots; their mean value is probably somewhat higher.

It is clear from Table 5.1 that there is a wide spread in the observed values of α . In view of the number of variable factors that enter into these experiments it is perhaps not surprising that closer agreement is not obtained.

The value of α obtained in the present experiment is considerably lower than has previously been obtained at sea-level. The experiment is however unique in the radial distance covered (>300 metres) which could suggest that α is a function of distance, r. This would lead to a size dependence in the lateral structure function for muons, f(r)

Author	Minimum Energy	Distance	Size	Altitude
Greisen (1960)	.75 1Gev			
Clark et al. (1958)	.70 1Gev	Near core	10^6-10^8	Sea-level
Vavilov et al. (1957)	.62 1Gev	200m.	10^5-10^6	3,860m.
Linsley et al. (1962)	.77 10cm.Pb	200-400m.	10^7-10^9	820grms/cm^2
Hasegawa et al. (1962)	.65 1Gev	200m.	10^5-10^6	Sea-level
Escobar (1963)	.9 .5Gev	10-50m.	10^5- 10^7	5,200m.
Chatterjee (1963)	.44 .5Gev	50m.	10^5-10^7	800grms/cm^2
Chatterjee (1963)	.60 1Gev	50m.	10^5-10^7	800grms/cm^2
Present Experiment	.50 .25Gev	550m.	$5x10^6$-10^8	Sea-level

Table 5.1 Comparison of α values.

(equation 5.3). However if f(r) is assumed to be a simple power law over the distance range under observation, results to be shown in section 5.12 are consistent with a constant exponent over the size range 10^7-10^8 particles.

There is a possibility that some of the non-proportionality in the N_μ-N relation is caused by a bias in the detection of showers by the array. Showers of size below 2×10^7 have to fall in preferred positions within the "collecting triangle" in order to trigger the array. The "collecting triangle" is the region enclosed by the three perpendicular bisectors of lines joining the three outer stations to the central one. All showers of size greater than about 2×10^7 falling within this region will trigger the array. A bias might occur due to the part played by smaller showers with abnormally flat distributions (i.e. low value of n in equation 5.2) triggering the array from positions at which a normal shower of equivalent size could not. This produces a detection bias towards flat showers at small sizes.

Results presented in section 5.12 confirm that such a bias probably does occur. However this is unlikely to be the cause of the experimental results as even for efficient showers ($>2\times10^7$) a value of α not far different from 0.56 must be fitted to the experimental points on Figure 5.4.

Another bias effect which might apply to showers over the whole size range is a systematic error in shower analysis caused by fluctuations in the density measurements. The importance of such a bias is discussed in section 5.12.

5.8 Dependence of α on Shower Size

A more significant conclusion which is suggested by the results of Table 5.1 is the possibility of a size dependence of α. The low value of α could be peculiar to the size range around 10^7-10^8 particles.

This would tie in closely with theoretical suggestions made recently to explain the steepening of the size spectrum of EAS in the range 5×10^5 — 5×10^7 particles. It is suggested that this region of shower size marks the change-over from showers produced by galactic primaries to those produced by metagalactic particles.

The galactic magnetic field is too weak to contain primary particles with energies much in excess of 10^{15} eV per nucleon. Particles of higher energy could escape into metagalactic space and a measurable intensity would not be built up inside the Galaxy as at lower energies.

The escape threshold depends on the rigidity of the particle and heavier nuclei will remain trapped to a higher

total energy than protons. Thus in the transition region a higher proportion of heavy galactic primaries than at lower energies will be expected.

Experimental results on multi-cored showers (Winn et al., 1965) lends support to this theory. Moreover experimental results on showers of size greater than 10^8 particles suggest that protons may predominate at these highest energies (Linsley,1963).

It is known experimentally that the proportion of muons decreases with increasing shower size. Thus if an EAS produced by a multi-nucleon primary can be regarded as a superposition of a number of lower energy proton initiated showers, the proportion of muons will be higher than in an equivalent size EAS produced by a single proton.

In the transition from galactic to metagalactic primaries it would therefore be expected that a fairly high value of α applies in the region 5×10^5 – 5×10^6 particles and a much lower value in the region 10^7-10^8 particles where the heavy galactic primaries give way to metagalactic protons. Above a size of 10^8 particles α should then return to its pre-transition value.

It is suggested that the present experimental value of α =0.50 for the shower size range 5×10^6-10^8 particles adds

weight to a theory as outlined above. Closer examination of the M.I.T. results reveal that both sets of data (Clark et al.,1958;Linsley et al.,1962) are not inconsistent with this idea.

The earlier M.I.T. figure of $\alpha \simeq 0.7$ was derived from a best straight line fit over the whole size range 10^5-10^8 and the results are by no means inconsistent with a change of α (from high to low) at around 10^7. Linsley's results cover the range 10^7-10^9 particles but a much lower value of α than that quoted in Table 5.1 could be applied to his points in the narrower size range of 10^7-10^8 particles.

5.9 The Mean Lateral Density Distribution of Muons

In order to plot the mean lateral density distribution of muons the distance range 300-1,200 metres was divided up into eight intervals. A mean density of muons normalised to a shower size of 2×10^7 was then determined for each distance interval.

To calculate this mean density the complete size range 5×10^6-10^8 was divided into twelve size intervals. In each size interval the total of the muon densities for the events were added and the sum normalised to 2×10^7 by using the $\rho_\mu \propto N^{0.56}$ relation. The total of the muon densities in

each event were given a statistical weight proportional to the square root of the total number of muons in that interval. The sum over all size intervals was then made. The mean muon density in the distance interval is given by:-

$$\rho_\mu(r) = \left[\frac{\sum_N W(dN,dr)(2\times10^7/N)^{0.5}}{\sum_N nW(dN,dr)}\right]\sum\rho_r \qquad \ldots\ldots 5.9$$

where n is the number of events in each interval, and W is is given by;-

$$W(dN,dr) = \sqrt{t(dN,dr)}$$

where t is the total number of muons detected in the size interval. This weighting is necessary to offset the importan given by the normalisation procedure to the low densities, and therefore the most susceptible to fluctuations, in the smaller size range.

Figure 5.5 shows a plot of the results for the zenith angle range $\theta < 40^\circ$. The errors shown are based on the total number of muons detected in each distance interval.

The zenith angle distribution for Haverah Park showers is rather broad due to the different relative sensitivity of the detectors to the various shower components (Wilson et al.,1963). The mean zenith angle for $\theta < 40^\circ$ is about 24°. The mean depth of the atmosphere for showers plotted in Figure 5.5 is therefore about 1,100 grms/cm^2.

A best fit straight line, of slope -2.1 ($\pm$0.1), has been drawn through the points. This line can be represented

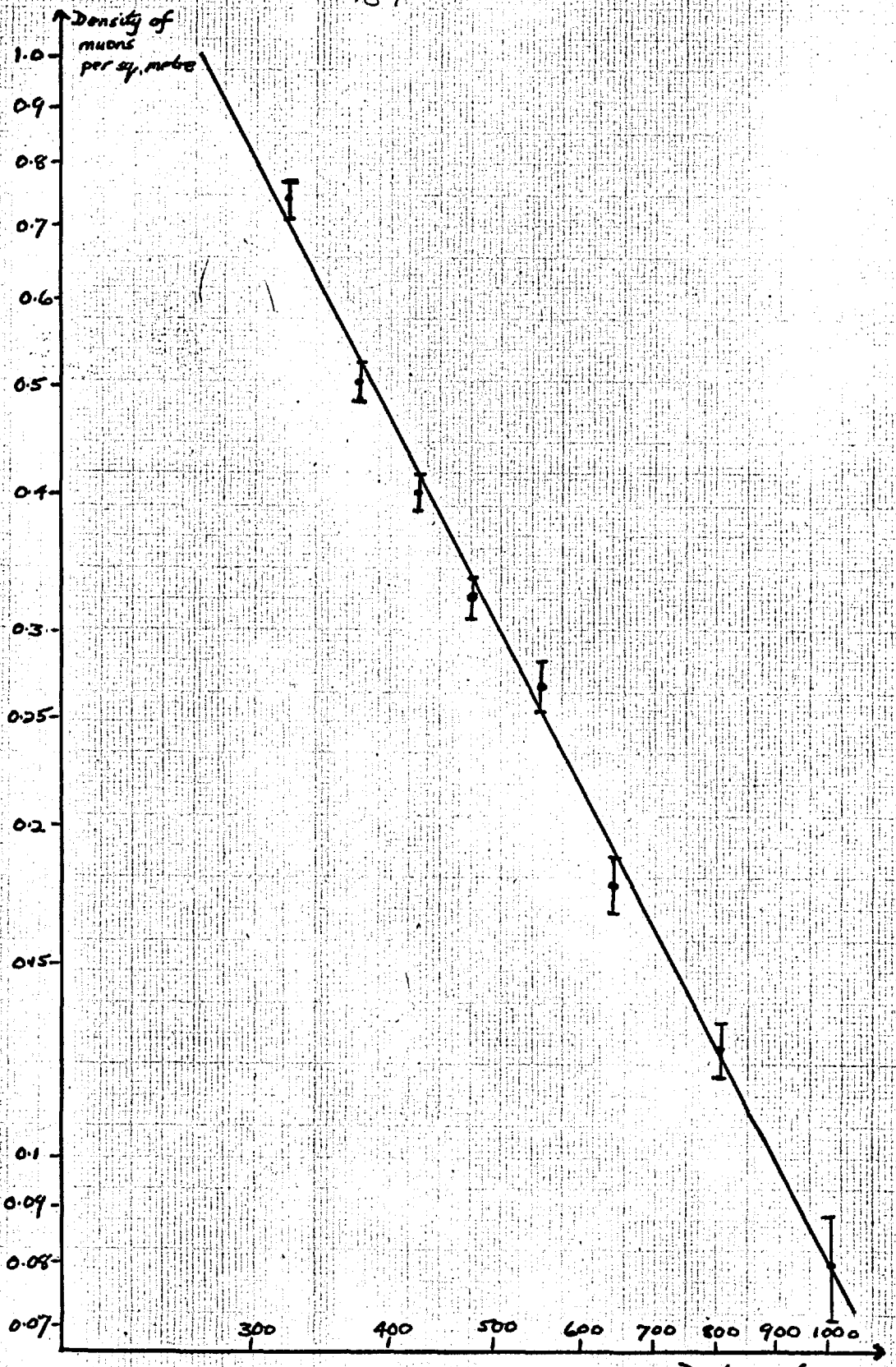


FIGURE 5.5 Lateral distribution of muons of energy greater than 250Mev for showers of size 2×10^7 particles

by the equation:-

$$\rho_{\mu}(r) = 1.35 \times 10^{5} r^{-2.1} \quad \ldots\ldots 5.10$$

for a mean shower size of 2×10^{7}, zenith $< 40^{\circ}$, energy > 250 Mev in the interval range 300-1,000 metres from the core.

5.10 Comparison With Other Work

The exponent of the muon density distribution, -2.1 ($\pm$ 0.1) is in close agreement with Greisen's 1960 review equation (5.1) over the distance range considered. This was based on results obtained at M.I.T. by Clark et al.(1958) for showers around 10^{6}.

In figure 5.6 the experimental points obtained from the Haverah Park results are compared with Greisen's formula using the energy dependence derived by Bennett et al. (1962) to adjust the low energy threshold down to 250 Mev. The experimental points of Clark et al. for showers of size $1 - 3 \times 10^{7}$ are also shown. The points at 200 and 275 metres were obtained under 60 cm. of lead ($E > 1$Gev) and the 850 m. point under about 30 cm. ($E > 0.5$ Gev) for $\theta < 25^{\circ}$. Also shown are the results from the Moscow group (Abrosimov et al., 1960) using a large area detector shielded by 5 cm. of lead plus 5 cm. iron having a low threshold of about 100 Mev.

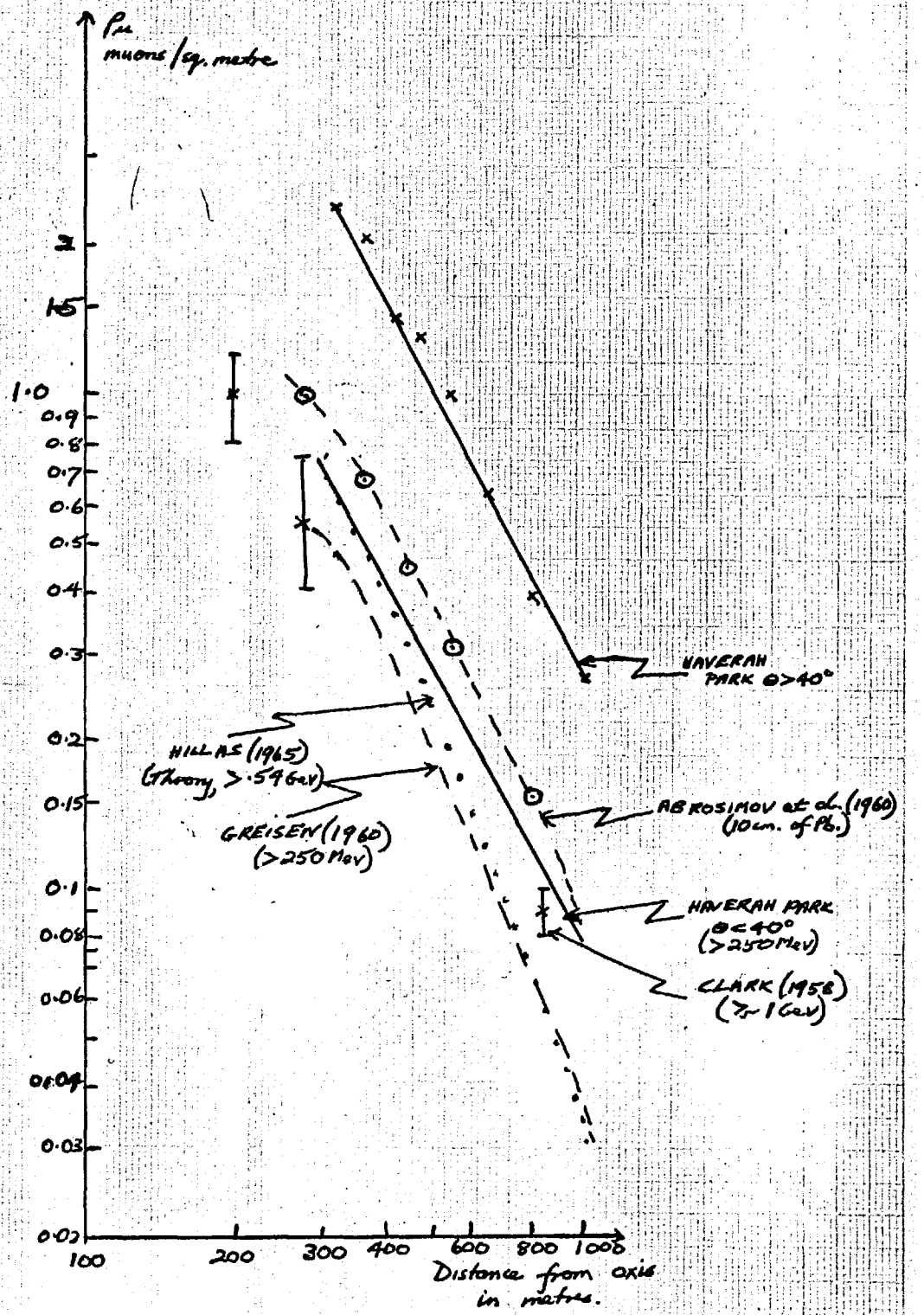


FIGURE 5.6 Comparison of Lateral distribution of muons as found by various workers. Normalised to showers of 2×10^7 particles.

Within the limit of quoted errors the present results are in good quantitive agreement with both sets of results. Greisen's formula appears to underestimate the number of muons per sq.metre by about 35% in this distance range, even after the energy correction has been made. It should be noted that the formula was normalised from a shower size of 10^6 using the $N^{0.75}$ dependence.

The Russian workers assumed that $\alpha = 1$ for their computations. They say however that if a value of 0.75 is assumed no significant change is obtained.

Hillas (1965) has computed the muon density distribution expected at sea-level from a 10^{17} eV proton corresponding to a shower size of about 2×10^7 particles. In preliminary calculations the muon distribution was attributed entirely to the initial projection angle of the parent pions and the subsequent slowing down, decay and magnetic deflection of the muons in an exponential atmosphere, were taken into account. The effect of Coulomb scattering was shown to be small and was ignored in the preliminary calculations.

These theoretical calculations are in close agreement with the experimental results obtained (Figure 5.6). Beyond 500 m. from the shower axis the integral muon energy spectrum (as computed by Hillas) is no longer flat in the region

below 500 Mev. The difference between the lower threshold of muons assumed by Hillas (540 Mev) and that set by the thickness of absorber in the present experiment (250 Mev) can almost completely account for the discrepancy between the theoretical and experimental results beyond 500 metres.

5.11 Variation of Lateral Distribution with Zenith Angle

In Figure 5.6 the lateral distribution for showers of zenith angle $40^{\circ} < \theta < 65^{\circ}$ is also shown. Again the showers have been normalised to 2×10^7 assuming that $\alpha = 0.8$. It should be pointed out that the distances from the axis are calculated in the plane of the shower front, normal to the shower axis.

The results are consistent with a best straight line slope rather flatter than that for smaller zenith angles. This is to be expected, since at these zenith angles the atmospheric depth (mean of about 1,900 grms/cm^2.) is such that showers are well past their maximum development. The nuclear cascade with its accompanying electromagnetic component will have almost died out. The lateral density distribution of the muons is slightly flattened by radial spreading.

There is an apparent increase in density of the muons

because at these zenith angles a large proportion of the secondary particles making up a shower of size N particles are muons. Consequently in normalising to 2×10^7 particles, the normalising factor (generally much greater than unity at these zenith angles) will raise the integrated number of muons in the recorded shower to a sizeable fraction of 2×10^7, with a corresponding increase in the computed muon density.

5.12 Variation of Lateral Distribution with Shower Size

In Figure 5.7 an attempt is made to plot the lateral distribution of muons as a function of shower size. Showers are selected in three size intervals:- $5 \times 10^6 < N < 1 \times 10^7$; $1 \times 10^7 < N < 2 \times 10^7$; $2 \times 10^7 < N < 10^8$. The muon densities are normalised to a mean shower size in each range as done in section 5.7.

Although the resulting plots are not statistically very accurate the following comments can be made:-

(a) For showers of less than 10^7 particles there is a bias towards detecting flat showers (i.e. with low value of the exponent n). This is indicated by the slope of -1.9 which is lower than that

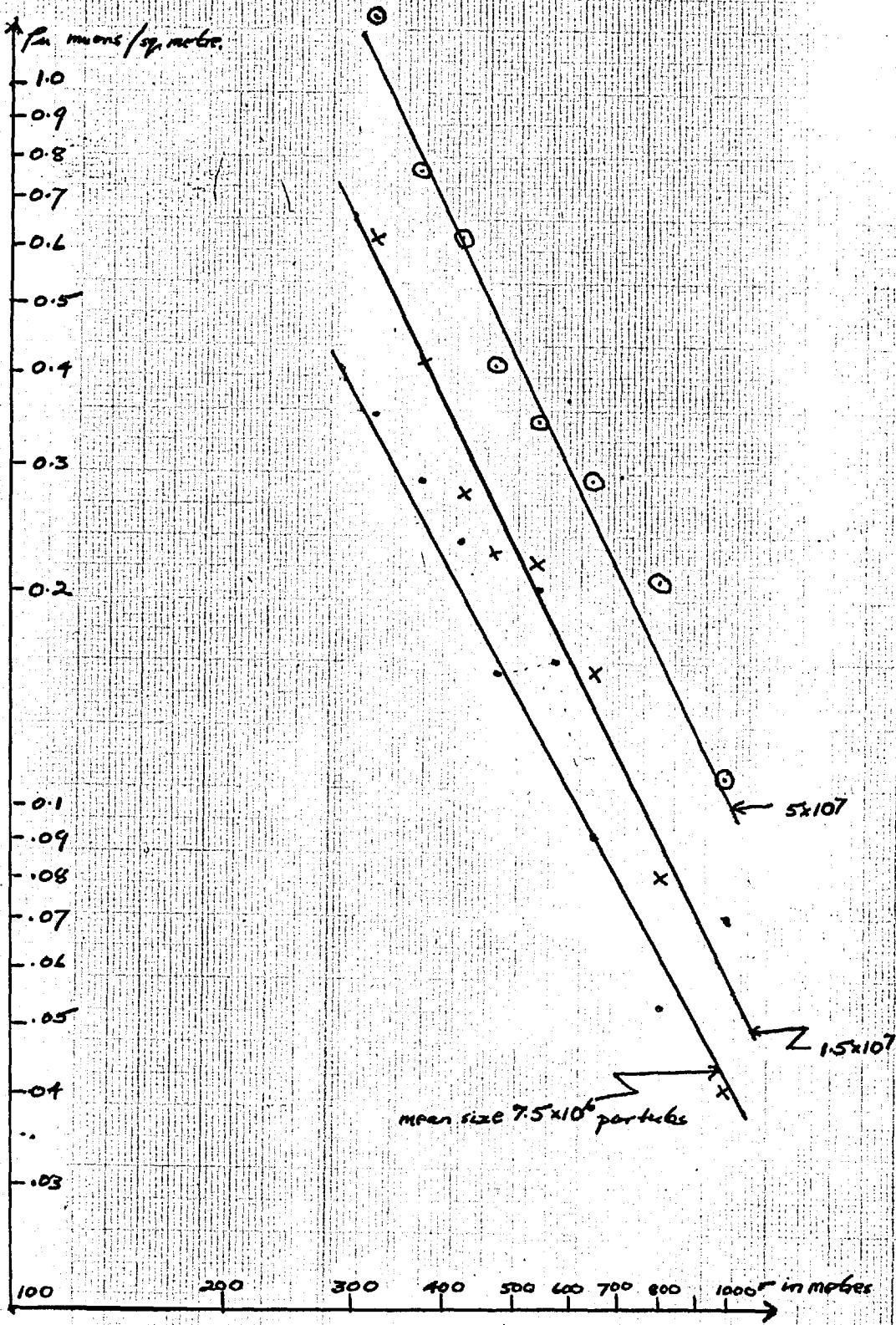


FIGURE 5.7 Lateral Distribution of muons as a function of shower size.

obtained by other workers for the same size range.

(b) There is no significant change with size for showers of around 10^7 particles.

(c) The absolute density of muons at a fixed distance from the core appears to increase roughly in proportion to $N^{0.5}$ in the size range $1x10^7 - 1x10^8$. This confirms the results of Figure 5.4.

(d) A significant distortion in the distribution occurs between 400 and 550 metres from the axis for all three size ranges.

These distortions are probably caused by a bias introduced by errors in the axis location of showers, arising from statistical fluctuations in the nominal densities at the four Cherenkov detectors. A large number of showers in this distance range from Hut 3 fall in regions where fluctuations can cause a systematic error in axis location and consequently in the size determination (Glencross,1963)(Figure 5.8).

The effect will be made larger than that suggested by Glencross for a smaller array due to the higher proportion of muons detected. The statistical fluctuations on an observed density of n electrons at 400 metres from the axis are much less than $n^{\frac{1}{2}}$ because the number of associated photons is large (about 10n). However with m muons the Poisson error distribution is just $m^{\frac{1}{2}}$ and this could be as

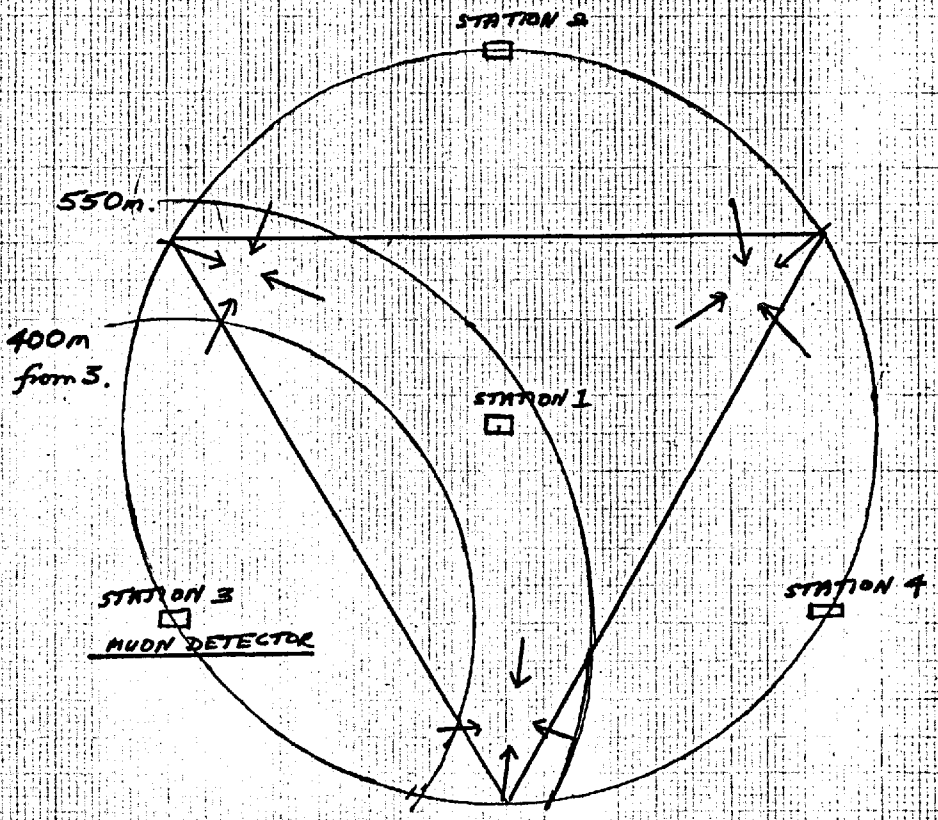


FIGURE 5.8. Diagram illustrating fluctuation effect of core location. There appears to be a systematic concentration of core positions near the corners of the collecting triangle

high as 50% of the total for showers just triggering the array It was shown earlier that about 55% of the nominal density at 500 metres is due to muons.

Without undertaking the difficult task of calculating quantitatively the effect of such fluctuations it seems unlikely that the errors are large enough to explain the discrepancy in the size spectrum or the low value of α .

5.13 General Conclusions

The lateral density distribution of muons presented in Figure 5.5 will be little affected by the errors discussed above. The agreement with other workers is good and little significance can be attached to the discrepancy with Greisen's formula which was based on a small amount of experimental data. There appears to be no significant change in the exponent of the lateral distribution with size at these distances. This is true over the full size range, 10^5-10^9 particles, as covered by published work.

It is suggested that the low value of the exponent, α , is probably associated with a change in composition of the primary particles in the energy range 10^{17}-10^{18} eV. The possibility of instrumental bias contributing to this low

value cannot however be disregarded.

Before a definite conclusion along these lines can be made a more detailed analysis of fluctuations introduced by a four detector array, as at Haverah Park, must be undertaken.

Future experimental work on muons over a wider range of size (10^5-10^8 particles), making use of the extensions to the detector array now being introduced at Haverah Park (see Chapter 6) should help to clarify this issue.

CHAPTER 6

FURTHER INVESTIGATIONS OF THE MUON COMPONENT OF EAS

6.1 Introduction

In addition to the determination of the muon lateral distribution of muons, the shielded detectors are useful for studying a number of other characteristics of EAS. In this chapter a description is given of the work done up to present and of the plans for future investigations.

A comparison of the lateral distribution of the response of unshielded and shielded detectors has been carried out in the distance range 300 — 1,000 metres from the shower axis. The initial results from such a study are presented in the following three sections.

The rest of the chapter is devoted to an outline of future plans. The 10 sq.metre shielded detector has just been moved to the central station where the lateral distribution experiments are to be continued and extended. Here the muon detector will be in operation close to a large shielded magnetic spectrograph which has been installed by the University of Durham Group to measure the energy of muons in EAS.

The construction of two smaller EAS detector arrays inside the present 500 metre array has just been completed. These will enable a detailed study of muons to be carried out over a much wider size range (10^5-10^8 particles) than has previously been the case at Haverah Park.

6.2 The Ratio of the Response to EAS of Shielded and Unshielded Scintillators

A 10 sq.metre area of unshielded plastic scintillator (NE102), 7.5 cm. thick, was installed for some time above the muon detector. This enabled a direct comparison to be made between the responses of the unshielded and shielded scintillators as a function of radial distances from the axis.

The wide statistical variation in the small number of muons detected for each event necessitates the use of average values taken over all showers within a certain distance interval. The ratio has therefore been derived from the experimental mean lateral distributions of the muon and unshielded detectors.

Figure 6.1 shows a plot of the radial distribution of the ratio for zenith angles, θ, less than 40°. The densities were normalised to showers of size 2×10^7 particles.

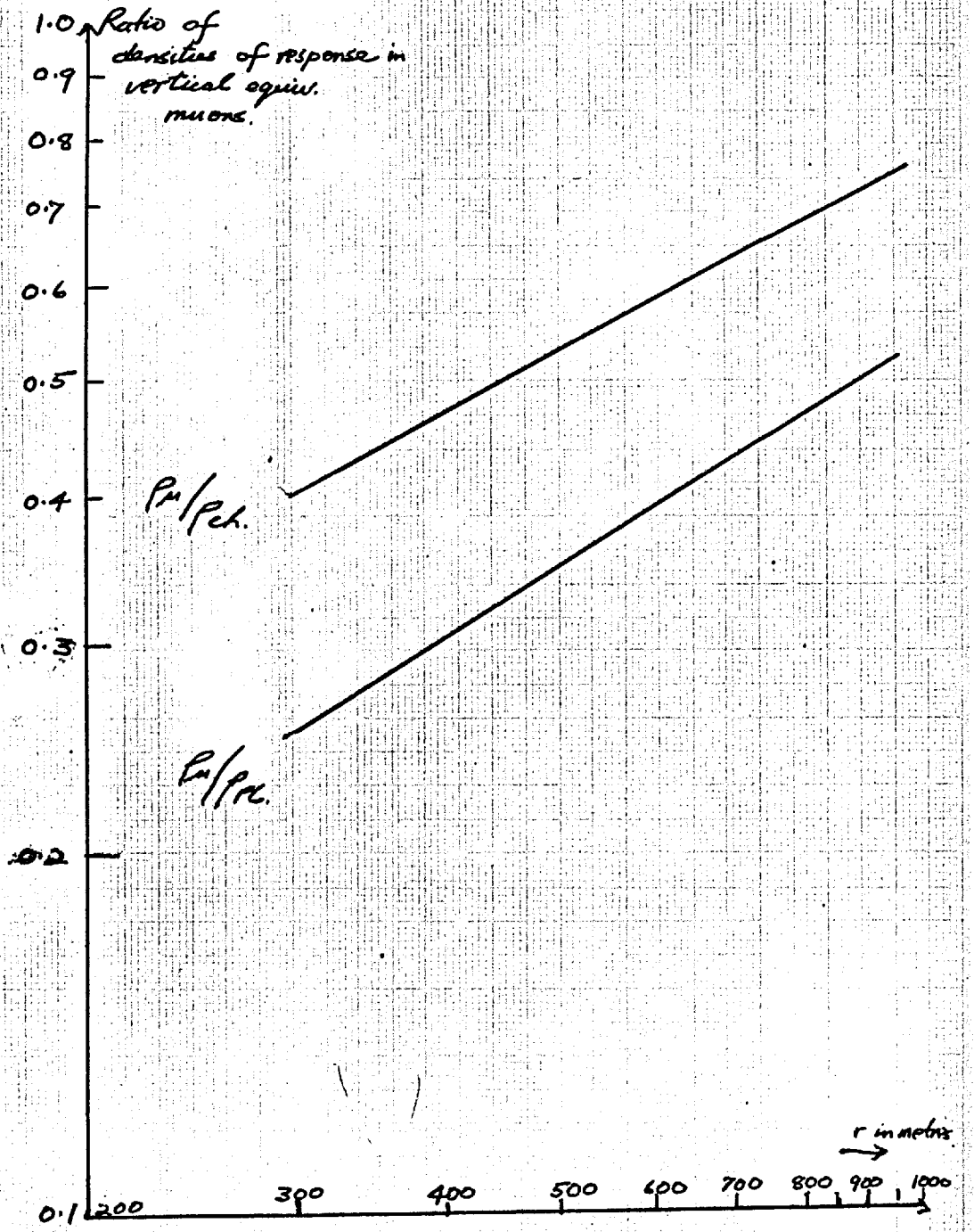


FIGURE 6.1 Variation of ρ_μ/ρ_{ch} and ρ_{em}/ρ_{ch} with distance from axis of shower (normalised to 2×10^7 particles) for zenith angles less than 40°.

The density response of the plastic scintillator is expressed in units of mV per vertical penetrating muon. Results have indicated that at these distances from the axis of EAS the response of the plastic scintillator represents fairly closely (within 10%) the actual density of charged particles (Towers, private communication).

On this assumption Figure 6.1 represents the proportion of muons to all charged particles in EAS as a function of radial distances. It is clear from the curve that at 1,000 metres from the core of a shower some 45%-50% of the secondaries are still electrons. The agreement with other workers at sea-level is well within their statistical errors.

There has not been sufficient work at lower shower sizes to determine how the muon:electron ratio varies over a wide shower size range. Such a determination over a range 10^5-10^8 particles should yield an important clue for any change in the composition of primaries. It is hoped that with the expansions now taking place at Haverah Park (Section 6.6) a detailed analysis over such a wide shower range can be made.

6.3 Comparison of Muon and Water Cherenkov Detector Response

The deep water Cherenkov detectors (3.4 radiation lengths deep) used in the main 500 metre array at Haverah

Park yield a mean response to shower secondaries intermediate between the shielded and unshielded scintillators when expressed in units of equivalent vertical penetrating muons. Whereas most shower muons go right through the tanks to give one unit of response, the response to the electron-photon component expressed as equivalent vertical muons per electron is less than one. A comparison of the two types of detector should help to determine tha amount of energy loss of this 'soft' component in the Cherenkov detectors.

The radial distribution of the ratio of the shielded scintillator response to that of the Cherenkov tanks is shown in Figure 6.1 for $\theta<40^{o}$. The curves show clearly the higher sensitivity of the tanks to the muon component.

Using the two curves shown in Figure 6.1 one can calculate how the mean response of the Cherenkov tanks to the electron-photon component of showers varies with distance from the shower axis. Figure 6.2 shows a plot of the mean response to the electron-photon component per electron expressed in units of equivalent vertical muons as a function of distance.

The solid line curve is obtained assuming that in the plastic scintillator there is a mean response per shower

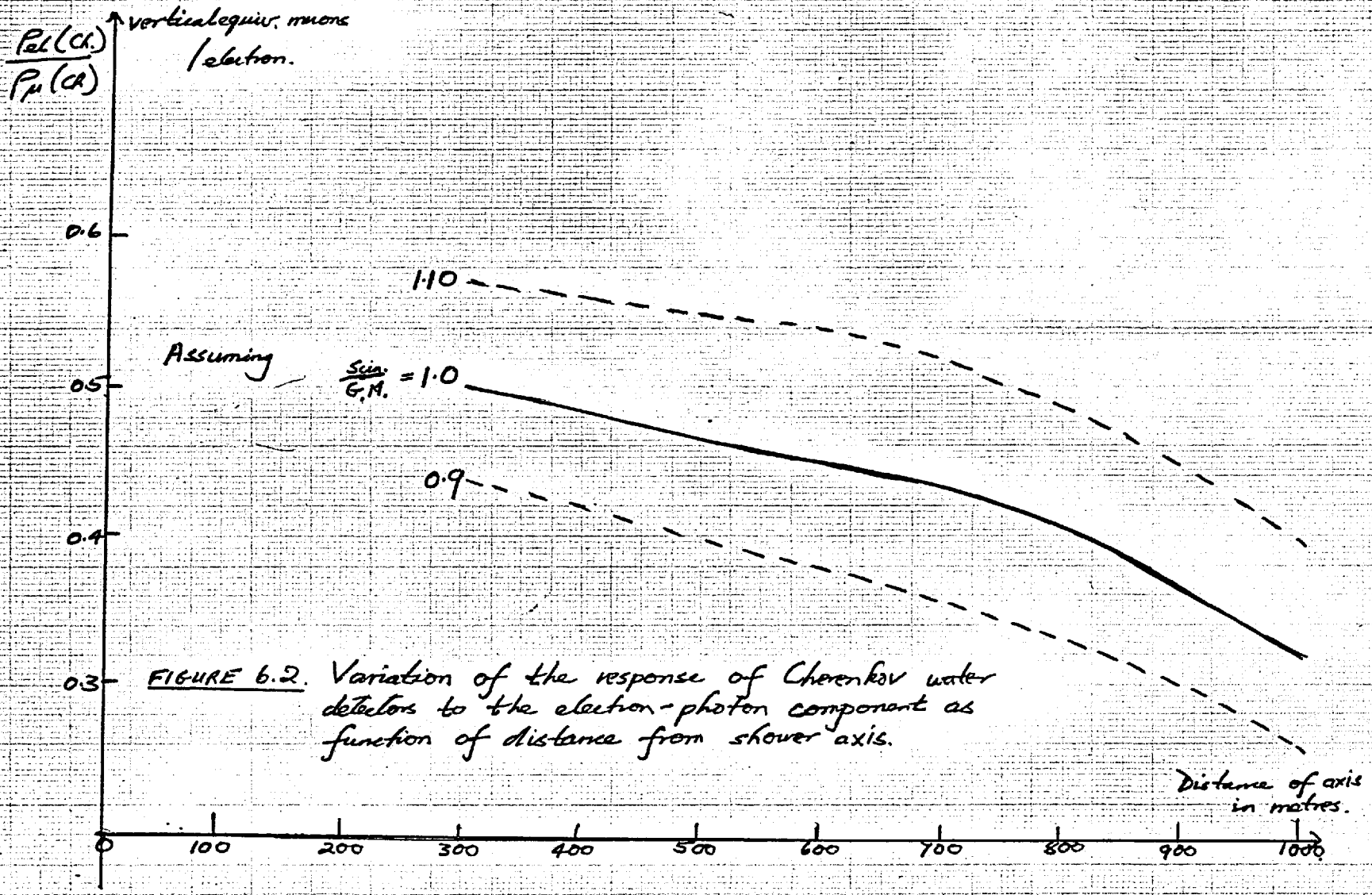


FIGURE 6.2. Variation of the response of Cherenkov water detectors to the electron-photon component as function of distance from shower axis.

electron of 1.0 vertical muons. There is still some doubt about the accuracy of this figure and the dotted curves are calculated from lower and upper limits.

A gradual decrease in relative response is observed with increase in distance from the core. This indicates the way the energy of the electron-photon component falls off at large distances from the axis.

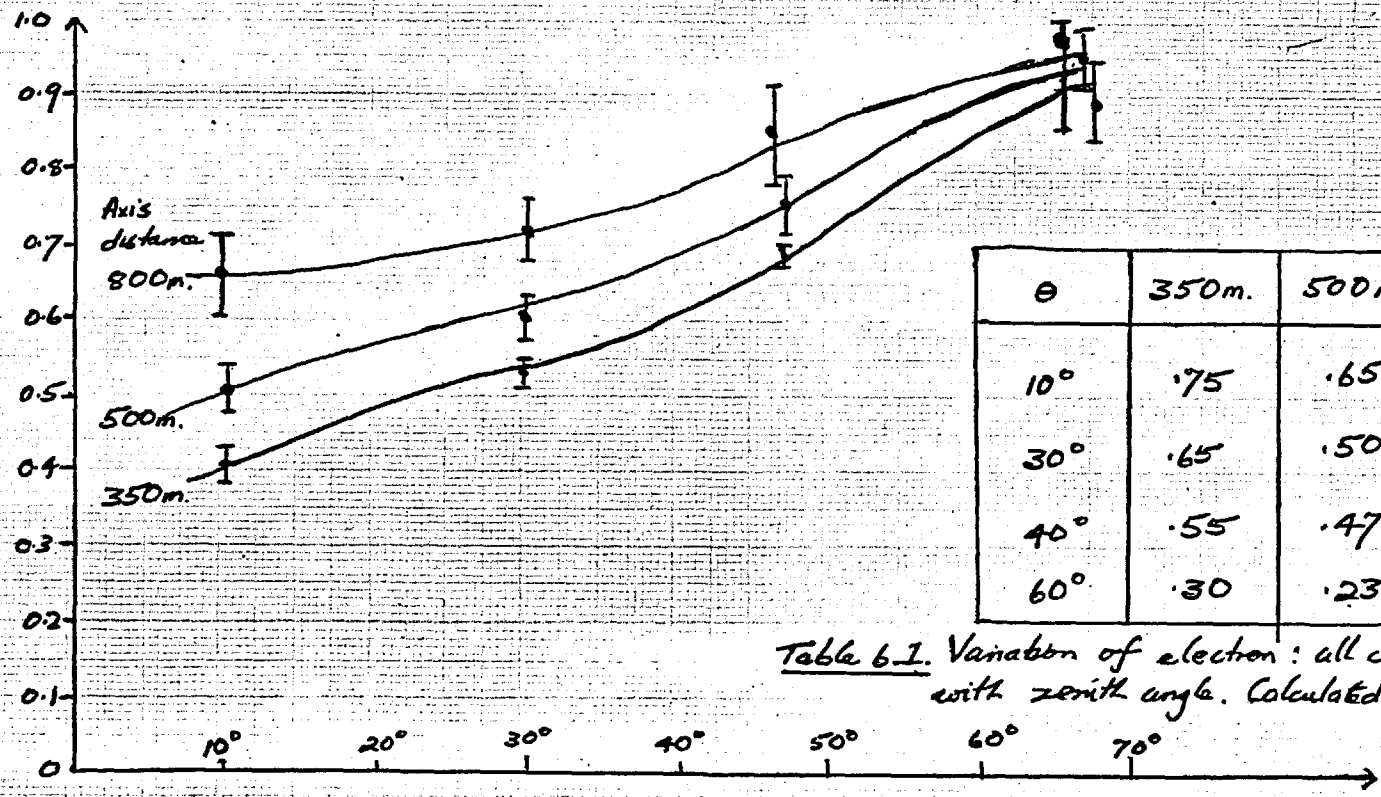
The curves are in reasonable agreement with what is expected theoretically. If it is assumed that at these distances most of the energy in the electron-photon component is carried by photons (see Chapter 3), the most penetrating of which have an absorption length of around 60 grms/cm^2, a limiting value of 0.42 is obtained for the relative response (Lillicrap,1963).

A more detailed analysis of the data obtained by comparing the scintillator and Cherenkov responses will be presented in subsequent theses from the Haverah Park Group.

6.4 The Ratio of Muon to Cherenkov Response as a Function of Zenith Angle

In Figure 6.3 the variation in the ratio of muon to Cherenkov response with zenith angle is plotted for three mean distances from the shower axis. Table 6.1, calculated

FIGURE 6.3. Variation of ρ_e/ρ_{ch} with zenith angle.



θ	350m.	500m.	800m.
10°	·75	·65	·50
30°	·65	·50	·46
40°	·55	·47	·37
60°	·30	·23	·15

Table 6.1. Variation of electron : all charged particle ratio with zenith angle. Calculated from Figure 6.3.

from the curve, represents the proportion of electrons to all charged secondaries assuming the equivalent vertical muon response discussed above.

The errors on the percentages for 60° are quite large but there is an indication that the proportion becomes practically independent of distance at these high zeniths. If such is the case it would be reasonable to conclude that these electrons are secondary products of muon decay or knock-on processes. At 60° zenith the atmospheric depth ($\sim$2,000 grms/cm^2) represents about 25 nuclear interaction lengths. The electron-photon component produced as the result of neutral pion decay in the remnant N--component must be small at these distances from the core.

At 60° zenith the results indicate that around 15-20% of the charged particles are still electrons. However the thickness of the lead shield also varies with zenith angle. At high zenith some muons may be stopped in the lead without penetrating to the detector. If such is the case the proportion of electrons will be less than is apparent from Table 6.1.

Again a more detailed study of this effect will be possible with the increased statistical accuracy obtained with the muon detector moved to the centre of the 500 metre array.

6.5 Further Study of the Lateral Distribution of Showers of Size 2×10^7 Particles

The 10 sq.metres of muon detector is now being set up at the central station of the 500 metre array. Here experiments on the lateral distribution of muons will be continued. The distance range covered at the centre is shown by the histogram in Figure 6.4. A distribution over the range 100 metres to 500 metres from the shower axis should be obtained. This overlaps the distance range covered by the results obtained at the outside station (presented in Chapter 5) as well as extending the results much closer to the core. A more accurate comparison with other workers' results can then be made.

6.6 The Small EAS Arrays

Two smaller Cherenkov detector arrays have now been built at Haverah Park centered on Hut 1 (Figure 6.5).

The 50 metre array will detect showers of size around 10^5 particles at a high rate of recording ($\sim$1,000/day) while the 150 metre array will detect 10^6 particle showers most efficiently.

The 10 sq.metre shielded detector will be operated in conjunction with both arrays. Although for each array the

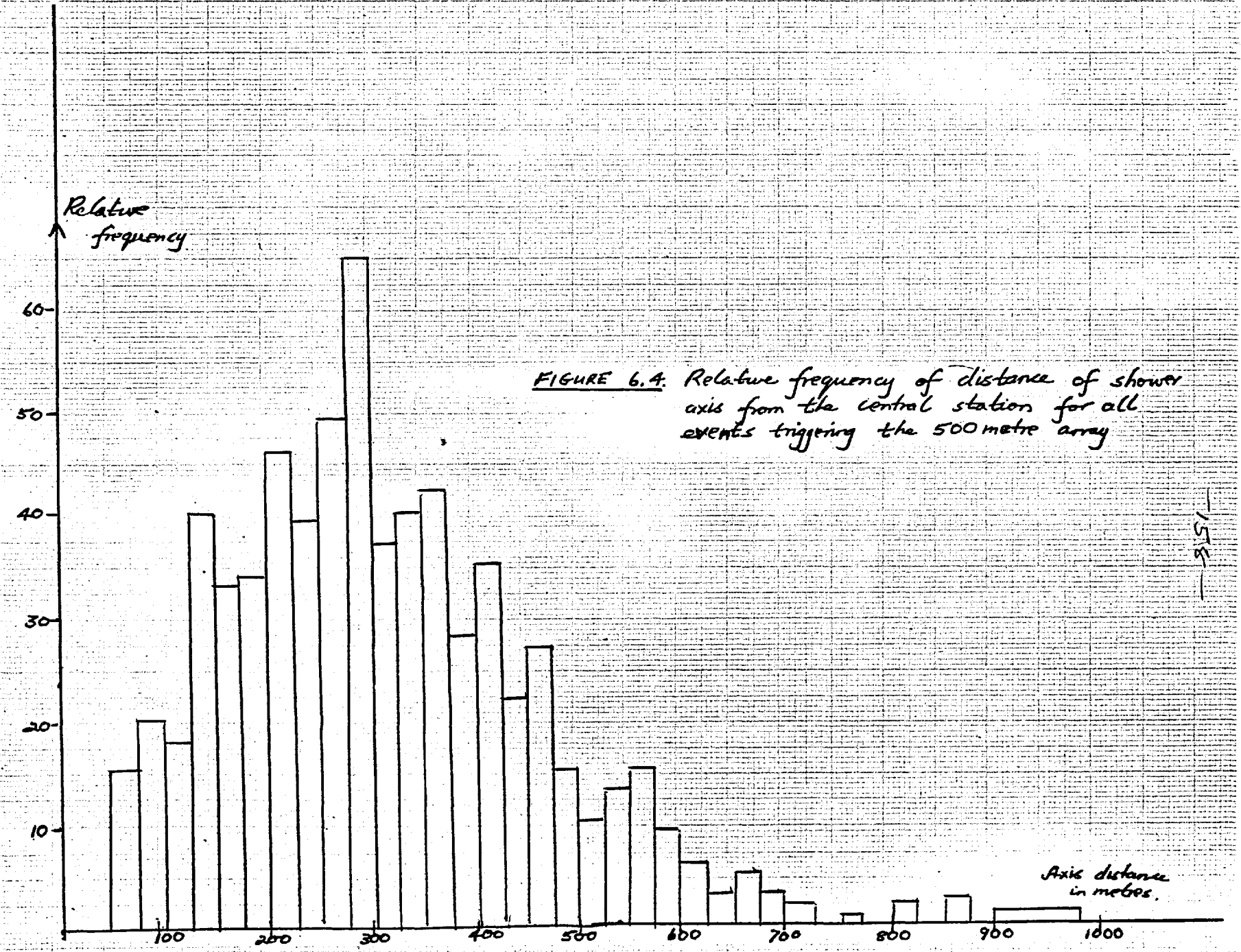


FIGURE 6.4. Relative frequency of distance of shower axis from the central station for all events triggering the 500 metre array

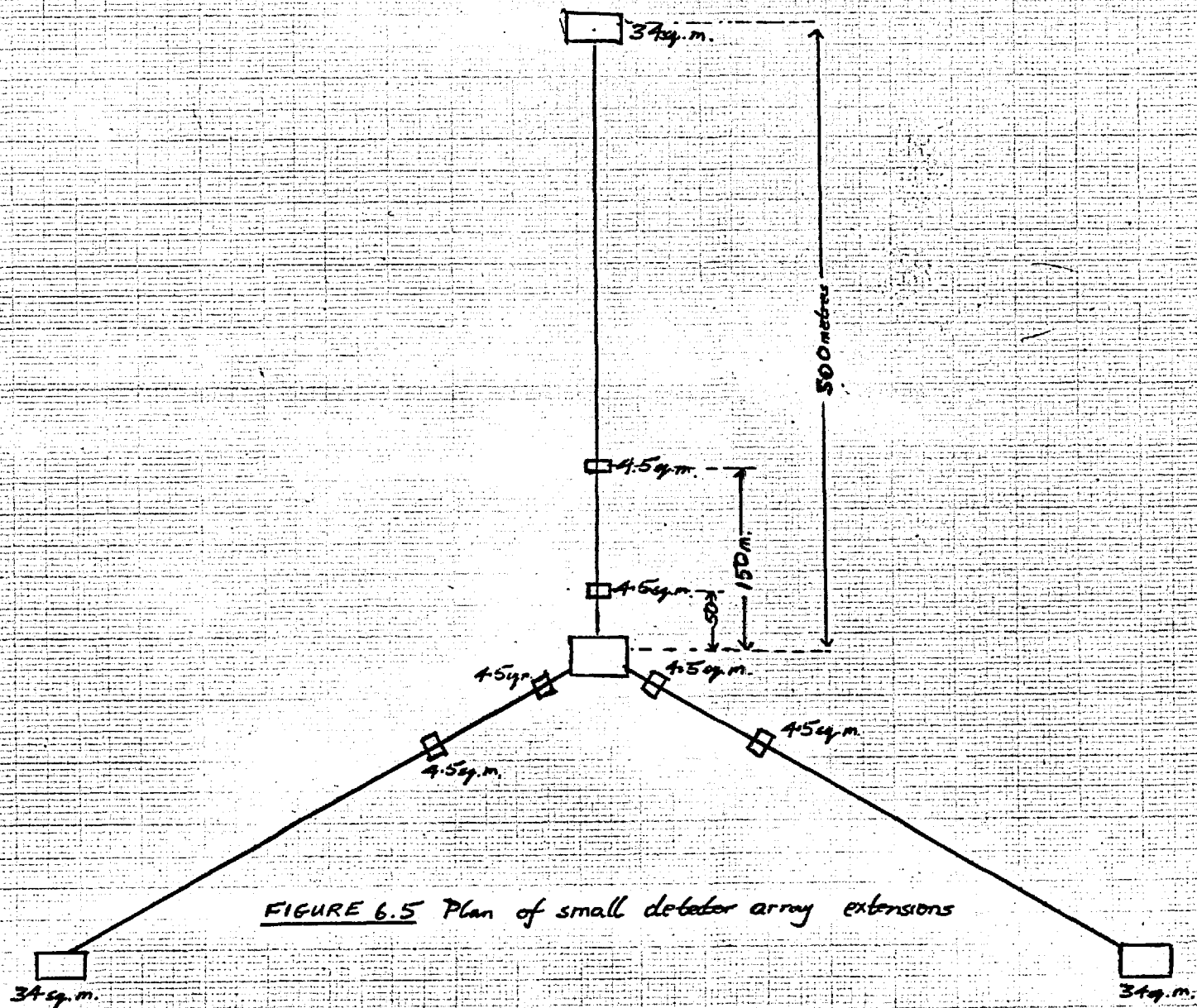


FIGURE 6.5 Plan of small detector array extensions

lateral distribution of muons will have to be determined over different distance ranges the arrays have been designed so that sufficient overlap occurs to make comparison possible. In particular an accurate determination of how N_μ varies with shower size, N, over the size range 10^5-10^8 particles should be possible. Such results should prove conclusively if any sharp change in mean muon content of showers occurs within this size range.

6.7 Energy of Muons

A shielded magnetic spectrograph has been in operation for about a year at the central station of Haverah Park. Using neon flash tubes as track indicators a study is being made of the energy spectrum of muons in showers (Rochester et al.,1955). With the density detector also at the centre a detailed assessment of the total energy carried by the muon component in showers should be possible. Also correlation between energy and density of muons in individual showers could lead to a better understanding of the development processes.

6.8 Time Spread in Arrival of Secondary Particles

The arrival time of secondaries in an EAS at a sea-level detector can be spread over intervals up to at least one microsec. Recently analysis has been carried out on the rise times of Cherenkov tanks pulses from EAS at Haverah Park (Baxter et al.,1965). It is found that 25% of the shower particles arrive within 25 nanoseconds of each other and it is suggested that this group is largely muons.

During the film analysis of the muon detectors it has been noted that occasionally muons arrive with substantial relative time delays (up to at least $\frac{1}{2}\mu s$). A detailed analysis of this phenomenon has not yet been carried out.

It is hoped to pursue the study further, using the shielded detector to identify muons. Such experimental investigation can again be usefully tied in with theoretical models of shower development.

6.9 Search for Anisotropy of "Muon-Rich" and "Muon-Less" Showers

By moving to the centre station a larger number of muons (mean about 4) than previously will be recorded in the showers. It should therefore become possible to select showers on their muon content and search for anisotropy in

arrival directions.

There is some evidence that such asymmetries do occur in both "muon-rich" and "muon-poor" showers. If agreement could be found between different research groups for the direction of such an anisotropy then greater confidence could be placed in the results.

6.10 Large Array Extension

Construction is also under way on a large scale extension of the detector array. Six small arrays are being set up at a distance of about 2 kilometres from the central station, spaced roughly symmetrically, in a circle around the 500 metre array. This will enable the upper limit of shower size recorded at Haverah Park to be raised to around 10^{10} particles. Even over such a large area array however the rate of recording even 10^{9} particles showers will be extremely slow, about one per week.

6.11 General Conclusions

The experiments described in this thesis and the results obtained are just the beginning of an intensive investigation over three or four years of the muon component of EAS

observed at Haverah Park. Although no definite conclusions ca can yet be made from the results concerning the nature of the primaries and the details of shower development, a number of questions have been raised and interpretations proposed.

The significant result presented in Chapter 5 of the way the mean muon content of showers varies with size, N, cannot as yet be regarded as a definitely real effect related to the primary composition. However it should not be difficult to establish this with the operation of the new detector arrays.

The lateral distribution of muons presented in Chapter 5 over the range 300-1,000 metres appears to be the most statistically accurate so far obtained. Extension of the measurements into regions closer to the core will enable a fairly complete structure function of muons in showers of size 2×10^7 particles to be established.

APPENDIX 1

A.1 The Optical Design of the Detectors

Since the refractive indices of liquid paraffin and perspex are very nearly equal (n = 1.49) the scintillator and tray can be regarded as a homogeneous slab.

Light is emitted isotropically from any point P in the slab due to the passage of a charged particle (Fig.A.1.1). The absorption of light in the scintillator is assumed negligible in the first instance and the surfaces are considered as plane smooth perpendicular sides.

The angle between a given light ray inside the body and the surface normal is denoted by r, and the corresponding angle outside the slab by i. Then

$$\frac{\sin i}{\sin r} = n$$

and the critical angle, r_c, for total internal reflection at the liquid (or perspex) to air interface is given by

$$r_c = \sin^{-1}\frac{1}{n} = 42^{\circ}(\text{approx})$$

All rays of light from the point P which are not totally internally reflected by a plane surface will lie within a cone whose axis is normal to the surface and with a half angle equal to r_c. In the case of the rectangular slab there are six plane surfaces, so that six escape cones exist (Fig.A.1.2). Rays that lie within the cone of one surface

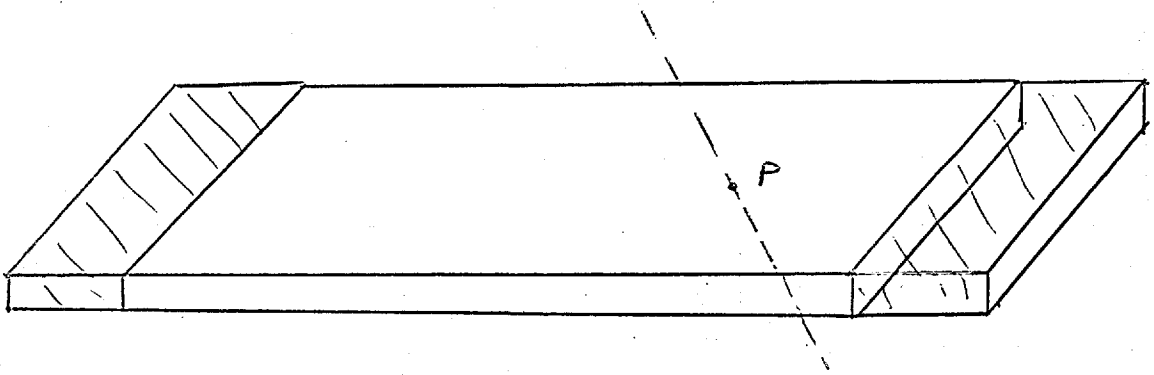


FIGURE A.1.1.

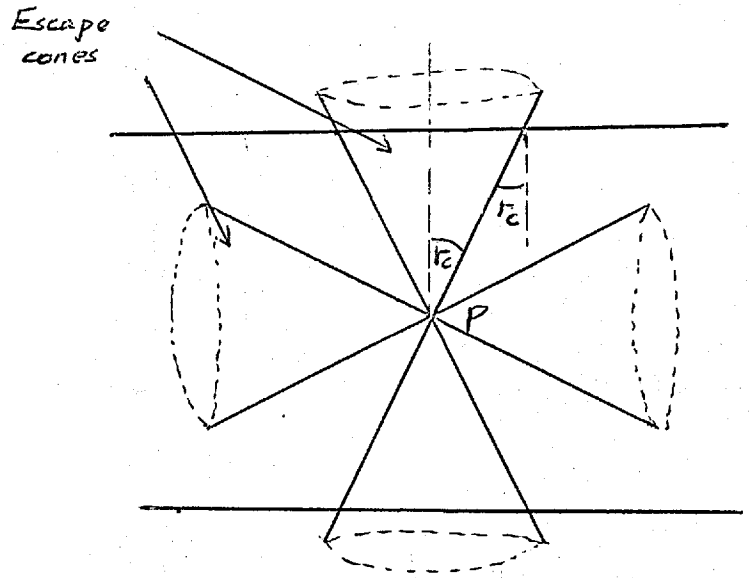


FIGURE A.1.2

may be reflected internally by another perpendicular surface, but such reflected rays will still lie within their original cone and will escape.

Rays emitted from P outside the escape cone will always be internally reflected and will remain trapped within the slab.

The fraction of light F, thus trapped can be calculated, since

$$F = \frac{1}{4}\Omega_{ext}$$

where Ω_{ext} is the total solid angle that lies outside the escape cones.

Since $r_c < 45^\circ$ the cones do not overlap and hence Ω_{ext} can be easily calculated:-

$$\Omega_{ext} = 4\pi - 6\Omega_{cone}$$

and $$\Omega_{cone} = 2\pi(1-\cos r_c)$$

hence $$F = 3\cos r_c - 2$$

$$= 0.23$$

i.e. 23% of the light emitted from P is trapped inside the slab. The fact that this amount of trapped light is independent of the position of P is important for the uniformity of the detector.

In the optical arrangement of transparent sides, light from four of the six escape cones is lost. Light in the remaining two cones (26%) emerges through the two viewing faces of the scintillator.

To ensure that the light received by the photomultipliers is independent of the scintillation position it is best that the scintillation should not take place at a distance less than $L = d \tan r_c$ from the photomultiplier face, where d is the diagonal of the viewing side (Brini et al.,1955). With the dimensions used here L = 36". Although for complete uniformity, in the absence of absorption, the light guides should theoretically be at least this length, 16" long guides were used due to shortage of space in the detector units. Tests described in section 2.8 show that satisfactory uniformity is obtained with such an arrangement.

The influence on light collection of the absorption in the scintillator and at the surface walls should also be considered. Exact information on the emission and absorption spectra are needed for a detailed study of the problem. There will certainly be a reduction in collection efficiency because of these effects.

Since each photocathode covers about 10% of the viewing side about 1% of the light output will finally reach the photo-cathodes.

One possible way of improving on this light collection is to capture the entrapped light by having the phototubes in optical contact with the sides of the detector. The efficiency thus gained would be offset by the difficulty of ensuring good contact and the troublesome techniques involved.

It is possible to capture the light from the other four escape cones by making the walls of the detector reflecting. Such a counter would have a uniform collection if it were not for absorption and a reflection coefficient which is always less than one. The rays with large angles, r, at the viewing surface reach the surface after many reflections. They thus undergo an attenuation through reflection and absorption which grows with increasing distance of the scintillation from the collecting surface. Such a counter will be very non-uniform.

The use of a transparent walled light guide with such an arrangement will help to eliminate the worst of the non-uniformity.

Diffusely reflecting walls are only of use in detectors of approximately spherical shape, and even then only when the collecting surface is small and direct light has little effect.

The design adopted in the present experiment, i.e. a rectangular parallelepiped with transparent walls, leads to good uniformity provided the absorption length of the light in the scintillator is not shorter than the length of the detector. However the fraction of light collected is fairly low.

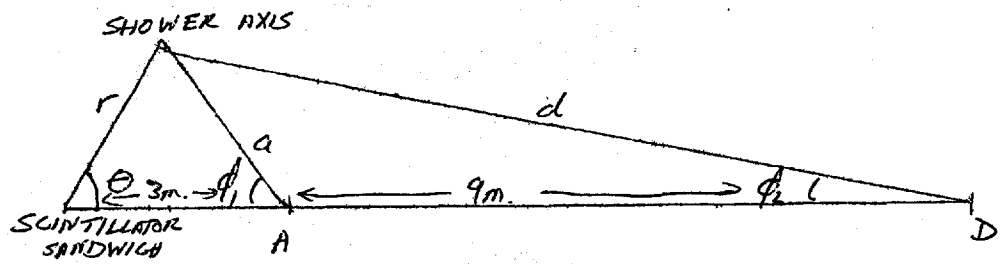
APPENDIX 2

A.2 Interpretation of Selected Showers

In the following it will be assumed that all showers fall vertically. The detector response structure function is assumed to be of the form:-

$$j(r) \propto r^{-m}.$$

Then for a small Cherenkov tank array Lilliorap (1963) shows that the best value of m is 1.48($\pm$0.2).



If the response of the nearest group of tanks to the scintillator is denoted by A, and that of the furthest by D:-

$$\frac{A}{D} = \frac{j(a)}{j(d)} = \left(\frac{a}{d}\right)^{-1.48}$$

where a, d are the distances of the shower axis from groups A, D respectively.

For "Near" showers, the selection criterion requires a minimum value of A/D such that

$$\frac{A}{D} = 5 = \left(\frac{a}{d}\right)^{-1.48}$$

i.e. $$\frac{d}{a} = (5)^{\frac{1}{1.48}} = 3.0 \qquad \ldots\ldots \text{A.2.}$$

From Figure A.2.

$$a\text{Cos}\phi = 3 - r\text{Cos}\theta$$

$$b\text{Cos}\phi_2 = 12 - r\text{Cos}\theta$$

$$a\text{Sin}\phi_1 = r\text{Sin}\theta$$

$$b\text{Sin}\phi_2 = r\text{Sin}\theta$$

where r is the distance of the shower axis from the scintillator.

Then $$a^2 = (3 - r\text{Cos}\theta)^2 + (r\text{Sin}\theta)^2$$

$$= r^2 - 6r\text{Cos}\theta + 9$$

$$b^2 = (12 - r\text{Cos}\theta)^2 + (r\text{Sin}\theta)^2$$

$$= r^2 - 24r\text{Cos}\theta + 144$$

From equation A.2.1. for "Near" showers

$$9(r^2 - 6r\text{Cos}\theta + 9) = r^2 - 24r\text{Cos}\theta + 144$$

i.e. $$8r^2 - 30r\text{Cos}\theta - 63 = 0.$$

Maximum r occurs when $\text{Cos}\theta = +1$, i.e. $\theta = 0$

Then $$8r^2 - 30r - 63 = 0$$

From which $$r_{max} = 5.2 \text{ metres.}$$

Hence "Near" showers have cores lying within 5.2 metres of the scintillator.

For "Distant" showers as D > C > B > A, the core of the shower must fall nearer Group D than Group C of the tanks. Hence its core position is greater than 10 metres from the scintillator stack.

ACKNOWLEDGEMENTS

The author wishes to acknowledge the following for their help in various ways:-

Professor H. Elliot of Imperial College for his advice and interest in the experiment.

Professor J. G. Wilson for his co-operation and generosity in allowing the author to use the facilities of the Physics Department of the University of Leeds.

Dr. H. R. Allan for much discussion and advice.

Mr. J. K. Jones, Mr. J. K. Pidcock and other members of the Imperial College Group for their willing help.

All other members of the Haverah Park Group for the help and co-operation received from them.

The Science Research Council for supplying a maintenance grant during the three years of study.

. . . . . .

REFERENCES

Allan H R; Blake P R; Jones J K; Lillicrap S C; Pidcock J K; Reid R J O; Turver K E. — 1965 London IUPAP Conf. (to be published)

Arley N. — 1938 Proc.Roy.Soc. A168 519

Askaryan G A. — 1962 J.Phys.Soc.Japan 17 Suppl. A3 257

Auger P. — 1938 C.R.Acad.Sci.Paris 207 907

Auger P; Maze R; Grivet-Meyer T. — 1938 C.R.Acad.Sci.Paris 206 1721

Auger P; Ehrenfest P; Maze R; Daudin J; Robley J; Freon A. — 1939 Revs.Mod.Phys. 11 288

Barnaby C F; Barton J C. — 1960 Proc.Phys.Soc. 76 745

Barton J C; Barnaby C F; Jasani B M; Thompson C W. — 1962 J.Sci.Inst. 39 360

Barton J C; Crispin A. — 1964 J.Sci.Instum. 41 736

Barton J C. — 1965 Private Communication

Baxter A; Watson A A; Wilson J G. — 1965 London IUPAP Conf. (to be published)

Belenky S Z; Ivanenko I P. — 1960 Uspekhi Sov.Physics 2 6

Bennett S; Delvaille J; Greisen K; Kendziorski F. — 1962 J.Phys.Soc.Japan A3 196

Bhabha H J; Chakrabarty S K. — 1948 Phys.Rev. 74

Brini et al. — 1955 Nuovo Cimento Supp. 2 1048

Broadbent D; Jamossy L.	1947 Proc. Roy.Soc. A191 517
Brooke G; Wolfendale A W.	1964 Proc.Phys.Soc. 83 843
Buja.	1963 Acta Physica,Polonica 24 No.3
Burbidge E M; Burbidge G R.	1965 London IUPAP Conf. (to be published)
Burbidge G R.	1963 Jaipur IUPAP Conf. 3 229
Butcher J C; Messel H.	1960 Nuclear Physics 20 15
Butcher J C; Messel H.	1962 Nuclear Physics 39 1
Carmichael H; Steljes J F.	1955 Phys.Rev. 99 1542
Charman N.	1965 London IUPAP Conf. (to be published)
Chatterjee B K; Murthy G T; Naranan S; Sreekantan B V; Rao M V S.	1963 Jaipur IUPAP Conf. 4 227
Chernavsky D S; Feinberg E L.	1963 Jaipur IUPAP Conf. 5 395
Chowdhuri B.	1948 Nature 161 680
Clark G; Earl J; Kraushaar W; Linsley J; Rossi B; Scherb F.)	1958 Nuovo Cimento Supp. 8 631
Clark G; Earl J; Kraushaar W; Linsley J; Rossi B; Scherb F; Scott D W.	1961 Phys.Rev. 122 637
Clark G; Bradt H; Pointe M La; Domingo V; Escobar I; Murakami K; Suga K; Toyoda Y; Hersil J.	1963 Jaipur IUPAP Conf. 4 65

Clay.	1927 Proc.Roy.Acad. Amsterdam 30 1115
Cocconi G; Tongiorgi V; Greisen K.	1949 Phys.Rev. 75 1068
Cocconi G.	1965 London IUPAP Conf.
Cousins; Nash F.	1962 Advances in Physics 11 349
Cranshaw T E; Hillas A M.	1960 Moscow IUPAP Conf. 2 210
De Beer; Cranshaw T E; Parham.	1962 Phil.Mag. 7 499
Dennis B R; Wilson J G.	1963 Jaipur IUPAP Conf. 4 258
Dennis B R.	1964 Ph.D.Thesis University of Leeds
Dufresne R.	1965 Priv. Communication
Evans.	1955"The Atomic Nucleus" McGraw Hill
Fowler P H.	1963 Jaipur IUPAP Conf. 5 182
Freier P; Lofgren E J; Ney E P; Oppenheimer F; Bradt H L; Peters B.	1948 Phys.Rev. 74 213
Furry W H.	1947 Phys.Rev. 52 569
Ginzburg V I; Syrovatskii S I.	1964 "The Origin of Cosmic Rays" Pergamon Press
Glencross W M.	1963 Proc.Phys.Soc. 82 501
Green J R; Barcus J R.	1959 Nuovo Cimento 23 708

Greisen K. — 1949 Phys. Rev. 75 1071

Greisen K. — 1956 Prog.Cosmic Ray Phys III 3

Greisen K. — 1960 Ann.Rev.Nucl.Sci. 10 63

Hasegawa H; Naranan S; Matano T; Miura I; Oda M; Shibata S; Tanahashi G; Tanaka Y. — 1963 J.Phys.Soc.Japan 17 A3 189

Hayman et al. — 1963 Proc.Roy.Soc. 275 391

Hersil J; Escobar I; Clark G; Olbert S; Moore C; Scott D. — 1962 J.Phys.Soc.Japan 17 A3 243

Hillas A M. — 1965 London IUPAP Conf. (to be published)

Janossy L; Lovell A C B. — 1938 Nature 142 716

Jelley J V; Graham-Smith F; Porter N A; Weekes T C; Porter R A; Charman N; Fruin J H; McBreen B. — 1965 Nuovo Cimento (preprint)

Johnson T H. — 1938 Rev.Mod.Phys. 10 193

Jones J K. — 1965 London IUPAP Conf. (to be published)

Kamata K; Nishimura J. — 1958 Prog.Theor.Phys. Suppl. 6 93

Kameda T; Toyoda Y; Maeda T. — 1962 J.Phys.Soc.Japan 17 Suppl. A3 270

Kazarov R E; Andronikashvili E L. — 1957 Sov. Phys.J.E.T.P. 6 1182-3

Lattes C M G; Muirhead H; Occhialini G P S; Powell C F. — 1947 Nature 159 694

Millicrap S C.	1963 Ph.D.Thesis University of London
Linsley J; Scarsi L; Rossi B.	1962 J.Phys.Soc.Japan 17 Supp. A3 91
Linsley J; Scarsi L.	1962 Phys.Rev. 128 2384
Linsley J.	1963 Jaipur IUPAP Conf. 4 77
Linsley J.	1963A Jaipur IUPAP Conf. 4 295
Lloyd; Wolfendale A W.	1959 Proc.Phys.Soc. 73 178
Malos J; Millar, C D; Wallace O S.	1962 J.Phys.Soc.Japan 17 Suppl. A3 114
Matano T; Miura I; Nagano M; Oda M; Shibata S; Tanaka Y; Tanahashi G; Hasegawa H.	1963 Jaipur IUPAP Conf. 4 129 & 248
McCusker C B A; Millar C D.	1951 Proc.Phys.Soc. A64 915
McCusker C B A; Peak L S.	1963 Jaipur IUPAP Conf. 5 35
McCusker C B A; Rathgeber H D; Winn M M.	1963 Jaipur IUPAP Conf. 4 306
Meyer P.	1965 London IUPAP Conf. (to be published)
Meyer et al.	1963 Nuclear Inst.& Meth 22 371
Miyake S.	1958 Prog.Theor.Phys. 20 844
Miyake S.	1962 J.Phys.Soc.Japan 17 Suppl. A3 291
Muira I; Hasegawa H.	1962 J.Phys.Soc.Japan 17 Suppl. A3 84

Morrison P; Olbert S; Rossi B.	1954 Phys.Rev. 94 440
Occhialini G P S; Powell C F.	1947 Nature 157 186
Oda M.	1965 London IUPAP Conf. (to be published)
Peters B.	1963 Jaipur IUPAP Conf. 4 317
Peters B.	1963A Jaipur IUPAP Conf. 5 423
Rochester G D; Somogyi A J; Turver K E; Walton A B.	1965 London IUPAP Conf. (to be published)
Rossi B.	1933 Zeits f. Phys. 32 151
Rossi B.	1952 "High Energy Particles" McGraw Hill
Schmeiser K; Bothe W.	1938 Ann.Phys.Lpz. 32 161
Scott W T; Uhlenbeck G E.	1942 Phys.Rev. 62 497
Shibata S; Nagano M; Matano T; Suga K.	1965 London IUPAP Conf. (to be published)
Sitte K.	1961 Handbuch der Physik 46/1
Sitte K.	1963 Jaipur IUPAP Conf. 4 225
Steinberger J; Panofsky W K H; Steller J.	1950 Phys.Rev. 78 802
Stoker P H et al.	1961 Proc.Phys.Soc. 78 650
Suga K; Escobar I; Mukakami K; Domingo V; Toyoda Y; Clark G; Pointe M La.	1963 Jaipur IUPAP Conf. 4 9

Swinson D B; O'Donnell B D; Prescott J R. — 1965 London IUPAP Conf. (to be published)

Toyoda Y; Suga K; Murakami K; Hasegawa H; Shibata S; Domingo V; Escobar I; Kamata K; Bradt H; Clark G; Pointe M La. — 1965 London IUPAP Conf. (to be published)

Turver K E. — 1963 Ph.D Thesis. University of Leeds

Ueda A. — 1960 Prog.Theor.Phys. 24 1231

Vernov S N. et al. — 1960 Sov.Phys.J.E.T.P. 10 1050

Walker. — 1953 Phys.Rev.90 234

Wilson et al. — 1963 J.Sci.Instr. (March)

Winn M M; Wand R H; Ulrichs J; Rathgeber M H; Poole P C; Nelson D; McCusker C B A; Jauncey D L; Crawford D F; Bray M D. — 1965 Il Nuovo Cimento 36 701

Woischnig; Burmeister. — 1964 Zeits Leift fur Physik 177 151

Wolfendale A W. — 1964 "Cosmic Rays" Newnes p.130

Zatsepin G T; Nikolsky S I; Khristiansen G M. — 1963 Jaipur IUPAP Conf. 4 100